A phase II randomised controlled trial of amiloride as a neuroprotective treatment in optic neuritis – studying in vivo neurodegeneration, neuroprotection and cortical plasticity after an inflammatory insult to the visual system

Justin McKee

A thesis submitted for the degree of Doctor of Philosophy

Wolfson College

University of Oxford

Trinity Term 2017

Abstract

Basic science and early clinical trial evidence suggest the safe diuretic drug amiloride, may exert a neuroprotective effect in multiple sclerosis (MS) through blockade of the acid sensing ion channel. Neuroprotective treatments are a key unmet need in multiple sclerosis. Optic neuritis (ON) is a discrete CNS inflammatory event leading to neuro-axonal injury in the optic nerve and retina.

The optic nerve is part of the visual system, one of the most functionally and structurally eloquent systems in the central nervous system, which affords a number of unique modalities to assess neurodegeneration and neuroprotection. The visual system can be classified into two parts, the anterior and posterior visual systems, which are defined by the lateral geniculate nucleus, where the two components synapse. The extent of neurodegeneration following ON in the anterior visual system can be imaged in vivo through scanning laser polarimetry (GDx) and optical coherence tomography (OCT).

The posterior visual system can be imaged by quantitative and functional magnetic resonance imaging (MRI) of the brain, giving insights into white matter structural integrity and cortical plasticity over time.

Combining these modalities in a longitudinal study, allows assessment of the impact of neurodegeneration in the anterior visual system on neurodegeneration downstream in the posterior visual system and on changes in functional connectivity over time in the visual cortex. Furthermore, in the clinical trial setting the neuroprotective effect of any intervention both on direct anterior neurodegeneration and downstream processes can be assessed. The functional relevance of changes in all of these biomarkers can be tested through a number of visual measures, including low contrast visual acuity.

In MS, the contribution of transsynaptic neurodegeneration to the global neuronal loss experienced by patients is an area of incomplete understanding. In addition, the role of the visual cortex, through neuroplasticity, in aiding visual recovery from optic neuritis, is unclear.

To address these issues, this thesis reports the results of the first clinical trial of amiloride in ON, and shows that despite the pre- and early clinical evidence of neuroprotection of amiloride, no neuroprotective benefit was found. It goes on to explore reasons for this lack of effect including the finding of early retinal neurodegeneration in ON, and the need for early recruitment windows in the future.

From there, it makes a detailed assessment of the longitudinal changes in retinal OCT for 12 months following ON, including a novel finding of the temporal evolution of inner nuclear layer swelling, previously reported only cross-sectionally.

Next, for the first time macular retinal neurodegeneration is shown to influence diffusion tensor MRI derived measures of white matter integrity in the optic radiations, indicating transsynaptic neurodegeneration.

Finally, longitudinal changes in resting state functional connectivity following ON are found in the visual system for the first time. The interaction between this cortical functional, retinal neurodegeneration and visual recovery is probed.

DECLARATION

I Justin McKee, confirm that the work presented in this thesis is my own. Where information has been derived from other sources I have indicated in this thesis. I applied for ethical approval, regulatory approval, wrote the protocol, standard operating procedures and investigators brochure for the clinical trial (with the exception of electrophysiology and MRI). I screened and consented the patients following referral from NHS clinicians, I performed and oversaw testing of vision, low contrast visual acuity, colour vision, visual field, OCT and GDx. I was present during the acquisition of the MRI scanning and was responsible for data retrieval and storage. I co-analysed all the data from the clinical trial (Chapter 2) and was responsible for the concept and analysis of the longitudinal observational OCT and MRI data (chapters 3-5), along with feedback and advice as outlined below. I wrote this thesis and prepared all of the figures and tables. In addition the following people and institutions contributed to data collection and analysis of the work described in this thesis.

Patients were recruited to the trial from the Oxford Eye Hospital, Frimley Park Hospital, Bristol Eye Hospital, The Western Eye Hospital, London, The Great Western Hospital, Swindon, Coventry University Hospital, The Royal Berkshire Hospital, Windsor and Stoke Mandeville Hospital in Aylesbury.

Trial safety checks were performed by Dr Matthew Craner as the treating physician for the trial.

The MS research nurses Anna Cavey, Catherine Peate, Alejandro Rubio Diaz and Christina Albarno tested vision, low contrast visual acuity and colour vision in the trial either alongside or independently of myself, and maintained the case records and trial master files. The same group were responsible for coordinating patient visit schedules along with myself, and trial administrators Joy Hodder and Abigail Koelewyn.

MRI scanning was performed on the John Radcliffe hospital site in Oxford, in the Oxford centre for Functional MRI of the Brain (FMRIB) and the Acute Vascular Imaging Centre (AVIC), by the radiographers Jon Campbell, Michael Sanders and Caroline Young, Juliet Semple and Peter Manley. Jon Campbell authored the SOP for MRI scanning and I approved it.

Dr Wilhelm Kuker reviewed the clinical MRI sequences (T1, PD/T2 and FLAIR) and provided clinical reports.

A minority of OCT scans (approx. 20%) were acquired by Lewis Smith and Angela Anstey in the Oxford Eye Hospital.

All of the electrophysiology data was acquired by Dr Charles Cottriall in the Oxford Eye Hospital.

The original study was designed by the trial working group who included; Dr Matthew Craner, Dr Jacqueline Palace, Prof Lars Fugger, Mr John Elston and Dr Valentina Tomassini who applied to the MS society for the grant that employed me.

Additional input and further refinement of the final trial design prior to protocol authorship including MRI sequence choice was provided by the same group above along with myself, Dr Lucy Matthews, Dr Yazhuo Kong and Dr Nikos Evangelou.

The PD/T2 MRI sequence was designed by Dr Mark Jenkinson. Dr Mark Jenkinson and Dr Ludovica Griffanti provided a pre-release version of the FSL tool BIANCA and trained me to use it. Matlab script for motion parameter calculation in chapter 5 was provided by Dr Saad Jbabdi. Other than this, all of the MRI sequences were standard FMRIB protocols and analysis performed with standard open source software as referenced.

The clinical trial powering calculations were performed by Dr Ly-Mee Yu and main trial data was analysed by Dr Stephen Gerry (chapter 2 amiloride placebo comparisons only), both from the Oxford Centre for Statistics in Medicine. I subsequently performed the same analysis post blinding in a different statistical package (SPSS) for figure generation purposes.

Dr Yazhuo Kong assisted in MRI analysis technique choice and in reviewing statistical design matrices and outputs.

Acknowledgements

My DPhil thesis would not have been possible without the continued support of a great many people, both in Oxford and elsewhere. In addition to being grateful to all those mentioned in my declaration I would like to give my personal thanks to the following:

My incredible supervisors, Matt Craner and Jackie Palace for their invaluable support and supervision, and for taking me on in the first place, and sticking with me.

Ana Cavey, Joy Hodder, Alejandro Rubio-diaz, Christina Albarno, Abigail Koelewyn, Catherine Peate, who are part of the wonderful MS trials team in Oxford for their help with the trial but most of all for being my supportive friends and making me laugh when I needed it the most.

Dr Charles Cottriall for his infectious enthusiasm for research, along with Patsy Terry and the Oxford Eye Hospital for being so accommodating for the trial procedures.

Mr John Elston and Professor Chris Kennard for their clinical support for the trial and for teaching me so much about neuro-ophthalmology.

In FMRIB I would like to thank Dr Yazhuo (Joe) Kong for his invaluable help with MRI analysis and for being a great conference companion. Prof. Mark Jenkinson and Dr Ludovica Griffanti for giving me their lesion masking software and helping me use it. Prof. Holly Bridge for providing invaluable feedback on my results at my confirmation viva and for my final results.

The other clinical fellows over the years including Jo Kitley, Sarah Finlayson, George Tackley, Ruth Geraldes, Jithin George and Adriana Rocca for their ideas, fun and support.

My flatmate David Parr for putting a roof over my head in Oxford and being a supportive friend both at work and at home.

My Mum, Dad, and siblings Colm, Philip and Norah, for their continued love and support over the years.

Dr John Olson, Dr Cynthia Santiago, Sam Loggie, Vikki McBain and all my friends and colleagues in the eye clinic in Aberdeen who supported me while working there and writing up

Moira Prior for her tireless proofreading and cooking, and putting roof over my head in Edinburgh while finalising this thesis.

The MS Society for generously funding this research.

Most importantly, I would also like to thank all the patients who gave up their time during a period of ill health in order to take part in this research. Their generosity was incredible.

List of Figures

List of Tables

List of Abbreviations

ACTION	Amiloride Clinical Trial in Optic Neuritis
AD	Axial Diffusivity
ANCOVA	Analysis of co-variance
ANOVA	Analysis of variance
AP	Antero-posterior
ART	Automated real time
ASIC	Acid-sensing ion channel
AVIC	Acute Vascular Imaging Centre
BET	Brain extraction technique
BIANCA	Brain Intensity Abnormality Classification Algorithm
BOLD	Blood Oxygen Level dependent
Ca2+	Calcium
CI	Confidence interval
CIS	Clinically isolated syndrome
CNS	Central nervous system
CRION	Chronic relapsing idiopathic optic neuropathy
CSF	Cerebro-spinal fluid
DMN	Default mode network
DTI	Diffusion tensor imaging
DVAR	Derivative variance in root mean squared
ECC	Enhanced corneal compensation
eGFR	Estimated glomerular filtration rate
EPI	Echo planar imaging
ETDRS	Early treatment of diabetic retinopathy study
FA	Fractional anisometry
FLAIR	Fluid attenuated inversion recovery
FC	Functional connectivity
FDT	FMRIB's diffusion toolbox
FLIRT	FMRIB's Linear Image Registration Tool
FM100	Farnsworth-munsell 100 hue test
fMRI	Functional MRI
FMRIB	Oxford Centre for Functional MRI of the brain
FNIRT	FMRIB's non-linear registration tool
FOV	Field of view

FSL	FMRIB software library
GCL	Ganglion cell layer
GCLIPL	Ganglion cell inner plexiform layer
GDx	Scanning laser polarimetry
HCVA	High contrast visual acuity
HVF	Humphrey visual field
IC	Independent component
ICA	Independent component analysis
ICC	Intra-class correlation
INL	Inner nuclear layer
IPL	Inner plexiform layer
IS/OS	Inner segment / outer segment layer
ISCEV	International Society for Clinical Electrophysiology of Vision
ITT	Intention to treat
K+	Potassium
LCVA	Low contrast visual acuity
LGN	Lateral geniculate nucleus
MD	Mean deviation
MNI	Montreal Neurological Institute
MRI	Magnetic resonance imaging
mRNFL	Macular retinal nerve fibre layer
MS	Multiple Sclerosis
Na+	Sodium
NMO	Neuro-myelitis optica
NO	Nitric oxide
OCT	Optical coherence tomography
ON	Optic neuritis
ONL	Outer nuclear layer
ONTT	Optic neuritis treatment trial
OR	Optic radiations
PA	Postero-anterior
PD	Proton density
PERG	Pattern-electroretinogram
PPMS	Primary progressive MS
pRNFL	Peri-papillary retinal nerve fibre layer
PVEP	Pattern visually evoked potential

RGC	Retinal ganglion cell
RD	Radial diffusivity
RNFL	Retinal nerve fibre layer
RRMS	Relapsing remitting MS
RSfMRI	Resting state functional connectivity
SD	Standard Deviation
SPMS	Secondary progressive MS
TBSS	Tract-based spatial statistics
TE	Echo time
TES	Total error squared
TFCE	Threshold free cluster enhancement
TR	Repetition time
VCC	Variable corneal compensation

Table of Contents

1 Chapter 1. Introduction

1.1 Multiple Sclerosis (MS) and neurodegeration

MS is characterised by inflammatory demyelinating plaques and neuro-axonal damage affecting the CNS. It is a major cause of disability and has a high societal and economic cost (1). Clinically, there are three main subtypes of MS, relapsing remitting MS (RRMS), primary progressive MS (PPMS) and secondary progressive MS (SPMS). In RRMS, patients suffer acute or sub acute inflammatory episode in the CNS resulting in transient clinical disability followed by partial or complete recovery (2). Around two thirds of RRMS patients will eventually convert to a pattern of steady decline in function, termed SPMS, which may or may not have relapses superimposed. Other patients experience a progressive neurological disability from first symptoms onset, and this is termed PPMS (3).

Diagnosis of MS is based on clinical and radiological criteria, with magnetic resonance imaging (MRI) being an essential tool for the diagnosis of MS (4). Characteristically, T2 weighted MRI in MS patients shows the presence of hyperintense white matter lesions disseminated in time, over repeat scans and disseminated in space. The age, and demyelination or remyelination status of lesions is not quantifiable from a T2 weighted MRI scan (5). Using gadolinium enhanced T1 weighted imaging can show enhancement of new lesions (6), and can be used as evidence of dissemination in time.

Pathologically, the majority of evidence indicates MS is primarily an inflammatory demyelinating disorder, with consequential neurodegeration. However, neurodegeneration in MS is a focus of increasing interest, and the possiblilty of MS

being a primarily neurodegerative disorder with inflammatory sequelae as an epiphenomenon, has been raised. Evidence for a primarily inflammatory component in MS comes initially from animal models, which have shown that peripheral sensitisation in animals inoculated with myelin leads to T cells transgressing the blood brain barrier, leading to CNS plaques of demyelination, activated macrophages and glial cells, giving a close approximation of the human disease (7). In post-mortem studies, MS plaques also demonstrate the presence of axonal loss associated with demyelination, active T-cells and microglia and a correlation between numbers of inflammatory cells and axonal loss has been reported (8). Moreover breakdown of the blood brain barrier is evident in vivo from the presence of gadolinium enhancing lesions on T1-weighted MRI, which along with hyperintense T2 weighted form the radiological hallmark of the disease (9).

However, others point to the distribution of active T-cells away from the active edge of inflammatory lesions (10) with their presence, along with B-cells, being detected in older, more established areas of lesions which are identified by the presence of remyelination - a recognised phenomenon in MS. Furthermore, additional pathology studies have shown a lack of correlation between lesion load and axonal loss in the brain as measured by brain weight (11).

Whilst there is debate about the extent to which inflammation and demyelination in MS are directly causative to neuro-axonal injury, neurodegeneration is a widely accepted key pathological determinant in the development of disability in MS (12). Treatment with immune modulating therapies, whilst effective at reducing relapses, has had a less clear benefit in reducing disability in MS. Some studies have shown no demonstrable long term effect on disability (13, 14), whilst others have been more favourable (15). Newer agents have shown early modest effects yet to be confirmed in long term outcomes (16).

Thus, therapeutic agents that can more directly target protection of neurons downstream from the effects of inflammation, could provide a useful augmentary treatment strategy to our current immune-modulating therapeutic approach. As in the eloquent analogy from Bermel and Inglese

"Immune-modulating therapies are the equivalent of a weather machine that prevents the storm from ever brewing, and in that way provide indirect neuroprotection. Primary neuroprotection would be achieved by another mechanism, something akin to installing storm shutters or reinforcing the structure of a home to help it weather the years. " (17)

1.2 The Acid Sensing Ion Channel (ASIC) a potential target for neuroprotection

Axonal loss in MS is likely to be multifactorial, but a key endpoint is intracellular influx of sodium (Na^+) and calcium (Ca^{2+}) ions. A major contributory factor to the influx of Na^+ is from ion channels, which drives reversal of the Na^+/Ca^{2+} exchanger (18, 19). A number of ion channels including voltage gated potassium (K^+) channels (20), TASK K^+ channels (21) have been assessed as targets in animal models of MS with some efficacy. In addition voltage-gated Na^+ channel blockade with phenytoin has shown evidence of efficacy both in an animal model of MS (22), and in a recent phase II clinical trial in ON (23).

Recent evidence has implicated the acid-sensing ion channel type 1 (ASIC1), capable of fluxing both Na^+ and Ca^{2+} as a mediator of neuronal injury in stroke and CNS inflammation (18, 24, 25). The inflammatory milieu of nitric oxide (NO) induced

inhibition of mitochondria and demyelination can produce a virtual state of hypoxia and lactic acidosis. ASIC1 is activated by this subsequent drop in pH and further sensitised by the presence of NO (26). ASIC1 activation leads to increased intracellular Na^+ and Ca^{2+} concentration and triggers injurious cell signalling cascades, the net result of which is protein lysis, loss of the cellular cytoskeleton, and axonal loss (Figure 1.1).

Not only is ASIC active under the acidotic conditions found during CNS inflammation, but it has also been found to be highly expressed white matter axons and oligodendrocytes in acute MS lesions, compared to control specimens (25). Therefore, blockade of ASIC has been explored as a neuroprotective target in experimental models and in early clinical studies.

Since the identification of ASIC in 1997 (27), it has been known to be blocked by amiloride, a licensed diuretic in clinical use in the UK (28). Amiloride was found to be significantly neuro- and myelo-protective within in-vitro studies and in experimental autoimmune encephalomyelitis (EAE), an animal model of MS (18, 25). This was supported by results of a pilot longitudinal crossover study, which used surrogate MRI markers of neurodegeneration, to examine the neuroprotective efficacy of amiloride in patients with PPMS (29). In PPMS a significant reduction in normalized annual rate of whole brain volume change during the treatment phase, compared to the pre-treatment phase ($p=0.018$ corrected), was observed.

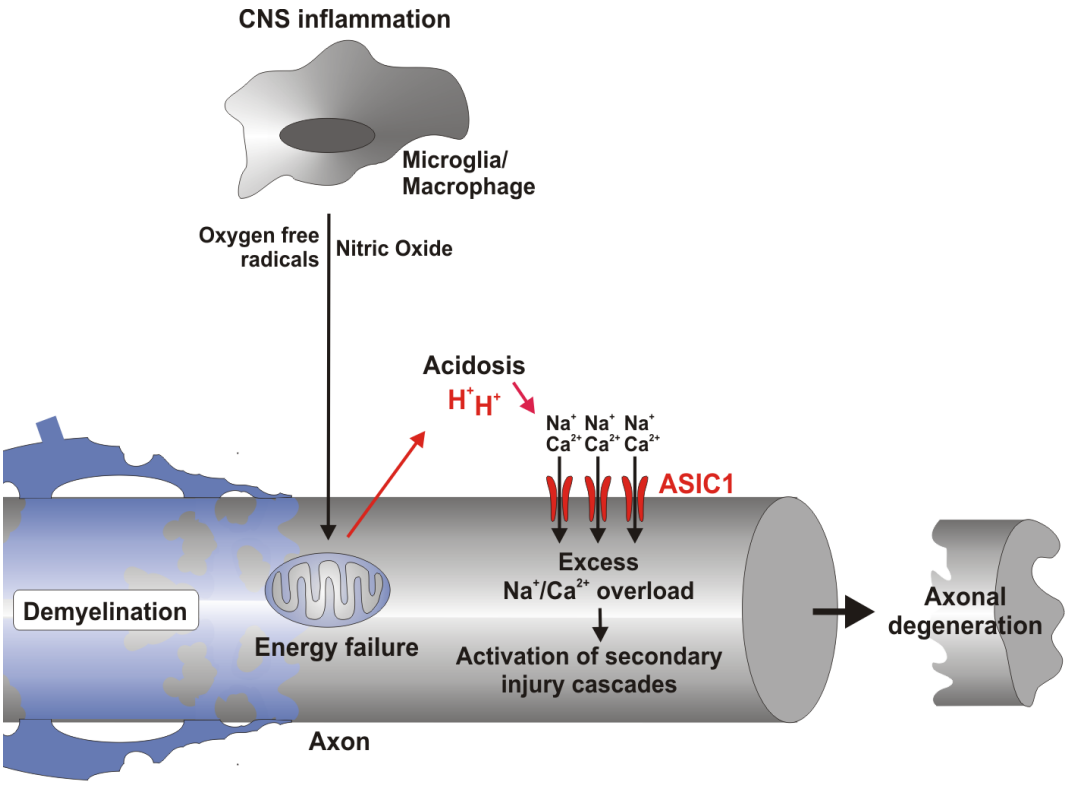

Fig 1.1 Schematic demonstrating the basic science that due to inflammation there is a combined state of virtual tissue hypoxia (mitochondrial inhibition) that leads to tissue acidosis. This in turn activates the abnormally expressed ASIC channel found on axons and oligodendrocytes. The consequent channel activation leads to the influx of injurious Na+ and Ca2+ and activation of secondary injury cascades.

1.3 Challenges in trial paradigms in MS

Phase 2, proof of concept trials in multiple sclerosis examining neuroprotection are challenging. Disability in multiple sclerosis accrues slowly in the majority of patients. Therefore, studies examining neuroprotective therapies can be protracted and expensive. Efficiencies can be gained by using surrogate markers of disability, such as MRI measures of brain atrophy. Nevertheless, MRI studies often require relatively long duration and large participant numbers and lack pathological specificity as they can be confounded by active inflammatory swelling, reducing the certainty of brain atrophy measurements (2, 30)

1.4 Optic Neuritis

Optic neuritis (ON) is a common precursor to the development of multiple sclerosis with approximately 50% of patients developing multiple sclerosis within 10 years of presentation with ON (31). The presence of hyperintense white matter lesions on T2 weighted MRI at diagnosis of optic neuritis increases the probability of developing MS substantially, with 70 % of those with one or more lesions developing MS at 15 years compared to only 25% of those who had no lesions at baseline (32). In addition, 70% of patients with multiple sclerosis will show evidence of optic nerve involvement over time (33). Pathologically, ON shows inflammatory demyelination and associated axonal loss, which is common to that observed in other white matter structures in multiple sclerosis (34). This means that translational research conducted on patients with optic neuritis is likely to be applicable to the wider patient group affected by multiple sclerosis.

1.4.1 Clinical features of ON

Diagnosis of ON is largely clinical. Patients typically present with painful visual loss that progresses for a maximum of two weeks and then recovers over the following 2-6 weeks, with further prolonged recovery of up to a year (35). Diagnosis is based on a combination of some or all of several key clinical features. These include pain on eye movement, sub-acute reduction in visual acuity over hours or days, presence of a central or paracentral visual field defect, presence of a relative afferent pupillary defect, and either a swollen or normal appearing optic disc with an absence of pallor in the acute phase (36).

The optic neuritis treatment trial (ONTT) was a landmark study examining the effect of corticosteroid administration in ON in 448 patients with acute ON, which reported in 1993 that whilst there was a slight improvement in the IV methylprednisolone group at 6 months (37), this effect disappeared at 12 months (38). This large cohort of ON patients improved our understanding of the clinical course and range of the disease, and range of snellen visual acuities at onset from 6/6 to no perception of light (though this was a very small group of 3.1%), with 92% of patients having pain at presentation (87% of those having an association between pain and eye movement), and the typical patient being female (77.2%) and caucasian (85%).

1.4.1.1 Atypical ON

Since the ONTT the concept of typical and atypical ON has emerged. Prevalence of aytpical ON amongst ON cohorts is highly variable depending on the cohort presented. One recent study from an ethnically diverse quaternary referral centre in London found an incidence as high as 10% in a series of 86 new onset ON (39). In a more regional setting the incidence is likely to be lower. Atypical optic neuritis is again determined on clinical grounds, and presenting clinical features that should alert the clinician to an atypical optic neuropathy include (40);

- Optic atrophy on presentation without previous ON or MS
- Severe optic disc oedema with vitreous reaction
- Optic disc haemorrhage
- Bilateral loss of vision - simultaneous or sequential within 4 weeks
- Previous history of neoplasia
- African, African-American or Afro-Caribbean patients with vision <6/12 and no early recovery
- Loss of vision to no perception of light with no early recovery

- Painless loss of vision to <6/60 with no early recovery
- Severe or persistent pain for >2 weeks since onset
- Visual loss progressing for >2weeks since onset of visual symptoms
- Lack of any recovery >3 weeks after onset of visual symptoms
- Worsening of vision after withdrawal of corticosteroids

The importance of identifying atypical ON is that unlike typical ON, such patients are likely to have a steroid dependent aetiology as opposed to typical ON where the ONTT and others (35, 41) have shown no benefit from steroid use. In addition, rarely, some infectious conditions such as syphilis, Lyme disease and Bartonella may also present with an optic neuropathy that is usually distinguishable from, but can mimic ON(42).

Steroid-dependent, autoimmune inflammatory conditions other than MS that can present with ON include Sarcoidosis, Lupus, and Neuromyelitis optica (NMO), or the non-specific chronic relapsing auto-immune optic neuropathy (CRION) (43). Of these NMO can currently be diagnosed with a sensitivity of 76% and specificity of 99.8% by aquaporin-4 antibody detection on a cell-based assay (44). In other conditions, particularly CRION, the clinical course of an atypical ON is such that the diagnosis may not be discriminated from a typical ON until after a poor recovery of vision in the initial weeks after ON. Such entities present challenges for recruitment to clinical trials in ON and it should be noted that both CRION and aquaporin-4 antibodies were both described after the ONTT was performed.

1.4.2 Neuroprotective clinical trials in ON

Despite these challenges, clinical trial paradigms examining acute inflammatory optic neuritis may help overcome some of the barriers of phase II trials in MS by efficiently demonstrating a 'proof of concept' neuroprotective benefit for re-purposed or novel therapies. Whilst there are no therapeutic strategies that have been shown to improve the visual outcome in optic neuritis, since the inception of the study described in this thesis, a number of groups have examined neuroprotective agents using non visual outcome measures (23, 45, 46). The increasing interest in examining neuroprotective strategies in ON is in part due to the unique modalities it affords to study the structural and functional changes in the CNS during and following inflammation (47).

The retinal nerve fibre layer (RNFL) is a major site of axonal loss after optic neuritis (48). Recent advances in retinal imaging allow accurate in vivo estimates of RNFL thickness, with the use of scanning laser polarimetry and optical coherence tomography. Indeed, since the inception of the study described in this thesis, RNFL measurement has been employed in neuroprotective trial frameworks (Table 1.1) (23, 45, 49) allowing neurodegeneration to be quantified in vivo both sensitively and longitudinally within a 6 month timeframe (50, 51). Thus, optic neuritis affords the opportunity to accurately and efficiently assess the impact of neuroprotective strategies in inflammatory CNS disease.

These unique imaging modalities afforded by studying the eye in ON, can be complemented with brain imaging to assess the impact of interventions on the posterior visual pathways, and moreover, longitudinal study of both aspects of the visual system can increase our understanding of the subsequent impact of neurodegeneration in the retina, and on the brain structures to which they send afferent neural connections.

Citation	Drug	Time to recruitment	Primary Outcome measure	N	Result
Tasikiri et al 2012	Simvastatin 80mg	28 days	Arden grating contrast sensitivity	64	Trend for improvement in POC, (p 0.06) improvement in SOC (PVEP p 0.01)
Esfahani et al 2012	Memantine 5mg then 10mg	8 days	OCT pRNFL (raw value at 3 months)	60	Significantly better POC (p0.01)
Suhs et al	Erythropoietin 33,000 IU	10 days	OCT pRNFL (change within affected eye)	40	Significantly better POC (p0.0357)
Cadavid et al 2015	Anti-lingo-1 100mg/kg	28 days	PVEP latency	82	No significant effect (p 0.33)
Raftopoulos et al. 2016	Phenytoin 6mg/kg then 4mg/kg	14 days	OCT pRNFL (change from baseline fellow eye)	86	Significantly better POC (p0.021)

Table 1.1 Recent clinical trials in ON (POC = primary outcome measure, SOC secondary outcome measure, OCT = optical coherence tomography, PVEP = pattern derived visually evocked potential, pRNFL = peripapillary RNFL)

1.5 Visual system

A key concept in this thesis, is the interaction between changes in the anterior visual system as measured by retinal imaging, and changes in the posterior visual system detected on non-conventional MRI. Thus a brief overview of the physiology and anatomy of the visual system follows.

Conceptually the visual system can be divided into two parts - the pre-synaptic anterior visual system, and the post-synaptic posterior visual system. The pre-synaptic anterior visual system comprises the neurosensory retina, the optic nerve, optic chiasm, optic tracts and lateral geniculate nucleus (LGN) of the thalamus. The posterior visual system, contains the geniculostriate axons of the optic radiations. These arise from the LGN and take afferent signals to the visual cortex, synapsing in layer 4 the primary visual cortex (also termed, V1 or striate cortex), other early visual areas V2 and V3, and from there into the higher visual areas.

1.5.1 Retina

The outer retina contains rod and cone photoreceptors. In these cells phototransduction occurs. Photoreceptor cell bodies synapse with bipolar cells at the outer nuclear layer. Bipolar cells are the first order neurons of the visual system (52). Bipolar cells can either depolarise (ON bipolar cells) or hyperpolarise (OFF bipolar cells) in response to loss of GABA release from photoreceptors when phototransduction occurs. Bipolar cells synapse with retinal ganglion cells (RGCs), the neurons whose axons go on to form the retinal nerve fibre layer (RNFL) (Figure 1.2).

Figure 1.2. Schematic of retinal layers. from Syc et al, Brain 2012.

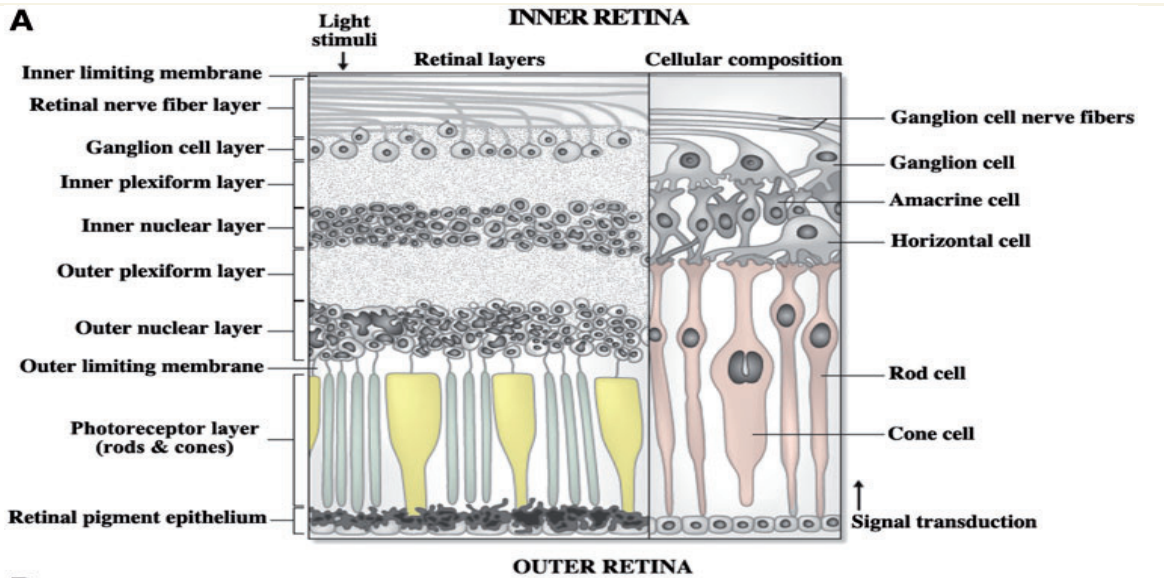

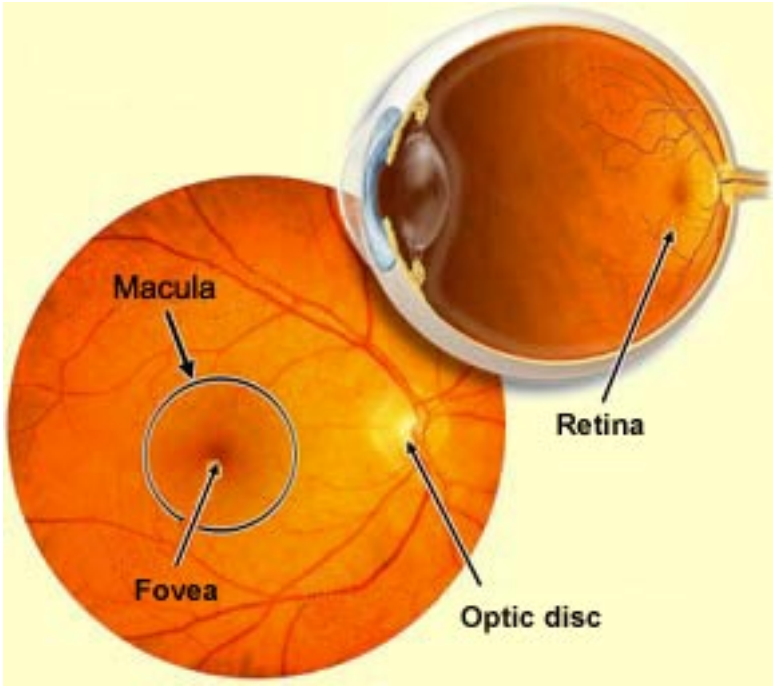

Figure 1.3. The position of the retina, fovea and optic disc within the eyeball. From www.thebrain.mcgill.ca

The centre of the retina contains the fovea and the surrounding macula. In this area, light rays are focused by the cornea and lens and is the area of highest visual acuity, and has several anatomical features that enhance this function. At the fovea photoreceptors are exclusively cones. Phototransduction in cones occurs in bright (photopic) conditions, and the three types of cones each have an opsin molecule of differing sensitivity to wavelengths along the visible spectrum (blue, short wavelength S-cones, green, medium wavelength M-cones, and Red, long wavelength L-cones), enabling colour vision (53). At the fovea there is a high ratio of photoreceptor to RGC, peaking at 1:1 meaning that visual information in this area is transmitted at high spatial frequency in small receptive fields. Architecturally, the RCG axons are displaced from the centre of the fovea, reducing any impedence to light striking the photoreceptors, resulting in a “hump” of RCG cells collected in a doughnut around the fovea to accommodate the high cone: RGC ratio (53).

By contrast, the opsin molecule in rods is more sensitive to phototransduction in scotopic (dark) conditions with peak activity in rhodopson is in the middle of the visible light wavelength range (500nm) (54). Rods are more prominent in the peripheral retina and multiple Rods are organised into large receptive fields - meaning that the receptive field can be simulated easily but encodes very low visual acuity.

Further specialisation is found in the types of RGC cells that predominantly receive input from different photoreceptors. The small central, cone based, receptive fields service small "midget" RGCs. These cells are relatively slow signal transducers, have a high concentration in the fovea. This makes them sensitive to high spatial frequencies, colour vision, and texture. "Parasol" cells are more frequent in the peripheral retina and predominantly synapse with rods. They are organised in large receptive fields with input from numerous photoreceptors. They are more sensitive to

high temporal frequency visual input such as fast motion and fast flicker, and are less sensitive to colour and high spatial frequencies. This functional separation that begins in the retina continues to be marked in the lateral geniculate nucleus with parvo and magnocellular cell types synapsing with midget and parasol cells respectively (53, 55).

In addition to the vertical transmission of photoreceptor signalling, the receptive fields are also determined by horizontal synapsing from amacrine and horizontal cells (53). The cell bodies of horizontal, amacrine and bipolar cells are grouped in the inner nuclear layer in the retina, underneath the cell bodies of the RGCs, the unmyelinated axons of which forming the RNFL.

The RNFL fibres from RGCs gather at the optic disc, pierce the sclera and become myelinated through the lamina cribrosa. The optic nerve then traverses posteriorly exiting the orbit at the optic canal, and moving superomedially where the right and left optic nerve form the optic chiasm (56).

Throughout this portion of the visual system, and indeed up to V1, the visual system maintains a strict topographic or “retinotopic” arrangement. The visual field is quartered along a vertical and horizonal meridian, and within these qaudrants RCGs representing adjacent receptive fields traverse the optic nerve together. At the chiasm, this is enforced by decussation of approximately 50% of the RNFL fibres. The nasal fibres of each eye cross to the contralateral optic tract (the portion of white matter tract between the chiasm and the LGN) meaning that the neurones sensitive left and right halves of the visual field from each eye travel to the contralateral visual cortex together (52).

The LGN are a bilateral pair of nuclei situated at the undersurface of the pulvinar of the thalamus. The majority of the axons from the optic nerve synapse at the LGN (the retinogeniculate pathway). The LGN is arranged in 6 layers, with 3 layers receiving input from the ipsilateral eye's fibres, and 3 layers receiving input from the contralateral eye's crossed fibres. The arrangement of the synapses from the retina is such that within the layers the retinotopic map of the corresponding hemi-retina is maintained. The ventral two layers form the magnocellular layers with input from, primarily the large parasol cells, and the dorsal 4 layers form the parvocellular layers with input from the midget cells (57). Of note, studies of the LGN in MS have shown an increased susceptibility of the parvocellular layers to neurodegeneration (58). A third class of LGN efferent cell - the koniocellular cell type, is less well understood but thought to have a key role in colour vision, as it receives input exclusively from midget RGC cells specific to S cone cells (57, 59).

Posterior to the LGN, the optic radiations carry fibres between the LGN and the V1 (56). Anatomically, the fibres split between those associated with the superior and inferior field of vision, (the lateral and medial portions of the LGN respectively). The fibres from the lateral aspect of the LGN loop anteriorly round the temporal horn of the lateral ventricle before turning posteriorly along the retrolenticular tract of the internal capsule. The fibres from the medial aspect of the LGN have a more direct lateral orientation on exiting the LGN before turning posteriorly along the superior portion of the retrolenticular tract. Fibers from the retrolenticular tract then turn inwards towards V1 cortex.

V1 (Broadmann's area 17) is a highly dense area of cortex, with c. 350 million neurons processing the input from the c. 2.4 million RGC cells combined that exit the eye (52). V1 is arranged around the calcarine fissure and maintains the retinotopic map, with the left and right V1 corresponding to the contralateral visual field

(ipsilateral temporal retina, and contralateral nasal retina). It can be identified by a thick band of myelin at the 4th of its 6th layer (60), lending the term “striate” cortex to V1. Central visual field information from the fovea is processed at the occipital pole, and moving anteriorly along the calcarine fissure areas that represent increasingly peripheral parts of visual field. In line with the high number of RCG cells that supply the central visual field, a large proportion of V1 serves the central portion of visual field. The input from the LGN enters V1 at level 4, at this level ocular dominance is maintained, with separate columns representing the same visuo-spatial area of input from each eye. In the superficial and deeper layers of V1 cells are binocularly stimulated. Visual processing continues from area V1 to adjacent areas V2 and V3. Allocating specific functions to these regions has proven challenging and they combine to process visual inputs to discriminate information on orientation, direction, colour, spatial frequency and assimilating signals from on and off receptive fields, and from magno and parvocellular inputs (61).

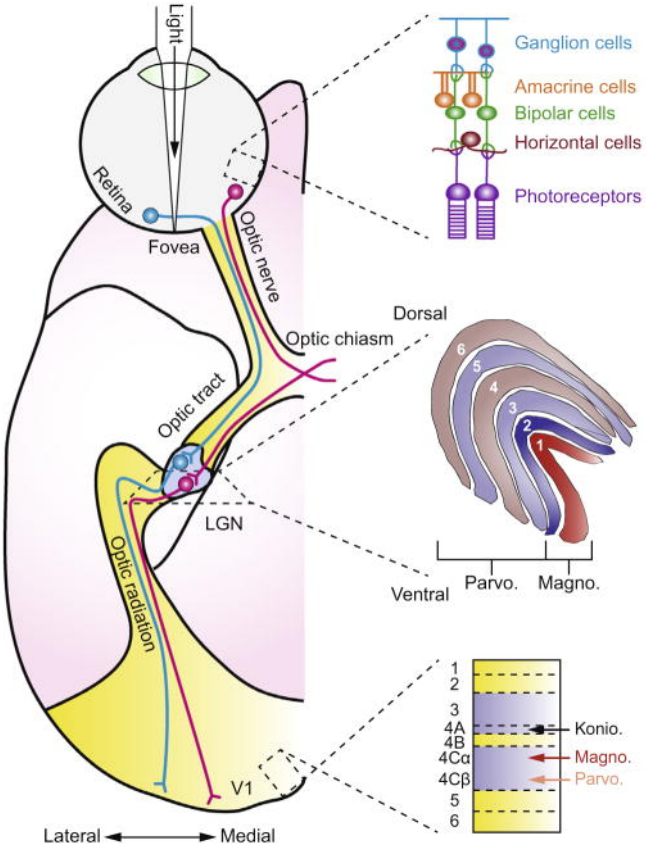

Figure 1.3. Schematic of the visual system of the macaque monkey, which mirrors that of humans as described. This is a ventral view of the right hemisphere. Visual information is transmitted from photoreceptors the the RGCs and RNFL via bipolar cells (see also figure 1.3), and fibers from both ON join at the optic chaism and synapse in the LGN, where in separate layers arranged retinotopicaly. From there signal are carried to V1 in the primary visual cortex, most fibers synapse at layer 4. (from Jeffries et al, J Physiol Paris, 2014)

1.5.2 Higher visual processing

Processing visual information beyond the visual cortex is complex and the subject of an evolving debate. Since the late 20th century, visual processing beyond V3 has been postulated occur in a two visual system model (62), based on research in primates and by neuropsychological testing of subjects with known circumscribed lesions in candidate visual areas. In this model the “dorsal” stream proceeds anatomically from V5 and the middle- and supero-temporal regions, through multiple parietal regions to the dorsal aspect of the prefrontal cortex (63). The ventral stream begins at V4 and from there continues along the inferior temporal lobes (64).

The two visual system model separates the two streams both anatomically and functionally. The ventral stream is the processing pathway to visually recognise

targets and goals (the “what” stream) and the dorsal stream processes visual information for action within the visual environment and movement towards, or away from, those goals (the “how?” stream). This model has provided impetus for subsequent research, and has been re-examined in the era of in vivo functional MRI (fMRI). Such research has suggested that the true dynamics of higher visual processing may be more complex than the two visual system model allows.

One recent study for example, using a large resting state fMRI dataset from the human connectome project (65) has identified three streams based on connectivity patterns - the dorsal stream was maintained, however the ventral stream is broken down into the ventral stream (ventral aspect of the temporal lobe) and a lateral stream (lateral aspect of the temporal lobe). This three-stream model had been suggested by other recent groups, who cite the duplication of facial and limb recognition centres within the traditional ventral stream (66). The precise functional separation of the two ventral streams requires further elucidation, however proponents suggest lateral stream has a more prominent role in integrating vision with other sensory inputs such as tactile sensation and language, and in tandem with this, the lateral stream appears to be unique to the human visual processing system and is not identified in primates. The ventral stream is held to have a role primarily in vision for memory (66).

In the dorsal stream, other authors point to evidence of separation. They find that the dorsomedial stream uses visual input from primary visual areas to recognise self motion and object motion, whereas the dorsolateral stream uses the same input to continuously monitor the location of stationary and moving objects while the self moves around, to allow for grasping of such objects even if the self is in motion (67). Not only do the authors point to multiple networks within the dorsal visual stream, but they also make the case for interaction between the two streams, and more broadly

promote the idea that the same cortical areas are not specific to one functional property, but encode multiple functional aspects depending on the situation and environment. This concept is reiterated by others who show that in task-based fMRI, the interaction between the frontoparietal complex (dorsal stream) and the occipitotemporal complex (ventral stream) is no only present, but dynamic in response to the demands of changes in the task paradigm (68).

Thus, whilst yet to be fully resolved, it is clear that visual processing beyond the occipital cortex involves multiple cortical and white matter regions. Human visual processing displays a dynamic and adaptable arrangement to suit the diverse range of visual environments and tasks that retinal information is used for. Therefore, studies focusing on posterior visual pathways and plasticity in response to an insult such as ON, may benefit from looking beyond the primary visual areas when assessing for brain changes over time and in response to neuroprotective agents.

1.6 Studying neurodegeneration, neuroprotection, and neuroplasticity in the visual system

From the above, it emerges that studying optic neuritis affords several opportunities to investigate key questions in MS and visual neuroscience. The visual system presents an anatomically well defined system that can be tested with direct and translatable clinical measures of function, in the form of visual acuity, low contrast visual acuity and colour vision.

In the pre-synaptic, anterior visual pathway, direct retinal imaging can be obtained from OCT and GDx as biomarkers of neurodegeneration. Furthermore, objective

electrophysiological measures of optic nerve function in the form of visually evoked potentials, and macular retinal function in the form of pattern electroretinogram can be applied to the anterior visual system. These techniques can be non-invasively applied to provide outcomes for clinical trials of neuroprotection.

Proof of concept of neuroprotective studies in MS are a key unmet need in clinical research in the disease, and assessing neuroprotective treatments in optic neuritis can hasten our understanding of the effectiveness of neuroprotective treatments applied to MS. ASIC has been identified from basic science as a key target of interest, which can be blockaded by the licenced drug amiloride.

Clinical trial outcomes assessing the anterior visual pathway can be supported by assessments of the post-synaptic white and grey matter structures in the cortical visual pathways. In the context of neurodegeneration in the anterior visual pathway, two key areas of exploration in the posterior visual pathways emerge.

The first is whether findings of neurodegeneration, or indeed a neuroprotective effect, in the anterior visual pathways have consequential findings in the posterior visual pathways. One region of the posterior visual pathways in which this can be addressed is the optic radiations (OR). Analysis of the OR can assess whether loss of input to the LGN from neurodegeneration in the optic nerve, is reflected on measures of white matter integrity in the optic radiations (OR). Such measures of white matter integrity can be explored using the quantitative MRI technique of diffusion tensor imaging.

The second key area that can be addressed is that of neuroplasticity in the visual system in response to deafferentation from the anterior visual pathway. As we have seen, there is a large neural network in the visual cortex that receives input from the

LGN. Thus, the question of whether this large neuronal area can re-organise to enhance recovery from ON is a pertinent one. Potential mechanisms of neuroplasticity are manifold and include axonal sprouting, dendritic branchings with synaptogenesis and neurogenesis in the grey matter (69). Again, non-conventional fMRI can be used to probe changes in grey matter functional connectivity.

1.7 Thesis Aims

1.7.1 Research Questions

This thesis aims to address the following research questions;

Is ASIC channel blockade via amiloride neuroprotective in ON?

Can our understanding of the temporal evolution of retinal changes following ON be enhanced by assessing OCT longitudinally, how do these changes influence visual outcomes, and this ameliorated by amiloride?

Is transynaptic neurodegeneration present in the posterior visual pathways following ON and this ameliorated by amiloride?

Is there evidence of neuroplasticity in the visual cortex following ON, and is this influenced by amiloride?

1.7.2 Research Aims

The objective of each experimental chapter is as follows;

Chapter 2 To report the study design, and results of a phase II, randomised, placebo controlled clinical trial of amiloride in ON

Chapter 3 To report detailed longitudinal analysis of the retinal layers in segmented macular OCT collected in the clinical trial, to assess the effect of amiloride on changes in these layers, and to assess which of these individual layers has the greatest influence on vision following ON.

Chapter 4 To assess whether transynaptic neurodegeneration in the OR is evident on analysis of the whole brain and region of interest (ROI), using the quantitative MRI technique of diffusion tensor imaging (DTI) derived measures of white matter integrity, and assess whether this is influenced by amiloride.

Chapter 5 To assess whether neuroplasticity can be demonstrated following ON on resting state functional MRI (RSfMRI), and to assess whether these changes are adaptive or maladaptive, based on their relationship to visual measures, and OCT-derived measures of neurodegeneration.

2 Chapter 2. The Amiloride Clinical Trial in Optic Neuritis

In this chapter the methods and results of a phase II randomised controlled trial of amiloride in ON are presented.

2.1 Introduction

In chapter 1, the pre-clinical and early clinical evidence supporting the potential for amiloride blockade of the ASIC1 channel as a neuro-protective mechanism was presented. Following on from this, a phase II proof-of-concept randomised controlled trial of amiloride in ON was performed - the amiloride clinical trial in optic neuritis (ACTION).

2.1.1 Outcome measures

A variety of outcome measures were included in the trial and are reported in this chapter, a brief description and rationale for the use of each is given, prior to reporting on the study design and outcomes.

2.1.2 Primary outcome measure

2.1.2.1 Scanning laser polarimetry (GDx)

The primary outcome measure selected for the trial was peri-papillary RNFL (pRNFL) as measured by GDx. GDx is used to measure the thickness of the peri-papilliary retinal nerve fibre layer (pRNFL) inferred from the phase shift occuring in a polarised light reflected back to a sensor from the retina. The retinal nerve fibre layer is the only layer in the retina that is birefringent to polarised light (70). Therefore, light that

has been reflected back to the scanner has passed through the RNFL twice. The degree of phase shift of two orthogonal beams of polarised light can then be used to calculate the thickness of the RNFL. This calculation must take account of the cornea and to a lesser extent the lens in the anterior segment of the eye, which are also birefringent to polarised light due to the parallel arrangement of collagen fibers in these structures. This can be compensated for via one of two methods; variable corneal compensation (VCC) or the more recently developed enhanced corneal compensation (ECC) (71). Both VCC and ECC were performed in this trial. Previously published literature on GDx in ON has been carried out on VCC, however ECC appears to have a closer structure-function correlate in glaucoma (72), hence, using this modality has potential added value and novelty in the field of GDx and ON.

In cross-sectional studies, the pRNFL on GDx has been shown following ON to be a mean of between 11-22μm less in eyes affected by ON, compared to unaffected fellow eyes and control eyes (50, 73, 74). Longitudinally, thinning of GDx pRNFL is present in 60% of eyes at 3 months from onset of ON (75). Thinning of pRNFL on GDx has been shown to correlate with visual function following ON(74).

GDx was selected as the primary outcome measure because the available evidence at the time of conception of the trial meant it afforded the most efficient powering of a phase II trial in ON. GDx was performed using the Carl Zeiss GDx Pro with ECC. An average of three readings were taken for each measurement in the study. All the scans were performed by me, and were deemed to be of adequate quality if they had a quality score of ≥ 7, and had a uniform brightness across the scan, consistent with previous studies (74)

2.1.3 Secondary outcome measures

2.1.3.1 Optical coherence tomography (OCT)

OCT uses near infra-red light (wavelength 870 nm in Heidelberg spectralis) to build up a series of "A" scans (single points) to build up a cross-sectional "B" scan or "slice" of the retina – analogous to ultrasound. The signal in OCT is composed of measuring the delay in reflectance of an infra-red beam low coherence light shone on the retina, when compared to a reference beam. Spectral domain OCT collects each A-scan signal as a single spectrum covering all the depths of the A-scan point, and uses a fourier transform to convert into a time domain signal (76). Previous time domain systems required the position of a reference mirror to be moved to probe different depths in each A-scan (77). By obviating the need for this, a spectral domain system is much quicker at scanning, allowing innovations such as repeat scans and increased signal to noise ratio, and better quality images. The Heidelberg spectralis employs automated real time (ART) meaning that the operator can determine how many times each B-scan will be repeated to improve signal to noise ratio.

pRNFL thinning on OCT in ON has been widely demonstrated both cross-sectionally (73, 78, 79) and longitudinally (36, 51, 80, 81). A meta-analysis of pRNFL in 956 eyes showed a mean difference of –20·38 μm (95% CI –22·86 to –17·91) compared to 1107 control eyes(82). Moreover, like GDx, OCT pRNFL has been shown to correlate with visual acuity (36, 81) and low contrast visual acuity (74, 78).

Adding OCT to the trial protocol as a secondary outcome measure allowed not only the potential validation of GDx findings at the pRNFL, but also enabled scanning of the macula, a feature not available on GDx. In this chapter, baseline data on

combined ganglion cell and inner plexiform layer (GCIPL) volume is presented along with total macular volume. The GCLIPL contains the cell bodies of retinal ganglion cells which are the cell bodies of axons that form the RNFL. Prior to conducting the trial, a number of cross-sectional studies had shown cross-sectionally that the GCIPL is thinned in patients with a history of ON (51, 83, 84). Thus, it was added as an exploratory secondary outcome measure. As will be seen later, in this chapter and in chapter 3, a number of studies have subsequently further explored this metric as a biomarker of neurodegeneration in ON.

For pRNFL OCT scans, high-resolution 3.5mm diameter peripapillary circle scans were acquired with a minimum automated real time (ART) setting of 30. For Macular scans a high resolution macular scan centred on the fovea, (19 supero-inferior slices, 200μm apart, ART 25) was chosen for analysis. This allowed detailed analysis of the central 3mm radius annular zone around the fovea - anatomically this contains the bulk of the ganglion cell bodies and contains those supplying the fovea - thus a priori it can be anticipated they are the most closely responsible for the main functional correlations - visual acuity and low contrast visual acuity. B-scans were segmented using Heidelberg Heyex 6.0 and a volumetric measurements for retinal layers were derived from the 3mm annular area (figure 2.2). Additional quality assurance parameters were applied in line with published consensus OSCAR-IB criteria for quality control of data (85). The majority of OCT scans were collected by me and a minority by ophthalmic imaging staff who had been trained in the standard operating procedure for the ACTION trial.

The segmentation software employed in this data has been used in recent publications (86) and has also been shown to have good intra-class correlation (ICC) coefficient for all layers with the exception of ONL (87). In the ACTION trial, the standard operating procedure advised repeated measurements for OCT scans

wherever possible. This was done in order to take a mean of two measurements to increase signal-to-noise ratio and get closer to the true mean of the individual subject timepoint.

Figure 2.1 A patient presenting with swelling of the optic nerve in the affected (right) eye (A on OCT, C on GDx). Here OCT measures swelling of the affected eye compared to the unaffected eye (B, E). In GDx, as it relies on integrity of RNFL rather than volume of tissue for measurement, the pRNFL thickness around the discs of the affected eye is similar to the unaffected eye- GDX pRNFL is shown in D – affected eye in green and unaffected eye in purple

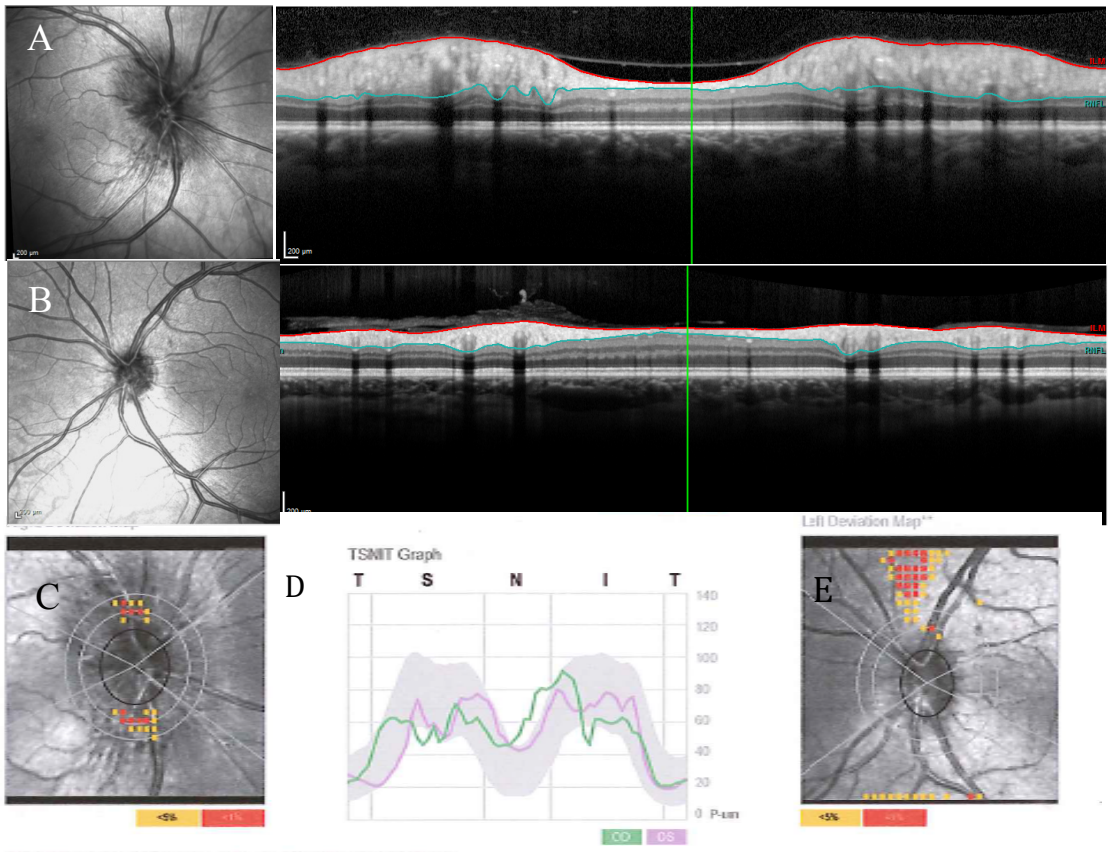

Figure 2.2. Macular OCT scanning in the ACTION trial High resolution OCT scan of the macula. (A) Illustrates the position of the 19 B-scans used to formulate the volumetric analysis. (B) shows the 3mm parafoveal annular area that is used for the volumetric analysis and a heat map of GCL thickness generated from the GCL volumes. (C) illustrates the segmentation of the macular layers (to the right of the picture, the left remains unmarked to illustrate the definition between layers). RNFL- retinal nerve fibre layer (macular), GCL ganglion cell layer, IPL – inner plexiform layer, INL – inner nuclear layer, OPL – outer plexiform layer, ONL – outer nuclear layer (the nuclei of the photoreceptors). IS/OS – outer retina, comprised of the inner and outer segments of the photoreceptors and the retinal pigment epithelium.

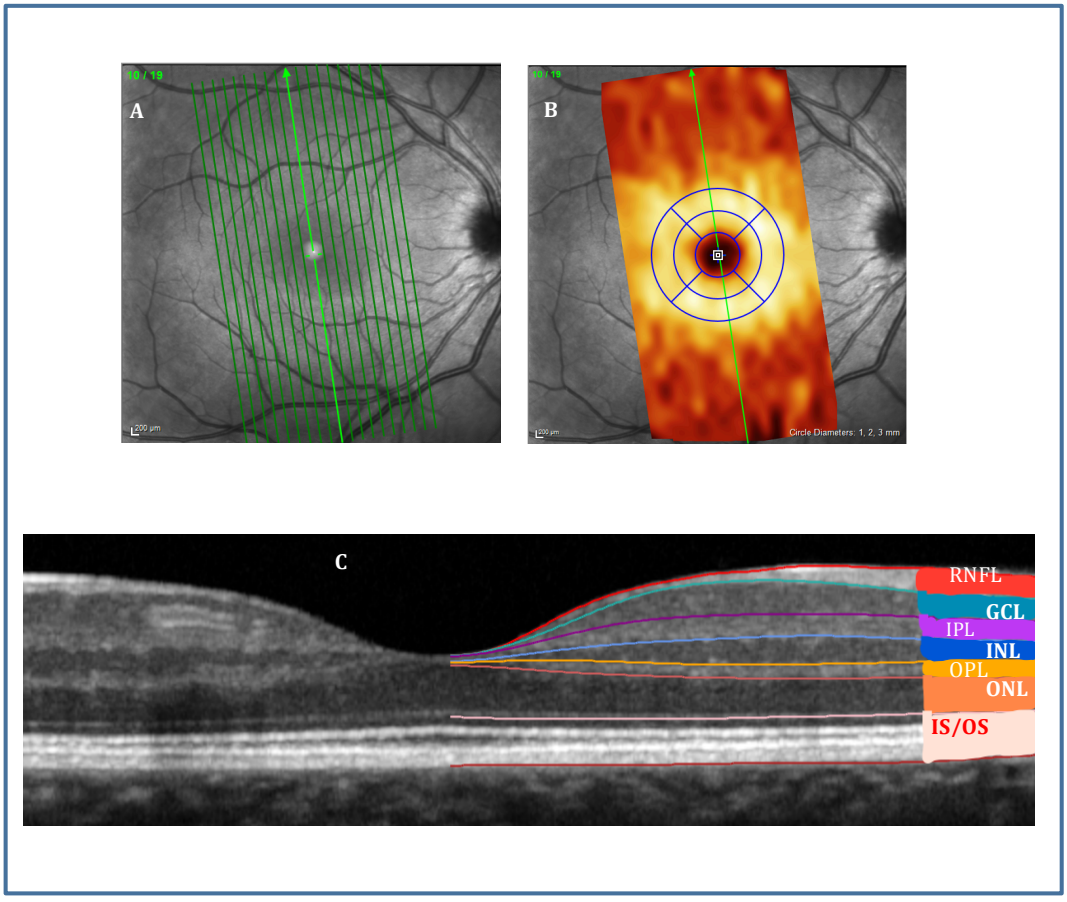

2.1.3.2 High contrast letter acuity (HCVA)

HCVA is the gold standard for most clinical trials in ophthalmology. In snellen acuity the numerator denotes the distance the subject is away from the letter chart, and the denominator refers to which line of the chart the subject can see. If the subject can

see 6/6 Then at 6 metres, the subject can see letters that subtend 5 minutes of arc (88), which is recognised as a normal high contrast acuity. Use of the traditional snellen chart creates a number of issues in clinical research, primarily that it creates categorical variables rather than continuous variables for subsequent multivariate comparisons, in addition to crowding of letters at smaller optotypes complicating the task of viewing small letters for subjects. Early treatment of diabetic retinopathy study (ETDRS) charts (89) overcomes these difficulties and allow a continuous variable of letter score to be applied to clinical data (35 letters = 6/60 snellen, 85 letters = 6/6 snellen).

In ON however, the usefulness of HVCA as an outcome is limited as most patients will recover to a good standard of HCVA with almost 70% of patients achieving 6/6 snellen vision and over 90% achieving greater than 6/12 vision at one year (38). Despite this, many patients remain symptomatic of visual problems. Further testing of vision can be achieved with additional methods including low contrast acuity, visual fields and colour vision. These can elucidate abnormalities and variability amongst ON patients, in keeping with ongoing symptoms, including those with 6/6 snellen acuity, and provide useful adjuncts to clinical trial design and assessments of structural biomarkers (90).

2.1.3.3 Low contrast visual acuity (LCVA).

Reduced contrast sensitivity post ON in eyes with normal high contrast acuity was demonstrated prior to the advent of retinal imaging (91), and was included in the composite primary outcome measure of the ONTT using Pelli-Robson charts (37).

Subsequently, due to lack of availability of Pelli-Robson charts for further MS trials in the late 1990's, Sloan low contrast letter charts were adopted for use in MS trials. Sloan charts are similar to ETDRS charts but have grey letters of increasingly faint appearance on separate charts of different contrast (separately 100%, 5%, 2.5%, 1.25% and 0.6% contrast charts are available) (92). Due to their use in MS trials of disease modifying agents as secondary outcome measures (93, 94) Sloan 2.5% and 1.25% charts were included in a number of studies in ON and have been found to correlate with pRNFL on OCT (74, 78), GDx (74) and GCLIP thickness on OCT (51, 84)

In the ACTION trial, HCVA was assessed for each eye in turn using a retro-illuminated early treatment of diabetic retinopathy (ETDRS) letter chart at 4 meters, and automatically assigned a score of 30 letters if 5 letters were seen at 4 meters (6/60 snellen equivalent) plus the number of letters read at 4 metres, with a maximum score of 100 (6/3 snellen equivalent). The chart was moved to 1 meter if the participant could not identify any letters at 4 metres. and the participant was assigned a score of 0-30 letters. Testing was performed with patients own refraction and with a pin-hole and the best letter score was used. Low contrast visual acuity was assessed using Sloan 1.25% and 2.5 % letter charts at 4 meters for each eye in turn with patient's own refraction.

Figure 2.3 ETDRS letter chart

2.1.3.4 Colour vision

Reduction in ability to discriminate colour is a key hallmark of optic nerve dysfunction and acute ON (95). Colour vision remains abnormal after recovery from ON (96). The Farnsworth Munsell 100 Hue test (FM-100) can be used to apply a continuous variable to dyschromatopsia in the form of the total error score (TES) (97). Whilst not designed to clinically assess acquired dyschromatopsia uni-ocularly, the FM-100 was an outcome measure in the ONTT (98) and confirmed that no clear pattern of red-green, or blue-yellow axis appears to be preferentially affected in ON(99). FM-100 error scores at baseline (within 32 days) and 3 months have also been shown to have a significant predictive value for pRNFL loss at 6 months (100).

For our trial, the FM-100 colour vision TES was acquired for each eye in turn using a standard illumination (97) on participants with vision of 6/60 or better at baseline and 6 months.

2.1.3.5 Visual Field

Visual field defects are an important clinical feature in diagnosis in ON, and like colour vision defects are heterogeneous and varied in severity (101). The Humphrey visual field analyser (HVF) is an automated perimeter which presents stimuli of different intensities to the subject, and by assessing scores across different stimuli points (74 different points in the visual field for a 30-2 30 degree protocol) the subject can be assigned a mean deviation (MD) score compared to a reference range corrected for age. A more negative MD indicates a more severely impaired visual field. Correlations post ON in pRNFL patients with severe pRNFL thinning (<75 μm) were shown in one paper (80), whilst another group have shown a strong exponential relationship between higher pRNFL thickness and HVF MD (102). Both findings suggest that for eyes with subtle loss of pRNFL, HVF lacks sensitivity in identifying functional impairment in milder ON cases. Moreover, performance of HVF demands a high degree of patient co-operation in pressing the button when stimuli are seen and this can be difficult for patients with ON, and particularly MS, to perform. A high degree of short and long term fluctuation has been demonstrated in patients who have recovered from ON (103). Nevertheless, HVF remains a translatable and extensively analysed outcome in ON, and uniquely amongst the visual tests in this trial gives an indication of peripheral retinal function.

In the ACTION trial visual fields were assessed using the Humphrey visual fields analyser using a 30-2 SITA protocol (104). Fixation losses, false negative and false positive rates of less than 33% were deemed of adequate quality (101).

2.1.3.6 Electrophysiology

2.1.3.7 Pattern stimulated visual evoked potentials (PVEP)

PVEP records the cortical (primarily V1) electroencephalographic activity in response to a checkerboard stimulus (105). Whilst PVEP requires the full visual pathway to be intact to be detected, it is relatively sensitive to pre-chiasmal abnormalities and relatively insensitive to post-chiasmal, cortical abnormalities. Thus PVEP provide a sensitive marker for optic nerve function. Characteristically, ON produces a delayed peak response (usually at 100ms - termed the P100) with relatively intact P100 amplitude. This delay typically improves from baseline over time, but remains persistently prolonged (106). This prolongation and subsequent improvement is thought to represent demyelination and remyelination of the optic nerve respectively (107), though ion channel re-organisation improving conduction in demyelinated segments of optic nerve may also contribute to this improvement. It should be noted that acutely, ON can produce a reduced amplitude with a less marked effect on latency of the P100, or indeed have an undetectable PVEP at presentation, postulated to be due to the effects of acute inflammation profoundly blocking conduction, rather than demyelination per se in the acute phase (108).

PVEP P100 time to peak has been correlated by some groups with pRNFL thickness in a mix of ON and MS patients (109), however other groups failed to find a significant correlation with P100 time to peak, despite finding a significant correlation with amplitude (81) 6 months after ON. These findings reflect the complex interplay between demyelination, remyelination and neurodegeneration in the optic nerve.

As ASIC was found to be expressed on oligodendrocytes and have a myeloprotective effect in animal models (25), inclusion of PVEP allows us not only to measure the effect of amiloride on a widely used clinical research tool in ON, but also to assess the effect of amiloride on de- and re-myelination following ON.

2.1.3.8 Pattern Electroretinogram (PERG)

PERG assesses retinal function at the macula, by stimulating with a reverse checkerboard pattern and recording the retinal biopotential via corneal or bulbar conjunctival electrodes (110). The early positive (P50) deflection of the PERG is thought to be primarily generated by outer retinal (photoreceptor) cells and the later, negative (N95) thought to be primarily derived from the RGCs. However, there is some crossover in that the p50 has been found to be reduced in amplitude and time to peak in optic nerve disorders. This is particularly the case in early ON (111), though reduced the N95 amplitude with relatively preserved P50 amplitude is generally the most characteristic feature of ON. N95 amplitude is taken as a peak-to-nadir measurement from the P50 peak as standard, thus reported N95 amplitudes incorporate P50 amplitude reductions.

In the context of ON the PERG can improve diagnostic certainty in that it can help exclude significant outer retinal dysfunction which could impact on PVEP recording, and can demonstrate RGC dysfunction (111). In the earliest ON OCT study PERG was found to correlate with pRNFL thickness both by GDx and OCT, (73), and has subsequently been found to correlate cross-sectionally with GCL volume on macular segmentation (112)

In the ACTION trial PVEP and PERG recordings were obtained according to published protocols from the international society for clinical electrophysiology of vision (ISCEV) (110, 113). Results from the 60’ check size are reported.

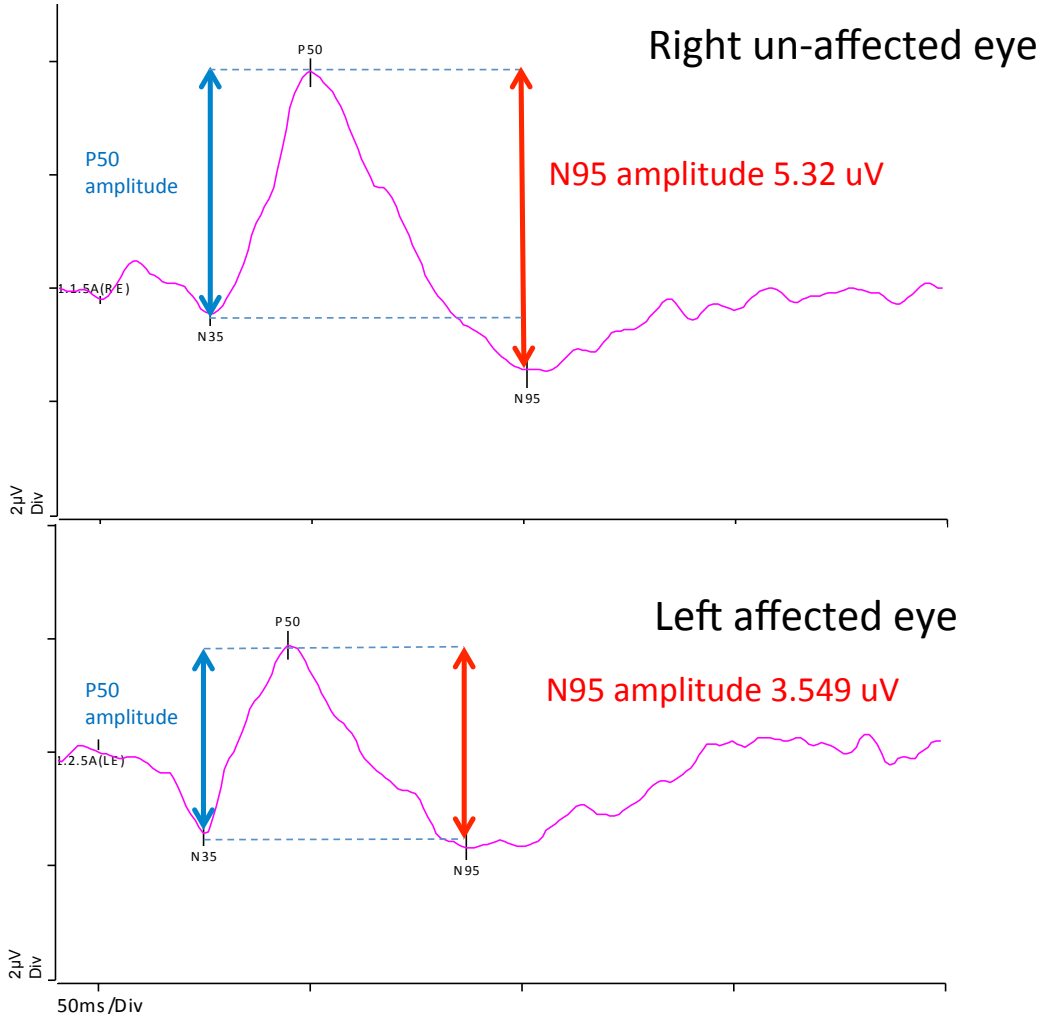

Figure 2.4. Example of PERG waveform in acute optic neuritis of the left eye, performed 11 days after onset of visual symptoms in a 38 year old female participant. As is typical in optic neuritis, the N95 amplitude is reduced primarily due to a muting of the N95 negative deflection and also partially from a reduction in p50 peak height and amplitude.

2.1.3.9 MRI

MRI for white matter lesion detection was obtained on a Siemens verio 3T MRI with a 32 channel head coil. Proton density (PD) and T_2 weighted images were obtained in 2 dimensional axial slices (0.9x0.9x1.1mm voxel size) from the same radio frequency pulse at different echo times (repetition time (TR) 10960ms, echo time (TE) 11ms proton density and 128ms T_2) (acquisition time = 5 mins 08 secs). In addition, fluid attenuation inverted recovery sequences (FLAIR) were obtained in 2 dimensional

axial slices (0.9x0.9x3 mm voxel size, repetition time 9000ms echo time 73ms) (acquisition time = 4mins 14 secs). All scans were reviewed by a neuro-radiologist (Wilhelm Kuker) for assessment of the presence of white matter lesions.

2.2 Trial Design for the Amiloride Clinical Trial in Optic Neuritis (ACTION trial)

We performed a randomised, parallel group, double blind, investigator led, placebo controlled trial. Participants were allocated on a 1:1 ratio to amiloride 10 mg once per day or placebo for 5 months duration of treatment. The primary outcome measure was difference in GDx-derived pRNFL thickness at 6 months compared to unaffected fellow eye at baseline. Secondary outcome measures were visual outcomes (visual acuity, LCVA, visual field), MRI and OCT measures at 0, 6 and 12 months, PVEP and PERG and colour vision at 0 and 6 months, with a further measure of GDx thickness at 12 months as a secondary outcome measure. The 12 month measurements were designed to ensure that any benefit from amiloride was sustained and to confirm the primary outcome measure. By using placebo treatment identical to amiloride, and blinding both the investigators and participants to treatment, bias was minimised.

All study procedures were conducted at the John Radcliffe Hospital site in Oxford, however recruitment of participants was from a network of hospitals throughout the south and south east of England.

All participants gave written informed consent in accordance with the declaration of Helsinki. The study was approved by the South Central Oxford B research ethics committee (reference: 13/SC/0022) and overseen by an independent data monitoring committee.

2.2.1 Inclusion and Exclusion criteria

2.2.1.1 Inclusion Criteria

- Participants with a first episode of unilateral ON
- Participants with an existing diagnosis of relapsing remitting MS and new onset of ON are eligible if they had:
    - ➔ Not had a previous episode of ON,
    - ➔ A duration of disease of ≤ 10years
    - ➔ An EDSS (Expanded Disability Status Scale) of ≤3.
    - ➔ No immune modulating treatment other than β-Interferon or glatiramer acetate at time of recruitment
- Able to be randomised within 28 days of onset of visual symptoms
- Visual acuity of ≤6/9
- Participant was willing and able to give informed consent for participation in the study and able to comply with study visits
- Male or Female, aged between18 – 55 years.
- Stable dose of current regular medication for at least 4 weeks prior to study entry.
- Female participants of child bearing potential had to be willing to use two effective methods of contraception (barrier methods, hormonal methods or abstinence) during the initial 5 month treatment period of the study and for one month thereafter
- Participants required clinically acceptable urea and electrolytes and estimated glomerular filtration rate (eGFR) >60
- Able and willing to comply with all study requirements.

- Willing to allow his or her General Practitioner to be notified of participation in the study.

2.2.1.2 Exclusion Criteria

- Previous diagnosis of ON
- Any concomitant immune suppressing or immune modulating therapy excluding β-interferon or glatiramer acetate.
- Female participants who were pregnant, lactating or planning pregnancy during the course of the study.
- Concomitant potassium supplements, angiotensin converting enzyme inhibitors, angiotensin II antagonists, cyclosporine, tacrolimus or lithium.
- Any contra-indication to MRI – severe claustrophobia, metal implant, pacemaker, etc.
- Participant who was terminally ill or is inappropriate for placebo medication
- Impaired renal function : eGFR ≤60, anuria, acute or chronic renal insufficiency and evidence of diabetic nephropathy
- Raised serum potassium (K^+ >5.5mmol/l)
- Diabetes
- Significant concomitant eye disease in either eye that may affect diseased or fellow eye results.
- Any other significant disease or disorder which, in the opinion of the investigator, would either put the participants at risk because of participation in the study, or may influence the result of the study, or the participant's ability to participate in the study.
- Participants who have participated in another research study involving an investigational product in the past 12 weeks.

We aimed to recruit 46 participants within 28 days of presentation with ON with visual acuity 6/9 or worse in the affected eye with or without a previous diagnosis of MS. ON was made as a clinical diagnosis based on a combination of some or all of several key clinical features. These included pain on eye movement, sub-acute reduction in visual acuity over hours or days, presence of a central or paracentral visual field defect, presence of a relative afferent pupillary defect, and either a swollen or normal appearing optic disc with an absence of pallor in the acute phase (36).

2.2.2 Aquaporin-4 antibodies

The clinical course of an atypical ON is such that the diagnosis may not be discriminated from typical (ie: MS associated or demyelinating) ON until after a poor recovery of vision in the initial weeks after ON. In addition, in the case of NMO, the diagnosis can be confirmed following positive anti-aquaporin-4 antibody testing. However, this result is not be available until 4 weeks after testing. Once identified, anti-aquaporin-4 antibody positive participants were removed from the intention to treat cohort and referred for appropriate care, and replaced in the ITT cohort untill 46 anti-aquaporin-4 antibody negative patients were recruited.

2.2.3 Randomisation

Subject numbers were assigned sequentially as each subject entered the study. The subjects were assigned a study drug through a centralised randomisation software hosted by the United Kingdom clinical research collaboration (UKCRC) registered Oxford Cognitive Health and Neuroscience Clinical Trials Unit. The randomisation was performed by study investigators whose access to the software did not allow unblinding. A random-deterministic minimisation algorithm was used to produce treatment groups balanced for important prognostic factors. The first 10% of

participants were allocated randomly without minimisation to avoid predictability. Subsequently the minimisation algorithm was applied with an allocation ratio that was not fully deterministic: there was an 80% bias in favour of allocations that minimised the imbalance.

The randomisation algorithm minimised for the following three variables related to prognosis at baseline:

- Sex (male or female)
- Number of weeks since onset of symptoms (<2 weeks; ≥2 weeks)
- Severity of visual impairment (between ≤6/9 and ≥6/18, ie, mildly affected; <6/18 and worse, ie, severely affected).

The study drug was labelled with the study number and unique pack identification number. The two treatments amiloride 10mg and placebo were indistinguishable to the investigators. Patients started the drug at the treatment dose on the day of dispensing of the drug after all the baseline investigations had been completed with the exception of electrophysiology, which could have been completed up to two weeks following randomisation. Medications were continued for 5 months, to allow a one month washout period before collection of the primary outcome measure.

2.2.4 Outcomes

The primary outcome was to measure the difference in pRNFL thickness as measured by GDx between the affected eye at 6 months and the fellow eye at baseline, and compare the amiloride and placebo groups.

As a secondary outcome, the same comparison with baseline fellow eye was made at 6 months with spectral domain OCT and with both OCT and GDx at 12 months.

The same comparison with baseline fellow eye was made for clinical outcomes (HCVA, 1.25% and 2.5% LCVA, TES, MD). All were done at 6 & 12 months with the exception of TES, which was only performed at 6 months.

Similarly, for electrophysiological secondary outcome measures a comparison between groups of the difference in visual evoked potential P100 amplitude and peak time, and pattern electroretinogram N95 amplitude from baseline unaffected eye to affected eye at 6 months, was made.

2.2.5 Statistical analysis of sample size

The primary comparison of GDx determinedpRNFL thickness was analysed using an analysis of covariance (ANCOVA). The response variable was the 6 month measure in the affected eye minus the unaffected eye baseline measurement. The baseline measure in the unaffected eye was added as a covariate, along with treatment group and the minimisation factors above, with time from onset of symptoms entered as a continuous variable in days rather than a binary variable as per the minimization algorithm.

Secondary analyses were made in the same way, with comparison being made with the unaffected fellow eye at baseline, with the affected eye at either 6 or 12 months. For visual evoked potentials, if the visual evoked potential was undetectable, the value of 200ms was used for peak time and an amplitude of 0μV (23). Correlations

were performed using Pearson's correlation coefficient if the data was parametric and Spearman's rho if non-parametric.

Statistical analyses were performed by the trial statistician (Stephen Gerry) using SAS 9.4 (SAS Institute, Cary NC), and reproduced by myself in SPSS 22 (IBM)

2.2.6 Statistical Powering

Thirty-six patients were required to provide 90% power and 5% alpha in order to detect a 21% effect size on the primary outcome measure. Based on previous data (74) this was a 7.4 μm difference between groups, with a common standard deviation of 6.6 μm. We allowed for a drop out rate of 10%, however, in addition we calculated that up to 10% of patients could have an atypical ON, over and above those with anti AQ-4 antibody (39). Therefore to ensure that there was enough power to detect a difference in the typical ON sub group, we aimed to recruit 46 patients in total.

2.3 Results

Between April 2013 and November 2014, 111 referrals were made to the trial and of those 48 participants were recruited and randomised to either placebo (n=26) or amiloride 10mg (n= 22), with follow up in the trial ongoing until November 2015, and with the trial finishing after the planned 12 month follow up for the last participant.

The final ITT cohort had 43 patients. In the amiloride arm two patients were withdrawn - one due to alternative diagnosis (functional visual loss) and one due to positive aquaporin-4 antibodies, therefore 20 patients were included in the primary analysis of the ITT cohort. In the placebo arm, one patient withdrew, one was lost to follow up and one patient was withdrawn due to alternative diagnosis, therefore 23

patients were included in the primary analysis (figure 2.1). These exclusions were made (as per the protocol), without knowledge of the patients' treatment allocations. No atypical cases of ON were identified from clinical follow up.

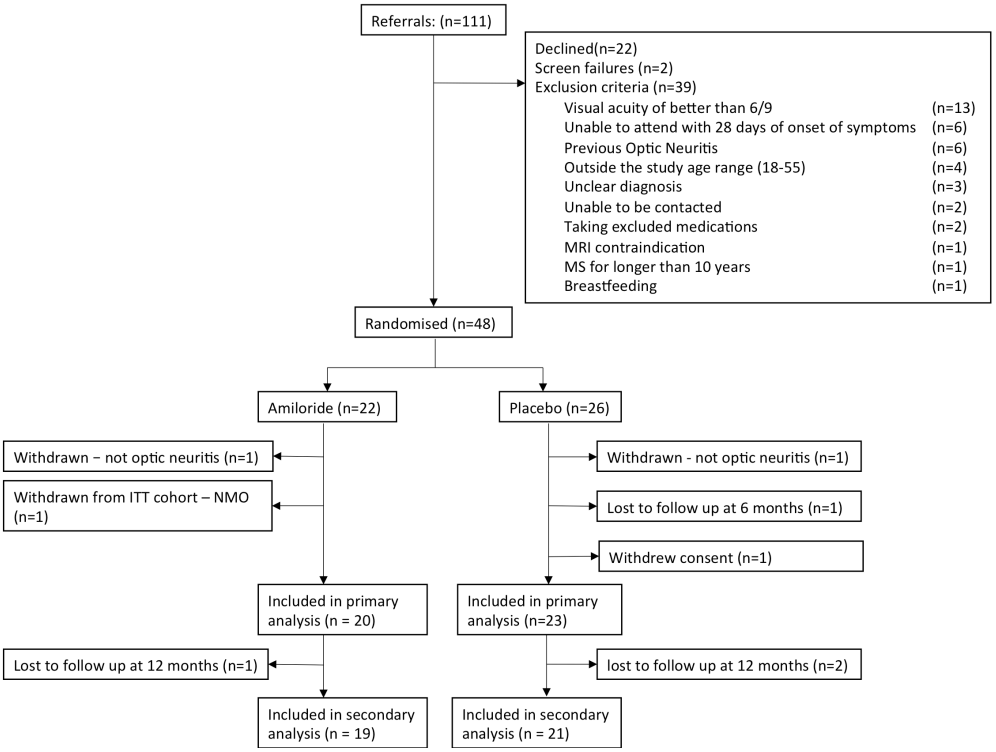

Figure 2.4 Flow diagram of recruitment to the ACTION trial

The baseline characteristics of both groups were similar as outlined in table 2.1.

Table 2.1 Baseline demographic and clinical characteristics of all patients in the intention to treat cohort.

	Amiloride n=20	Placebo n=25
Gender M:F	05:15	08:17
CIS	14 (70%)	14 (56%)
2nd CIS	3 (15%)	4(16%)
Subs MS [CIS]	3 (15%)	5 (20%)
known MS	0	2 (8%)
Steroids given	1 (5%)	5 (20%)
>2 White Matter lesions on MRI brain	14 (56%)	8 (40%)
	Mean (95% CI)	
Age (years)	34.70 (30.5302, 38.8698)	31.48 (28.0016, 34.9584)
Time from onset to randomisation (days)	14.70 (12.5736, 16.8264)	15.16 (13.0801, 17.2399)
Affected eye structural measures		
GDx		
RNFL thickness at baseline	53.28 (49.73, 56.83)	51.34 (48.54, 54.15)
Optical Coherence Tomography		
OCTpRNFL thickness at baseline (μm)	156.08 (116.55, 195.60)	119.75 (96.80, 142.70)
OCT macular volume (mm3)	2.41 (2.36, 2.45)	2.31 (2.21, 2.43)
OCT GCLIPL volume at baseline (mm3)	0.62 (0.59, 0.63)	0.60 (0.57, 0.62)
Affected eye visual measures		
High contrast letter score	43.90 (27.61, 60.18)	50.12 (37.63, 62.60)
1.25% acuity letter score	0.42 (-0.46, 1.30)	0.88 (-0.36, 2.12)
2.5% acuity letter score	1.42 (-1.14, 3.98)	2.44 (-0.14, 5.02)
Visual field mean deviation	-19.60(-25.38, -13.82)	-18.49(-23.00, -13.97)
Colour vision TES	324.73 (175.24, 474.21)	350.5 (277.69, 423.30)
Affected eye electrophysiological measures		
P100 amplitude (μV)	4.80 (2.46, 7.15)	5.016 (2.85, 7.19)
P100 peak time (ms)	152.93 (133.63, 172.22)	144.53(128.22, 160.84)
N95 amplitude μV	4.14 (3.46, 4.82)	4.11092 (3.4339, 4.788)

2.3.1 Primary outcome measure

There was no significant difference between the amiloride group and the placebo group in the primary outcome – difference between affected eye at 6 months and baseline unaffected eye in GDx derived pRNFL (table 2.2, figure 2.5). Furthermore, in the secondary outcome measure, at 12 months there remained no significant difference between the groups on GDx pRNFL (table 2.3, figure 2.5).

2.3.2 Secondary outcome measures

2.3.3 Structural and visual secondary outcome measures

In concordance with the primary outcome measure, OCT derived measurement of pRNFL at 6 (table 2.2, figure 2.5) and 12 months (table 2.3, figure 2.5) in the affected eye minus unaffected eye at baseline, showed no significant difference between the placebo and amiloride groups. Similarly, there were no differences between groups in macular thickness or any of the macular layers. In the visual outcome measures, there were no significant differences between the two groups in visual acuity, low-contrast visual acuity, FM-100 TES scores and HVF MD.

Figure 2.5 Scatter plot of pRNFL as measure by scanning laser polarimetry and optical coherence tomography in affected and unaffected eyes in both groups, for each dataset the mean and SD are marked with horizontal lines.

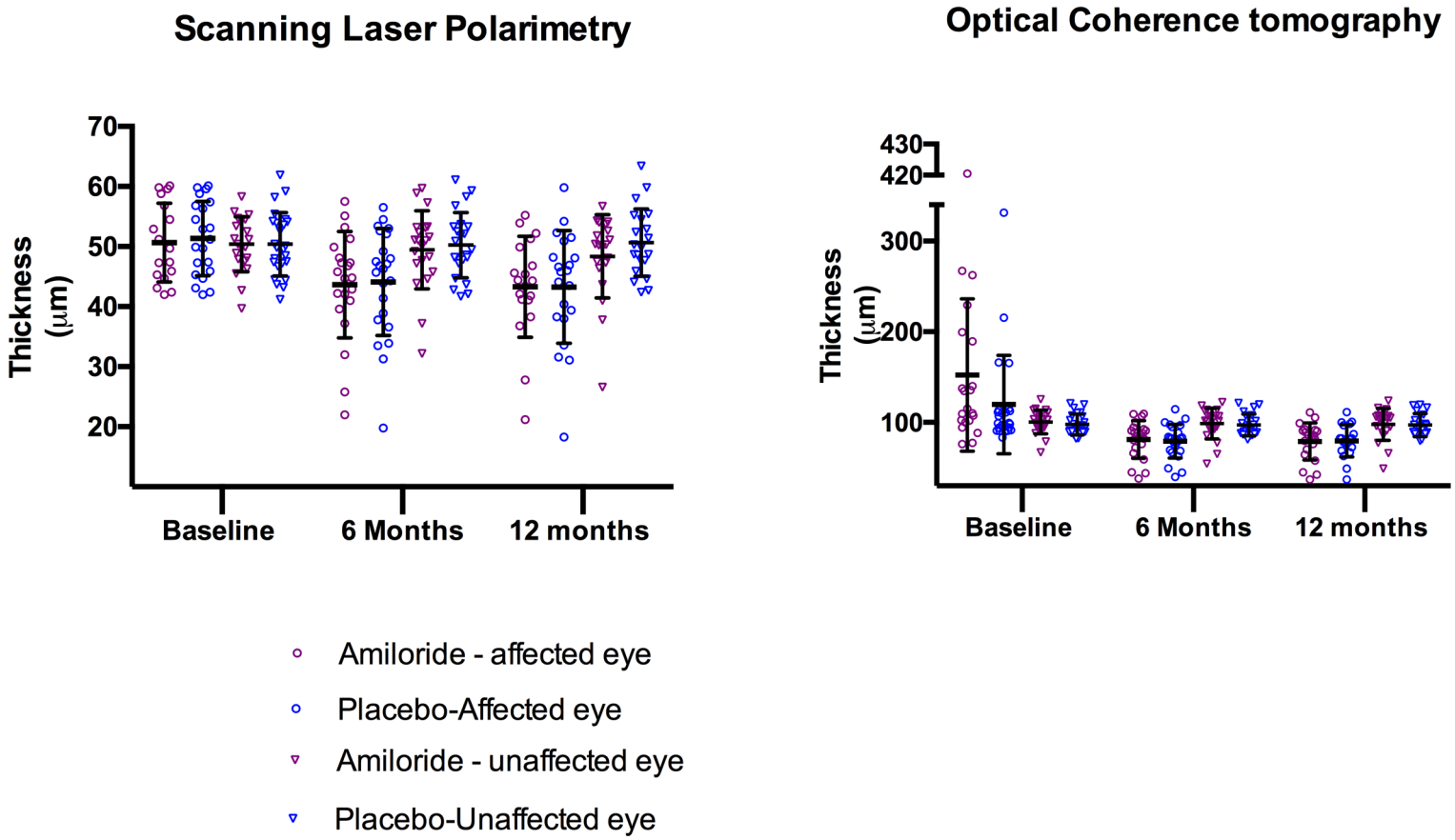

Table 2.2: Differences between the amiloride and placebo groups 6 month outcome measures the difference between the baseline unaffected eye and the affected eye at 6 months is shown as the outcome value, values given are adjusted for covariates, age, sex, and time from onset of symptoms.

	Measure	Amiloride change from baseline to 6 months (n=20) Mean (95% CI)	Placebo change from baseline to 6 months (n=23) Mean (95% CI)	Difference Amiloride - placebo, Mean (95% CI)	p-value
Structural measures	*Scanning laser Polarimetry*				
	pRNFL thickness (µm)	-7.04 (-11.04, -3.04)	-6.58 (-10.38, -2.79)	-0.46 (-5.02, 4.10)	0.840
	Optical Coherence Tomography				
	pRNFL thickness (µm)	-15.22 (-24.29, -6.15)	-16.99 (-26.25, -7.72)	1.77 (-9.13, 12.66)	0.745
	Total Macular volume (mm3)	-0.128 (-0.173,-0.084)	-0.124 (-0.165, -.082)	-0.005 (-0.058, 0.067)	0.884
	GCIPL volume (mm3)	-0.135 (-0.186, -0.092)	-0.139 (-0.186, 0.092)	0.004(-0.075, 0.067)	0.912
Visual measures	HCVA letter score	-11.67 (-25.75, 2.41)	-7.26 (-20.94, 6.42)	-4.41 (±-20.83, 12.02)	0.590
	LCVA 1.25% letter score	-15.13 (-21.87, -8.39)	-10.83 (-17.17, -4.49)	-4.30 (-12.06, 3.47)	0.269
	LCVA 2.5% letter score	-15.94 (-23.82, -8.06)	-13.34 (-20.69, -5.98)	-2.60 (-11.64, 6.43)	0.562
	Colour vision TES	26.40 (-24.14, 76.94)	29.00 (-23.91, 81.92)	-2.60 (-65.61, 60.40)	0.933
	HVF MD	-4.00 (-9.11, 1.10)	-1.98 (-7.09, 3.14)	-2.02 (-8.23, 4.18)	0.513
Electrophysiological measures	P100 peak time (ms)	27.27 (20.22, 34.31)	14.45 (7.27, 21.64)	12.81 (4.30, 21.33)	0.004
	P100 amplitude (µV)	-5.13 (-7.00, -3.26)	-3.43 (-5.36, -1.49)	-1.70 (-3.96, 0.56)	0.135
	N95 amplitude (µV)	-1.74 (-2.73, -0.76)	-1.20 (-2.21, -0.20)	-0.54 (-1.72, 0.64)	0.358

Table 2.3: Differences between the Amiloride and Placebo groups 12 month outcome measures the difference between the baseline unaffected eye and the affected eye at 12 months is shown as the outcome value, values given are adjusted for covariates, age, sex, and time from onset of symptoms.

	Measure	Amiloride change from baseline to 12 months (n=19) Mean (95% CI)	Placebo change from baseline to 12 months (n=21) Mean (95% CI)	Difference Amiloride - placebo Mean (95% CI)	p-value
Structural measures	*Scanning laser Polarimetry*				
	RNFL thickness (µm)	-8.33 (-12.81, -3.85)	-7.25 (-11.70, -2.80)	-1.09 (-6.39, 4.22)	0.680
	Optical Coherence Tomography				
	pRNFL thickness (µm)	-17.56 (-26.53, -8.59)	-17.52 (-26.93, -8.12)	-0.04 (-11.09, 11.02)	0.995
	Total Macular volume (mm3)	-0.135(-0.180, -0.90)	-0.143 (-0.185,-1.00)	0.007 (-0.057, 0.072)	0.815
	GCIPL volume (mm3)	-0.137 (-0.190, -0.085)	-0.150 (-2.00, - 1.00)	0.012 (-0.063, 0.087)	0.743
Visual measures	HCVA letter score	-9.76 (-23.28, 3.76)	-7.87 (-21.56, 5.82)	-1.89 (-18.37, 14.59)	0.817
	LCVA 1.25% letter score	-10.81 (-17.68, -3.94)	-11.34 (-18.15, -4.54)	0.53 (-7.76, 8.83)	0.897
	LCVA 2.5% letter score	-10.19 (-17.56, -2.82)	-12.62 (-19.78, -5.47)	2.43 (-6.55, 11.41)	0.585
	HVF mean deviation	-3.21 (-8.28, 1.85)	-1.21 (-6.49, 4.06)	-2.00 (-8.38, 4.38)	0.528

2.3.4 Electrophysiological secondary outcome measures

The difference between baseline fellow eye visual evoked potential P100 peak time, and affected eye peak time at 6 months was significantly prolonged in the amiloride group (27.27 95% CI 20.22, 34.31ms) compared to the placebo group (14.45 95% CI 7.27, 21.64 ms, *p* 0.004). There was a trend for a greater reduction in P100 amplitude between the two measures in the amiloride group and the placebo group, but this was not significant (*p 0.135).* Differences were not significant between the placebo and amiloride groups on pattern electroretinogram N95 amplitude difference. The difference in groups in PVEP P100 peak time remained significant when those with undetectable visual evoked potentials at 6 months were removed (1 patient in the amiloride group). It was noted however that there was an imbalance at baseline between the two groups in PVEP peak time, this was assessed via an unrelated samples t-test and found to be non-significant (p 0.491) . Furthermore, re-running the ANCOVA with the *affected* eye at baseline in PVEP P100 time to peak as an additonal co-variate, remained significant (p 0.002). However, in a post hoc analysis, a t-test of the change in P100 time to peak from 0 to 6 months in the affected eye's own visual evoked potential, there was no significant difference between groups.

2.3.5 Exploratory analysis of early neurodegeneration in macular OCT

Given the lack of effect in the randomised comparison, we further analysed our baseline macular OCT data to examine the possibility of pre-randomisation early neurodegeneration. At baseline, there was a significant thinning of the GCIPL volume, between affected eye and unaffected eye (*p* 0.002, figure 3), and this

difference correlated with the number of days between symptoms (r=-.415, *p* 0.005, figure 2.6) and OCT acquisition. Further analysis showed there was a significant correlation between the baseline affected-unaffected eye difference in GCIPL, and the 6 month affected eye minus the baseline unaffected eye in pRNFL (r=.463 *p* 0.002 Spearman's rho).

Figure 2.6 (A) Significant thinning of ganglion cell complex layer at baseline in affected eye compared to fellow eye (p=0.002, related samples Wilcoxon signed rank test) (B) Affected minus unaffected ganglion cell complex correlates with time from optical coherence tomography (r=.-415, p=0.005, Pearson's correlation coefficient)

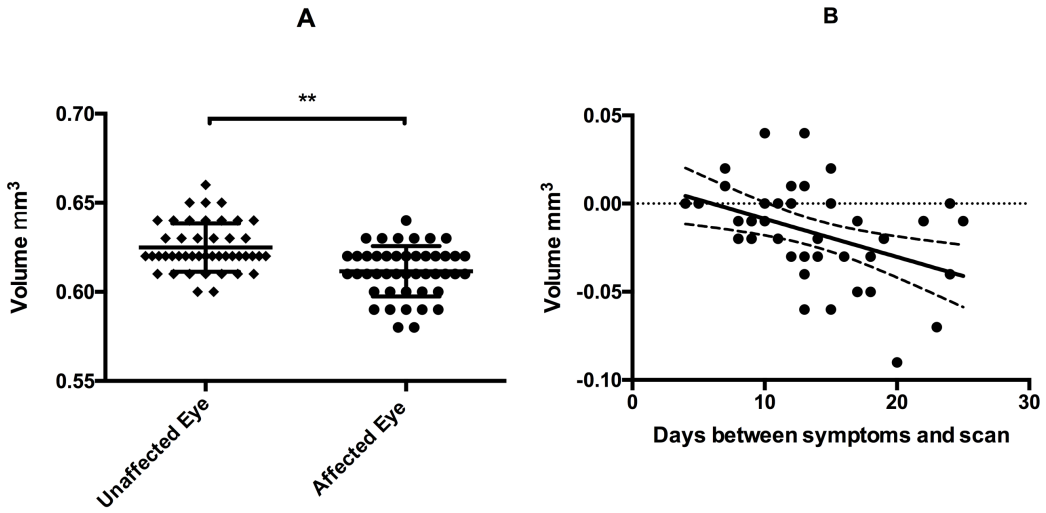

2.4 Discussion

Converging basic science and early clinical research indicated that amiloride may be neuroprotective in MS and its animal models. Based on this, we hypothesised that amiloride would also be neuroprotective in ON, the pathophysiology of which is closely related to that observed in MS. We conducted a prospective phase 2 randomised controlled trial of 43 patients in the ITT cohort comparing a group treated with amiloride for 5 months, and assessed at 6 months, to a placebo group. We assessed neuroprotection through imaging of pRNFL by GDx and compared the affected eye at 6 months, to the unaffected eye at baseline.

Contrary to our hypothesis, our trial failed to show any difference in the primary outcome measure of pRNFL on GDx between patients treated with amiloride, and patients treated with placebo following acute ON. In the electrophysiological secondary outcome of visual evoked potential peak time, the amiloride group showed

a poorer outcome than the placebo group. This suggests that amiloride does not have a neuroprotective effect in ON in the given clinical trial setting. However, there are other potential reasons for the lack of effect of amiloride on the primary outcome.

The timing of intervention in any neuroprotective trial is critical to demonstrate a potential effect but is offset by delivering study recruitment to target. Within our study, participants were initiated on amiloride or placebo within 28 days of visual symptom onset (mean 15 days). Other phase 2 trials of ON which have had positive primary outcome measures examining pRNFL have had windows of 10 days (mean 4.5 in the active group) (45) and 14 days (mean 8.2 in active group) (23). A study examining use of Simvastatin in ON, recruited within a slightly longer window of 4 weeks (mean 12 days in active group) (114) had a negative primary but positive secondary outcome. Analysis of our baseline data showed that even within our window of recruitment (28 days from symptom onset) there was a significant thinning of the GCIPL. Since commencing recruitment for our trial, other cohorts have reported similar findings (115, 116). In addition, this early GCIPL loss strongly correlated with later pRNFL loss, (r=0.46 in our data), which is consistent with other studies (115). This suggests that damage to the neuro-axonal unit had already been initiated prior to exposure to a putative neuroprotective effect of amiloride within our study (115). These combined factors demonstrate a critical time window for potential neuroprotective treatments.

Thus, the extended window of recruitment in our trial may have meant that, in late cases, neurodegeneration was already established limiting any potential benefit from amiloride. Therefore, future therapeutic trials should have as short a window, between symptoms and inclusion as possible. This involves educating clinicians and patients with a vision to developing an approach similar to stroke where “time is brain” (117), in ON, “delay is degeneration”.

The atrophy observed in the neural tissue in the retina is assumed to be due to a dying back wallerian neurodegenerative process, originating with axonal transection at the site of inflammation in the optic nerve (34). Whilst basic science models suggest that ASIC mediated mechanisms may be contributory to axonal injury, it seems likely that the mechanisms that contribute to axonal transection are manifold. Alternative mechanisms, for example more direct effects from T-cells and macrophages, may also hold a significant or even greater contribution to axonal transection (118). Additionally, in tandem with the recent finding of early GCLIPL loss on OCT, the potential role of primary retinal neurodegeneration in ON alongside wallerian degeneration, is of increasing relevance. In a recent analysis of an animal model of ON, RGC loss predated optic nerve axon transection in mice (119). Moreover, this study echoed human post mortem studies showing direct infiltration of the retina with microglia and macrophages (120). The contribution of ASIC to such cell body neurodegeneration could be limited, contributing to the lack of effect in our primary outcome measure from amiloride.

Our study was powered to detect a 21% difference between groups in GDx determined pRNFL thickness, based on a cross-sectional study from Frohman et al (74). We demonstrated a lesser difference between unaffected and affected eyes in our placebo group (6.58μm) compared the Frohman study (22.30μm). In tandem with this OCT measures showed a relatively preserved pRNFL at 6 months in both the placebo and amiloride arms when compared to other published cohorts. Our cohort had a mean drop in pRNFL of 17.52μm in the placebo arm and 17.56μm in the amiloride arm at 6 months. However, a recent study of phenytoin in acute ON had a mean loss of pRNFL of 24.16μm amongst their 42 placebo patients at 6 months, using the same OCT and acquisition parameters (23). These comparisons of our GDx and OCT assessments indicate our cohort had a less severe drop in pRNFL

than expected, lowering the power of our study to detect a potential neuroprotective effect on the pRNFL.

In view of the apparently mild disease course of our cohort, we further analysed our results as a per protocol group in sub-group analysis, pre-specified in our statistical analysis plan, with the aim to exclude those with no objective evidence of ON on baseline assessments. We excluded those who had a normal MRI brain, had a P100 amplitude and peak time of affected eye within 5% of unaffected eye at baseline, and a pattern electroretinogram N95 amplitude in the affected eye within 10% of the unaffected eye at baseline (2 patients in the placebo arm, 0 in the amiloride arm). Additionally, however, we also excluded patients who had a second clinical episode of ON in the affected eye within 6 months, thus removing the impact of any second "hit" of inflammation in the affected eye (2 patients in the placebo arm, 0 in the amiloride arm). However, this analysis also failed to find any significant difference between the placebo and amiloride arms of the trial.

Lack of effect of amiloride could be explained by insufficient bioavailability of the drug in the CNS to provide adequate blockade of ASIC in the CNS. Formal studies assessing amiloride's ability to cross the human blood brain barrier are lacking. However, though the dose used was higher compared to the maximum licensed dose used in this clinical study, pre-clinical studies of amiloride showed an effect through blockade of ASIC type 1 following intra-peritoneal administration (18, 25). In addition, it may be argued that the inflammation induced increased permeability of the blood brain barrier (121) would facilitate penetration of amiloride to the optic nerve.

Consistent with adequate CNS penetration of amiloride, and a biological target effect within the optic nerve, is the finding of a significant delay in P100 time to peak in the

amiloride treated group compared to placebo. P100 time to peak is a measure of myelination in the optic nerve and is significantly delayed in ON. Subsequent improvements in the P100 delay may reflect resolution of inflammation, remyelination and/or ion channel redistribution following ON (107). Remyelination is a function of oligodendrocyte cells. Oligodendrocytes are known to express ASIC, however the precise function of the expression of ASIC at this location is unknown. In the context of CNS inflammatory mediated injury of oligodendrocytes, a role for ASIC is suggested by its blockade being myelo-protective in animal models of MS. However, this is in contrast to our visual evoked potential findings in this study. In addition, the observed delay in the amiloride group was seen at 4 weeks after cessation of amiloride, which is more suggestive of persisting structural impairment of myelination status, rather than an ion channel mediated effect of amiloride. Such paradoxical effects between basic and clinical studies are not unique in MS, exemplifying the complex pathogenesis of this disease (122).

In conclusion, our trial failed to demonstrate a neuroprotective effect of amiloride in acute ON in any of the primary or secondary outcome measures. There was a signal from the secondary outcome measures that amiloride may have had a detrimental effect on recovery of the P100 peak time, which could be a reflection of amiloride impeding remyelination following ON. This was an unexpected result given laboratory evidence that amiloride preserved myelination through blockade of the ASIC type 1; this finding warrants further basic science research to explore the role of ASIC and its effects on myelin in CNS inflammatory disease. In the primary outcome measure however, analysis of our data emphasises that neurodegeneration is an early phenomenon in ON. Thus, future studies in ON should ensure capturing patients within the early window of opportunity for neuroprotection.

3 Chapter 3. Changes in macular retinal layers over time following optic neuritis

In this chapter a brief review of macular OCT studies with retinal segmentation is performed, and the cellular background to these segmented layers is reviewed.

The longitudinal data from OCT is then analysed after a drug effect from amiloride has been examined. In this analysis, patterns of neurodegeneration are shown in the inner retina which correlate with our functional and electrophysiological measures, but thickening of outer retinal layers is also found, which have negative correlations with these functional measures.

The dynamic nature of these changes in thickness are then explored, and the analysis is shown to add new insights into what was known about the sequence of changes in retinal layers following optic neuritis.

3.1 Introduction

The advent of spectral domain OCT has allowed in vivo monitoring not only of the pRNFL in the retina, but also the segmented layers of the retina at the macula.

The cellular basis of the retinal layers is shown in figure 3.1 along with an explanation of abbreviations used in this chapter. And a detailed description of the retinal structure can be found in the introduction.

Figure 3.1: Diagrammatic representation of the retinal layers (see figure 2.2 for OCT layers). OCT layers are on the left hand side of the diagram, and their cellular components on the right. RNFL- retinal nerve fibre layer (macular), GCL ganglion cell layer, IPL – inner plexiform layer, INL – inner nuclear layer, OPL – outer plexiform layer, ONL – outer nuclear layer (the nuclei of the photoreceptors). IS/OS – outer retina, comprised of the inner and outer segments of the photoreceptors and the retinal pigment epithelium. Adapted from Britze et al 2017

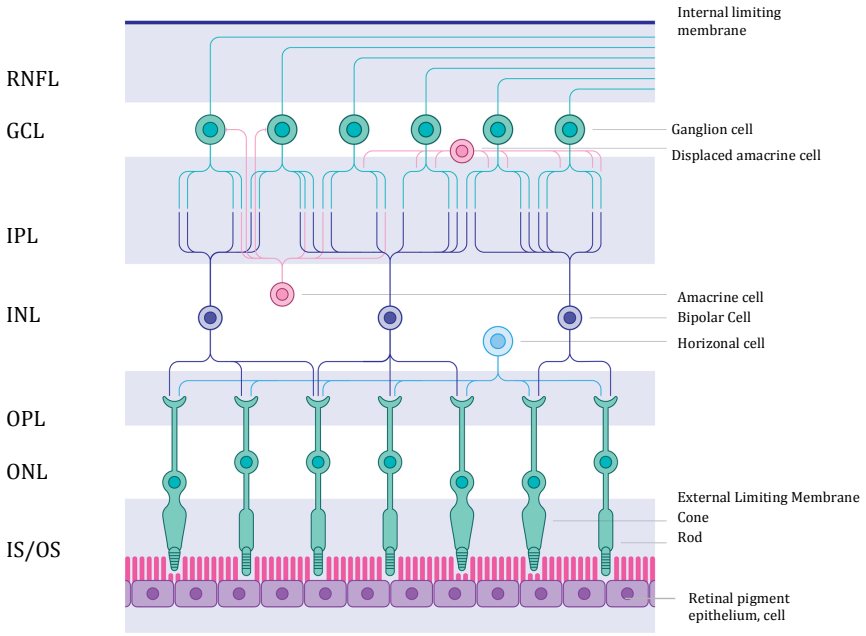

The focus of the primary outcome of the trial was on the pRNFL, the retinal layer that is continuous with the optic nerve, and this a key target to explore wallerian degeneration from retro-bulbar ON. However, many cross-sectional OCT studies of the macula in ON have shown marked changes in the retinal layers, which correlate well with visual outcomes. A major advantage of using OCT in the trial means that we can segment the retinal layers and assess how the thickness of the layers evolve over time following optic neuritis, and how the change over time correlates with clinical outcomes.

3.1.1 Pathology Studies

To my knowledge no literature exists describing post mortem human tissue directly following optic neuritis. However, the retina of post mortem MS eyes were studied in large numbers by Green et al (120). This showed not only retinal nerve fibre layer and ganglion cell layer atrophy, but also atrophy in the INL. Notably the authors did not find any change in the outer retinal layers beyond the INL. Inflammatory cells were found in a proportion of cases in the GCL and occasionally in the inner plexiform later (IPL) and INL. These findings give us some insight into the pathological basis underlying OCT changes in ON, however they reflect a broad spectrum of MS eyes, and none of the eyes were undergoing acute ON.

3.1.2 OCT studies

There have been a large number of cross-sectional OCT studies to date on retinal changes in eyes with a history of optic neuritis. These have established that there is thinning of the total macula and GCL (usually combined with IPL as some segmentation algorithms have difficulty in separating the two layers), and that GCL correlates with visual outcomes following optic neuritis - notably low contrast visual acuity (83, 84, 86, 123-125). One study has shown a correlation between PVEP amplitude and GCL thickness following optic neuritis (126). The reltionship between PERG and segmented macular OCT has been looked at cross-sectionally and n95 has been shown to correlate with GCL thickness (112).

To date no longitudinal studies have looked at PERG and PVEP with OCT in ON.

Longitudinal studies have also shown that GCL thinning is detectable early in the course of optic neuritis and has usually plateaued by around 3 months post optic neuritis (115, 116), or possibly as early as 2 months (127).

The INL however has been shown to be significantly swollen in eyes with a history of ON compared to non-ON and healthy control eyes in cross-sectional studies (86, 128), however longitudinal studies reporting on the INL, have not found affected eye INL to have significantly changed from baseline to 6 months (51, 127) or up to a year when segmented in combination with the OPL (129). Thus the temporal evolution of this cross-sectional finding remains unknown.

Microcystic macular oedema has been shown to be occasionally present in the INL following optic neuritis, however thickening independent to this phenomenon has been found(130)and it has been suggested that this phenomenon is part of a continuum of INL thickening in response to GCL thinning(128).

Whilst total macula and inner retinal layers thin following ON, and INL appears to thicken, the current literature is less clear for the outer, photoreceptor layers. Cross-sectionally there is some evidence for swelling in these layers (combined OPL, ONL and IS/OS) (86). However, longitudinally there is evidence for dynamic swelling that subsequently reduces. In one study this was found to peak around 2 months and return to normal but remain swollen at 6 months (127). A further study showed that the outer retina was significantly swollen at 6 months, but had returned to baseline at 12 months (129).

3.2 Aims

Thus, I set out establish whether the longitudinal post ON OCT data in the ACTION trial;

- Conformed to the pattern of GCL and inner retinal thinning reported previously
- Confirmed the dynamic nature of outer retinal changes following optic neuritis reported in small cohorts
- Could establish the temporal evolution of INL thickening within a 12 month time period
- Could enhance our understanding of the structural functional correlates between OCT and vision with further analysis of the full retinal layers.

In order to increase the reliability of our exploration of these aims I also;

- Evaluated the repeatability of our retinal layer measurements
- Assessed whether there was an effect of amiloride on any of the retinal layers

3.3 Methods

3.3.1 Data acquisition and preparation

OCT scans (pRNFL and macular) were acquired and segemented as described in chapter 2. Acquisition of HCVA, LCVA, PERG and PVEP is also described in chapter 2.

3.3.2 Statistical Analysis

3.3.2.1 Intra-Class correlation co-efficient of repeated scans at the same timepoint

The acquisition of repeat scans at each time point (see section 2.1.3.1) allowed us to assess the ICC for our chosen analysis parameters. As with all the subsequent statistical analysis, this was performed in IBM SPSS v 22.

3.3.2.2 Effect of Amiloride

First an assessment was made of whether there was an effect of amiloride on the change in thickness in macular layers. This was performed using the same statistical method as the primary outcome measure in the ACTION trial - ANCOVA, The response variable was the 6 month measure in the affected eye minus the unaffected eye baseline measurement. The baseline measure in the unaffected eye was added as a covariate along with treatment group and the minimisation factors above, with time from onset of symptoms entered as a continuous variable in days rather than a binary variable as per the minimization algorithm.

3.3.2.3 Effect of time

Next, the differences between the affected eyes and unaffected eyes at each timepoint were assessed. This was done using a paired samples t-test (131) at each time point if the data was found to be normally distributed and with a related samples wilcoxon signed rank test if either affected or unaffected eye group was non-parametrically distributed. Given the high number of data points and groups, parametric or non-parametric distribution was defined as whether the data was found to significantly deviate from the normal distribution in Shapiro-Wilk test of normality.

Following this, the effect of time on individual retinal layers was assessed. For this, a repeated measures ANOVA with subsequent pairwise analysis was used if the data was parametric, or if the data was non parametric, a related samples Friedman's analysis of variance by ranks with subsequent Wilcoxian signed rank test was used for pairwise analysis. Separate analyses and figures are presented for affected and unaffected eyes.

3.3.2.4 Structural-functional correlations

Following examination of the data for the effect of intervention and time, the correlations between the macular layers and functional measures were limited to VA, LCVA and electrophysiological parameters of p100 time to peak and amplitude.

A full correlation matrix for all the ACTION parameters would result in 484 correlations for each eye (from a total of 22 visual, electrophysiological and structural metrics). Within those variables, there is a high degree of co-variance. Of the visual measures initially collected VA and LCVA have a number of advantages over the remaining variables. They are highly relatable and transferable for clinicians as well as being rapid to acquire. This speed with which they can be acquired is advantageous in a multi-modalilty clinical trial setting, where our experience as investigators showed that patient fatigue was a major factor in performance. Testing visual acuity is also highly dependent on the fovea as opposed to the periphery of the retina. Given our OCT parameters were restricted to the foveal and para-foveal retina, VA and LCVA as functional measures that are most dependent on this architecture are of most interest in assessing structural/ functional relationships. FM-100 hue score (which was only collected at 0 and 6 months), and Sita standard HVF both suffer from being long, difficult tests that are not very comfortable for patients and induce a high degree of patient fatigue. As discussed in chapter 1, repeatablilty of HVF has been shown to be poor in ON patients(103), and shows a poor correlation to pRNFL in milder cases (80). Whilst the pre-specified error rate based on previous publications in optic neuritis (101) was 33% for HVF, in clinical practice, this would be deemed to be an unacceptable error rate, and has high risk of affecting the measured variable - mean deviation, in diseased populations (132).

In order to make use of the longitudinal nature of our data, for this analysis, linear correlations, (either a pearson's correlation coefficient, or Spearman's rho in the case of non parametric data) were calculated and are presented. Correlations are also presented between macular layers. It is assumed that there is a high degree of co-variance between macular layers and therefore between correlated in retinal layers and functional / electrophysiological correlations. On the same basis, raw p values are presented without adjustment for multiple comparisons ie: there are multiple comparisons of essentially the same correlation measured by different biomarkers.

3.4 Results

3.4.1 Intra-class correlation coefficient (ICC)

Analysis of our ICC coefficients within each layer over repeated measures at the same timepoint, was consistent with the Oberwahrenbrock (87) data. This showed that the OPL did indeed have generally lower ICC scores and displayed higher degree of variability in ICC across timepoints than other layers. However, our data outperformed that of Oberwahrenbock et al, with only one of 54 timepoints - OPL in the baseline affected eye - giving an ICC of less than 0.7 (0.699). ICC coefficients are displayed in figure 3.2, for comparison the data from the Oberwahrenbrock cohort are also presented.

Figure 3.2. Intra-class correlation coefficient (ICC) of repeated measures of retinal layers at each timepoint. ICC is a measure of the concordance of repeated measures. 0.7 or above is considered acceptable, 0.8 or above is considered good, and 0.9 or above is considered excellent. The variation in the OPL in particular is consistent with reported literature and should be considered when reviewing correlations for that layer. However, our use of the mean of two measurements means that we are more likely to have captured the true mean at each timepoint, thus improving the reliability of our results.

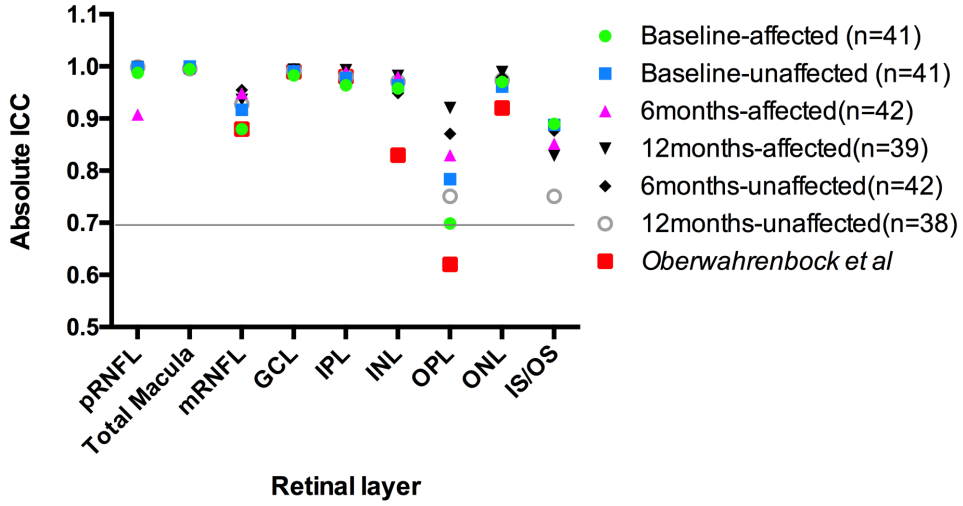

3.4.2 Effect of Amiloride on change in macular layers

In line with our primary outcome measure, there was no significant difference between the amiloride and placebo group in the change in macular layers at 6 or 12 months, compared to the unaffected eye at baseline, in our pre-specified ANCOVA analysis (Table 3.1). Thus, all eyes were included in subsequent analysis, regardless of whether they were in the amiloride or placebo group.

Table 3.1. ANCOVA of retinal layers assessing the effect of amiloride on change in retinal layer thickness. No significant differences are found between the amiloride and placebo groups

		Amiloride			Placebo					
Layer	Timepoint (months)	n	mean change (mm3)	95 % CI	n	mean change (mm3)	95% CI	Difference in means*(mm3)	CI of difference in means	p value
Total Retina	6	20	-0.128	-.165, -0.82	23	-0.124	-0.165, -.082	-0.005	-0.67, 0.58	0.884
	12	19	-0.135	-0.180, -0.90	21	-0.143	-0.185, -1.00	0.007	-0.57, 0.72	0.815
mrnfl	6	20	-0.21	-0.29, -0.14	23	-0.24	-0.30, -0.17	0.002	-0.008, 0.12	0.69
	12	19	-0.25	-0.32, -0.18	21	-0.27	-0.033, -0.20	0.002	-.008, 0.011	0.743
GCL	6	20	-0.084	-0.116, -0.053	23	-0.088	-0.117, -0.058	0.003	-0.041, 0.047	0.881
	12	19	-0.085	-0.118, -0.052	21	-0.095	-0.126, -0.064	0.01	-.037, -.056	0.678
IPL	6	20	-0.051	-0.070, -0.032	23	-0.051	-0.069, -0.034	0.001	-0.026, 0.027	0.962
	12	19	-0.052	-0.072, -0.032	21	-0.055	-0.074, -0.032	0.003	-0.026, 0.031	0.855
GCLIPL	6	20	-0.135	-0.186, -0.085	23	-0.139	-0.186, -0.092	0.004	-0.67, 0.75	0.912
	12	19	-0.137	-0.19, -0.085	21	-0.15	-0.2, -0.1	0.012	-0.063, 0.087	0.743
INL	6	20	0.008	0.000, 0.016	23	0.013	.006, 0.020	-0.005	-.016, 0.006	0.354
	12	19	0.012	0.003, 0.022	21	0.014	0.005, 0.023	-0.002	-0.015, 0.012	0.808
OPL	6	20	-0.008	-0.018, 0.003	23	-0.012	-0.022, -0.002	0.004	-0.011, 0.019	0.587
	12	19	-0.012	-0.024, -0.001	21	-0.014	-0.025, -0.003	0.001	-0.016, 0.018	0.886
ONL	6	20	0.028	0.10, 0.046	23	0.025	0.008, 0.042	0.003	-0.022, 0.028	0.807
	12	19	0.3	0.010, 0.049	21	0.25	0.007, 0.043	0.005	-0.022, 0.032	0.72
IS/OS	6	20	0.009	0.000, 0.018	23	0.012	0.004, 0.020	-0.003	-0.015, 0.009	0.638
	12	19	0.011	-.003, 0.019	21	0.005	-0.003, 0.014	-0.005	-0.018, 0.007	0.362
*Amiloride minus placebo										

3.4.3 Development of difference between affected and unaffected eyes

Scatter plots for all subjects' data for each layer at each time point are shown in figure 3.3.

Figure 3.3. Scatter plot of volume of each retinal layer in affected and unaffected eyes over time. Error bars show mean and standard deviation. Horizontal square brackets show significant differences between affected and unaffected eyes on paired samples t-test with varying levels of significance denoted by asterisks - * p <0.05, ** p <0.01, *** p <0.001

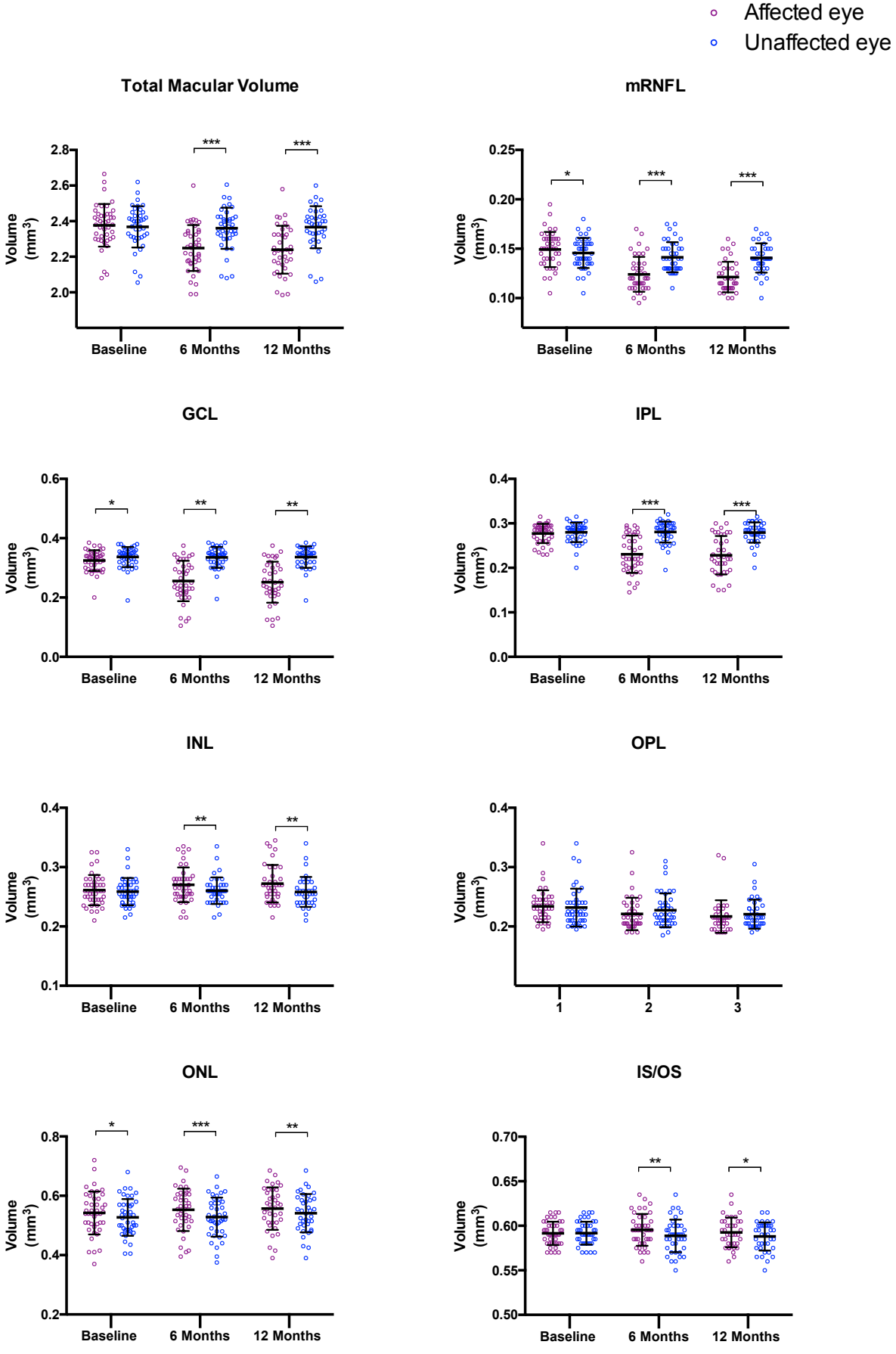

3.4.3.1 Baseline

At baseline, four layers showed a significant difference between affected and unaffected eyes on a paired samples t-test. There was significant thinning in the GCL and IPL of affected eyes, significant thickening of the mRNFL (presumably from peri-papillary oedema tracking into this layer acutely) and also a significant thickening of the ONL.

3.4.3.2 6 months

At 6 months, total macular volume was significantly thinner in the affected eye compared to the unaffected eye. The change in the mRNFL had reversed and was now significantly thinner in the affected eye. There was an increased thinning in the affected eye GCL and IPL compared to the unaffected eye.

The INL was significantly thicker in the affected eye by 6 months compared to the unaffected eye. There was no significant difference in the OPL. The ONL was increasingly thicker in the affected eye. The outer retina was also significantly thicker in the affected eye at 6 months.

3.4.3.3 12 months

At 12 months the total macula, mrnfl, GCL, IPL all remained significantly thinner in the affected eye.

The INL, ONL and outer retina all remained significantly thicker in the affected vs fellow eye. It is notable however that the 12 month comparison the ONL and IS/OS had both a reduced mean difference between affected and unaffected eye, and also

a lower probability value than at 6 months, suggesting some dynamism to their thickness over time in affected eyes.

3.4.4 Change over time within each eye

3.4.4.1 Affected eye (Figure 5a)

All of layers with the exception of the ONL had a significant change over time. Changes over time can be seen in figure 3.4(a and b). The Total retina, mRNFL, GCL and IPL and OPL all significantly reduced at baseline and 6 months and baseline and 12 months, but there were no significant changes between 6 &12 months.

The INL had a significant increase between 0 and 12 months but the trend was not yet significant at 6 months.

The IS/OS notably had a significant increase in thickness at 6 months, however this had returned to non-significance by 12 months.

3.4.4.2 Unaffected Eye (Figure 5 B)

The only layer that had a significant change over time in the unaffected eye was the ONL. This showed a significant rise however, this represent a 1.8% increase in thickness over time from baseline, and the significance was marginal (*p* 0.032).

*Figure 3.4. (A) Change over time in volume of retinal layers. Error bars are mean with 95% confidence interval of the mean (n=40 patients with three timepoint follow up) .Significant changes over time are marked by square brackets and asterisks based on parwise analysis from ANOVA or wilcoxian signed rank test, only shown for analyses where the F-test of all three timepoints was significant to a p value <0.05. - * p <0.05, ** p <0.01, *** p <0.001*

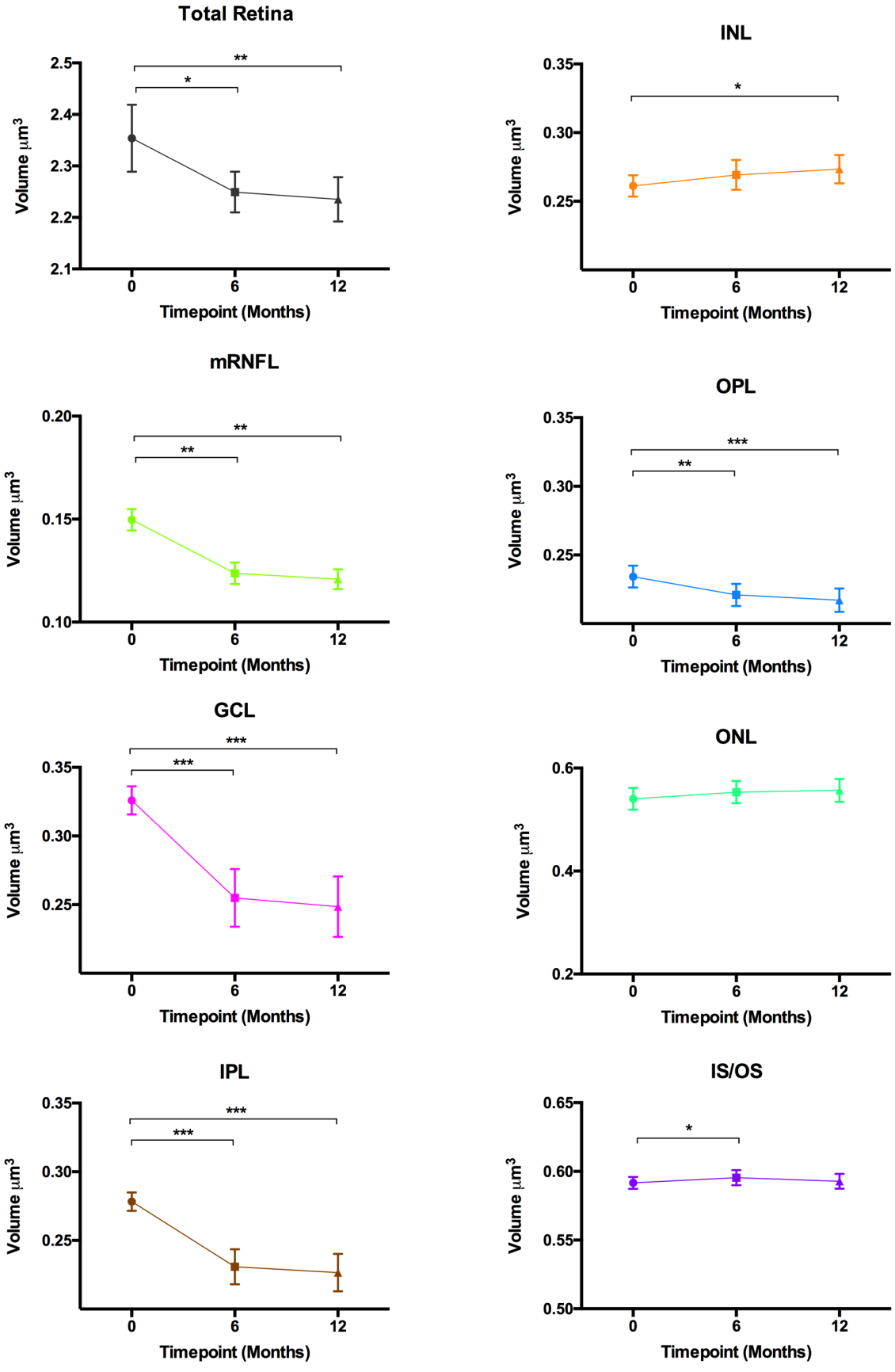

Figure 3.4. (B) the same analysis as figure 5 (A) for the unaffected eyes (n=37, excluded patients with bilateral ON during the 12 month follow up period)

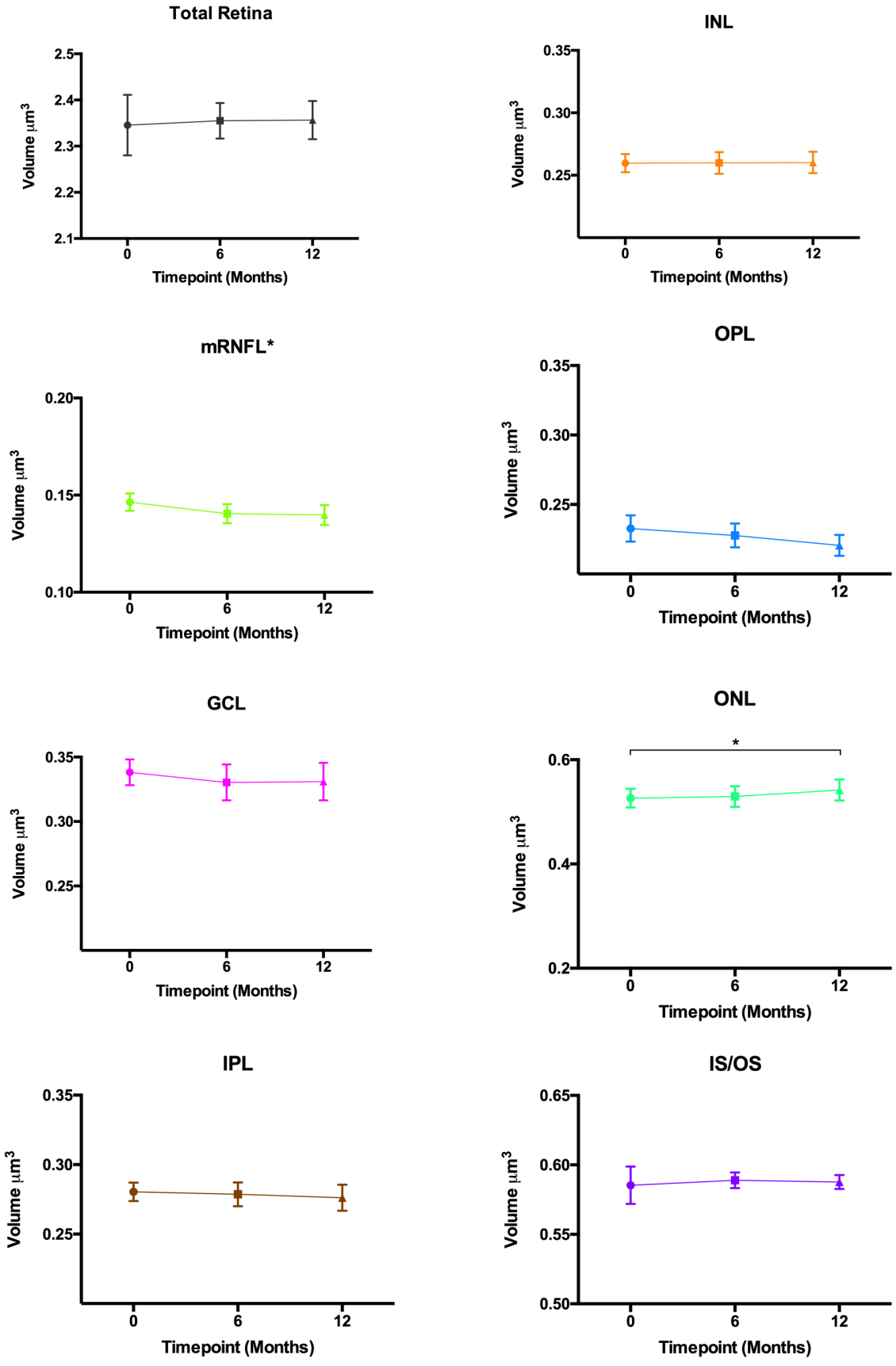

3.4.5 Correlations between visual, electrophysiological and structural measures.

Correlations are displayed in table 3.2 for 6 months and table 3.3 for 12 months.

3.4.6 Multiple Linear regression between OCT layers and 2.5% LCVA.

Due to the colinearity of the retinal layer variables, any model which includes combinations of more than one inner retinal layer or outer retinal layer fails assumptions on colinearity necessary for a valid multiple regression model. Multiple regression could be applied in order to assess whether additional variance in visual or electrophysiological parameters, could be explained by a combination model of retinal layers. Therefore a hierarchical model with initially GCL difference combined with INL difference between affected eye at 12 months and unaffected eye at baseline was assessed with 2.5% LCVA as the dependent variable. However, this had a minimal effect on the r value (increasing from .658 for GCL alone to .659 for combined GCL and INL). A further attempt with GCL combined with IS/OS had a non significant F test change (p0.165) with an increase in r from .658 to .679. These analyses and the correlation matrix of retinal layers, suggests that most of the variability in LCVA explained by retinal changes is carried in the positive correlation between change in GCL volume and change in LCVA. Thus, there appears to be little independent additional variability explained by either thickening or thinning of other retinal layers.

Table 3.2. 6 month correlations between visual and electopysiological measures and macular layers. For comparason, correlations with pRNFL on OCT and GDx are also included

	Statistic	Total Macula	mRNFL	GCL	IPL	GCLIPL	INL	OPL	ONL	IS/OS	PERG-N95	VEP- p100 amp	VEP - p100 ttp	pRNFL -OCT	pRNFL -ECC GDx	pRNFL VCC GDx
LCVA 1.25%	r	.449**	*0.172*	.584**	.512**	*.520***	-0.111	*0.187*	-.390**	-.334*	*.349**	.370*	-0.118	.470**	-.481**	.378*
	p	0.003	*0.27*	0	0	*0*	0.479	*0.23*	0.01	0.028	*0.024*	0.015	0.458	0.001	0.001	0.013
LCVA 2.5%	r	.508**	*0.293*	.503**	.578**	*.607***	-0.287	*0.094*	-.314*	-.404**	*.379**	.453**	-0.101	.552**	-.533**	.393**
	p	0.001	*0.057*	0	0	*0*	0.062	*0.549*	0.04	0.007	*0.013*	0.002	0.526	0	0	0.009
HCVA	r	.307*	0.266	.403**	.388*	.385*	-0.224	-0.06	-.410**	-.410**	0.209	.415**	-0.095	.396**	-.493**	0.24
	p	0.045	0.085	0.007	0.01	0.011	0.148	0.704	0.006	0.006	0.184	0.006	0.551	0.009	0.001	0.121
PERG-N95	r	.631**	*.471***	.640**	.649**	*.652***	-.320*	*0.223*	-.415**	-0.279	1	.505**	-0.168	.493**	.470**	.411**
	p	0	*0.002*	0	0	*0*	0.039	*0.156*	0.006	0.074	0	0.001	0.289	0.001	0.002	0.007
VEP p100 amplitute	r	.510**	0.296	.593**	.558**	.562**	-0.147	0.061	-.413**	-0.107	.505**	1	-0.262	.562**	.549**	.397**
	p	0	0.054	0	0	0	0.348	0.697	0.006	0.493	0.001	0	0.094	0	0	0.008
VEP - p100 ttp	r	-.362*	-0.242	-.404**	-.408**	-.403**	0.112	-0.113	0.22	.356*	-0.168	0.262	1	-.362*	-.347*	-.342*
	p	0.019	0.122	0.008	0.007	0.008	0.479	0.475	0.161	0.02	0.289	0.094	0	0.018	0.026	0.027
Italics - Parametric correlations (pearsons) otherwise non-parametric Spearman's Rho																
**significant to <0.01																
*significant to <0.05																

Table 3.3. 12 month correlations between visual measures, macular layers and for comparason, correlations with pRNFL on OCT and GDx are also included. No electrophysiological testing was done at 12 months as per protocol.

		Total Macula	mRNFL	GCL	IPL	GCLIPL	INL	OPL	ONL	IS/OS	pRNFL -OCT	pRNFL -ECC GDx	pRNFL VCC GDx
LCVA 1.25%	r	.542**	*0.269*	.549**	*.583***	*.594***	-0.26	*0.206*	-.360*	-0.207	.573**	.466**	.367*
	p	0	*0.093*	0	*0*	*0*	0.106	*0.201*	0.022	0.199	0	0.002	0.018
LCVA 2.5%	r	.503**	*0.249*	.560**	*.618***	*.640***	-.380*	*0.045*	-0.255	-0.184	.563**	.420**	.347*
	p	0.001	*0.121*	0	*0*	*0*	0.016	*0.781*	0.112	0.255	0	0.007	0.026
HCVA	r	.484**	0.29	.503**	.518**	.516**	-.399*	0.007	-0.181	-0.089	.558**	.398*	0.288
	p	0.002	0.069	0.001	0.001	0.001	0.011	0.966	0.263	0.585	0	0.011	0.068
Italics - Parametric correlations (pearsons) otherwise non-parametric Spearman's Rho													
**significant to <0.01													
*significant to <0.05													

Table 3.4. 6 month correlations between macular layers and electrophysiological testing.

6 months affected minus baseline unaffected (n=43)		Total Macula	mRNFL	GCL	IPL	GCL/IPL	INL	OPL	ONL	IS/OS
VEP time to peak p100	Spearman Coefficient	-.362*	-0.242	-.404**	-.408**	-.403**	0.112	-0.113	0.22	.356*
	Sig. (2-tailed)	0.019	0.122	0.008	0.007	0.008	0.479	0.475	0.161	0.02
VEP p100 amplitude	Spearman Coefficient	.510**	0.296	.593**	.558**	.562**	-0.147	0.061	-.413**	-0.107
	Sig. (2-tailed)	0	0.054	0	0	0	0.348	0.697	0.006	0.493
N95 amplitude	Spearman Coefficient~	*.603***	.471**	*.640***	*.652***	*.652***	-.320*	0.235	-.415**	-0.279
	Sig. (2-tailed)	*0*	0.002	*0*	*0*	*0*	0.039	0.134	0.006	0.074
**. Correlation is significant at the 0.01 level (2-tailed).										
*. Correlation is significant at the 0.05 level (2-tailed).										
~ for parametric correlations pearsons coefficient is given in italics										

3.4.7 Correlations between macular layers and electrophysiological measures

Correlations between the 6 months change in PVEP p100 time to peak and amplitude and PERG n95 are shown in table 3.4

3.4.8 Correlations within macular layers

Correlations at 6 and 12 months between each macular layer are shown in tables 3.5A and 3.5B respectively

Tables 3.5A and 3.5B. 6 month (A) and 12 month (B) difference in affected eye macular layers and unaffected eye baseline measurement, correlation matrix showing the correlation between each

A

6 months affected minus baseline unaffected (n=43)		Total Macula	mRNFL	GCL	IPL	GCL/IPL	INL	OPL	ONL	IS/OS
Total Macula	Pearson Correlation	1	.707**	.958**	.954**	.956**	-.448**	.372*	-.586**	-.311*
	Sig. (2-tailed)		0	0	0	0	0.003	0.014	0	0.042
mRNFL	Pearson Correlation	.707**	1	.723**	.674**	.697**	-.519**	0.176	-.511**	-0.19
	Sig. (2-tailed)	0		0	0	0	0	0.259	0	0.223
GCL	Spearman Correlation	.958**	.723**	1	.977**	.996**	-.556**	.333*	-.642**	-.315*
	Sig. (2-tailed)	0	0	.	0	0	0	0.029	0	0.04
IPL	Pearson Correlation	.954**	.674**	.977**	1	.991**	-.510**	.354*	-.630**	-.348*
	Sig. (2-tailed)	0	0	0		0	0	0.02	0	0.022
GCL/IPL combined	Pearson Correlation	.956**	.697**	.996**	.991**	1	-.556**	.334*	-.642**	-.316*
	Sig. (2-tailed)	0	0	0	0		0	0.028	0	0.039
INL	Spearman Correlation	-.448**	-.519**	-.556**	-.510**	-.556**	1	-0.2	.359*	0.113
	Sig. (2-tailed)	0.003	0	0	0	0	.	0.197	0.018	0.469
OPL	Spearman Correlation	.372*	0.176	.333*	.354*	.334*	-0.2	1	-.732**	-0.037
	Sig. (2-tailed)	0.014	0.259	0.029	0.02	0.028	0.197	.	0	0.814
ONL	Spearman Correlation	-.586**	-.511**	-.642**	-.630**	-.642**	.359*	-.732**	1	0.01
	Sig. (2-tailed)	0	0	0	0	0	0.018	0	.	0.949
IS/OS	Spearman Correlation	-.311*	-0.19	-.315*	-.348*	-.316*	0.113	-0.037	0.01	1
	Sig. (2-tailed)	0.042	0.223	0.04	0.022	0.039	0.469	0.814	0.949	.
**. Correlation is significant at the 0.01 level (2-tailed).										
*. Correlation is significant at the 0.05 level (2-tailed).										

B

12 months affected minus baseline unaffected (n=40)		Total Macula	mRNFL	GCL	IPL	GCL/IPL	INL	OPL	ONL	IS/OS
Total Macula	Pearson Correlation	1	.731**	.968**	.944**	.949**	-.453**	.528**	-.636**	-0.09
	Sig. (2-tailed)		0	0	0	0	0.003	0	0	0.579
mRNFL	Pearson Correlation	.731**	1	.735**	.625**	.653**	-.488**	.355*	-.548**	-0.02
	Sig. (2-tailed)	0		0	0	0	0.001	0.024	0	0.904
GCL	Spearman Correlation	.968**	.735**	1	.975**	.994**	-.492**	.432**	-.659**	-0.096
	Sig. (2-tailed)	0	0	.	0	0	0.001	0.005	0	0.556
IPL	Pearson Correlation	.944**	.625**	.975**	1	.988**	-.473**	.455**	-.663**	-0.091
	Sig. (2-tailed)	0	0	0		0	0.002	0.003	0	0.574
GCL/IPL combined	Pearson Correlation	.949**	.653**	.994**	.988**	1	-.509**	.457**	-.675**	-0.09
	Sig. (2-tailed)	0	0	0	0		0.001	0.003	0	0.583
INL	Spearman Correlation	-.453**	-.488**	-.492**	-.473**	-.509**	1	-.367*	.409**	-0.219
	Sig. (2-tailed)	0.003	0.001	0.001	0.002	0.001	.	0.02	0.009	0.174
OPL	Spearman Correlation	.528**	.355*	.432**	.455**	.457**	-.367*	1	-.692**	0.212
	Sig. (2-tailed)	0	0.024	0.005	0.003	0.003	0.02	.	0	0.189
ONL	Spearman Correlation	-.636**	-.548**	-.659**	-.663**	-.675**	.409**	-.692**	1	-0.14
	Sig. (2-tailed)	0	0	0	0	0	0.009	0	.	0.389
IS/OS	Spearman Correlation	-0.09	-0.02	-0.096	-0.091	-0.09	-0.219	0.212	-0.14	1
	Sig. (2-tailed)	0.579	0.904	0.556	0.574	0.583	0.174	0.189	0.389	.
**. Correlation is significant at the 0.01 level (2-tailed).										
*. Correlation is significant at the 0.05 level (2-tailed).										

3.5 Discussion

3.5.1 Summary of findings

This data adds to the known literature of changes over time in retinal layers following ON.

Reassuringly, in the inner retina our longitudinal data concurs with much of the published field. This suggests that the anterior visual system data is a robust foundation on which to move forward to assess correlations with posterior visual pathways in later chapters. In keeping with the early swelling that is found in pRNFL, significant swelling was found in affected eye mRNFL compared to unaffected eyes at baseline. However at 6 and 12 months mRNFL had followed the GCL and IPL and become significantly thinner in the affected eye.

In addition, this data shows that the structural functional relationship between OCT and visual function, is driven primarily by GCL thickness and has a less robust relationship to IS/OS thickening.

This is the first longitudinal dataset to correlate PERG n95 amplitude with retinal layers, r values are higher than in a previously published cross-sectional data set (112) and this data shows a correlation with the INL for the first time.

Correlations within retinal layers show considerable positive correlations between changes in layers. These are particularly striking in the positive correlations found in the change in the inner retinal (mRNFL, GCL and IPL) layers, but there are also highly significant correlations between the drop in inner retinal thickness and the gain in INL and ONL thickness. Notably, the IS/OS shows a weak but significant negative

correlations at 6 months with the inner retinal layers, but these have disappeared by 12 months.

This data is the first to my knowledge to show the evolution over time in swelling in the INL - which is significantly swollen at 12 months compared to baseline, but this has not reached significance by 6 months. However, in comparison with the unaffected fellow eye, the INL is significantly swollen by 6 months. This suggests a unidirectional trend evolving over time of an increase in time in the INL, which is in line with previous cross-sectional studies (86) but was not found to have reached significance in other longitudinal studies. In one study from Gabilondo et al this could relate to the fact the follow up period was limited to 6 months (127). In the other study from Al-louzi et al, the INL was in fact segmented along with the OPL for analysis, and this showed a dynamic change in this combined metric, with a rise at 4 months and a decline in thickness between 4 and 8 months (129).

Given a significant thickness observed in the INL in cross-sectional analysis over large numbers of patients performed by other groups, this suggests that the dynamic response observed in Al-louzi et al (129) in the INL may be as a result of less precise segmentation used in their study.

In the ONL - which comprises the nuclei of the rod and cone photoreceptors, no significant change is observed over time in the affected eye in this data. Conversely, this was the only layer to show a significant change over time in the unaffected eye, though it was of a very small magnitude (1.8%). However, of note, even at baseline there is a significant thickening of this layer in the baseline affected eyes vs unaffected eyes, and this difference is dynamic over time (4% at baseline, 5% at 6 months and 3% at 12 months) reflecting the dynamic pattern observed in the ANOVA of the outer segments of the photoreceptors. Unlike the GCIPL in chapter 2, the

difference between eyes at baseline in ONL and the time to OCT was not significantly correlated (r.012 p 0.942). Nevertheless, the early and persistent difference between the two eyes in ONL is suggestive of an early increase in thickness of the ONL. The finding in the unaffected eyes is difficult to explain on a pathophysiological basis, and may reflect a multiple comparisons effect.

This data also supports previous longitudinal studies which suggest a dynamic response to ON in the outer retina, primarily composed of the inner and outer segments of the photoreceptors, but also containing the thin layer of retinal pigment epithelial cells. In this data, the peak is at 6 months with a drift back towards baseline thickness at 12 months. This is also reflected in the change over time in the correlation between these outer-retinal layers and functional visual measures - correlations were present at 6 months but had waned by the 12 months timepoint. Furthermore, this chapter has broken down the retina into more layers than the study by Al-louzi et al (129) who combined GCL with IPL, INL with OPL, and ONL with IS/OS. This allowed me to confirm the dynamic change in the outer-retina more specifically related to the photoreceptor bodies, in data which has been shown to be robust from calculating ICC. The data from Gabilondo et al (127), which used the same degree of segementation as the study in this thesis, would suggest that this had in fact peaked at 2 months post optic neuritis, and returned to normal at 6 months, however, Gabilondo et al had a considerably smaller sample size than this data (n=27 vs n=43 at 6 months, n=40 at 12 months) therefore potentially reducing their power to detect trends present in our larger dataset. In addition, both studies also chose to examine a larger ETDRS area, which covers a wider area, but also means that they may be less sensitive to peri-foveal changes than in our analysis. Gabilondo et al used Spectralis OCT. Whilst the authors comment on their ART (mean 45) they do not comment on whether they used a high speed or high resolution acquisition.

3.5.2 Pathophysiological mechanisms for OCT changes

What remains unclear, are the underlying pathophysiological mechanisms effecting the changes observed in this longitudinal data and the similar findings observed in the literature.

As discussed in chapter 2, the recent finding of early neurodegeneration in the GCL and combined GCIPL in ON raised questions as to whether this process is entirely mediated by wallerian degeneration from an optic nerve lesion in ON. We have seen that in basic science, recent analysis of animal models of MS have shown that retinal ganglion cell loss predates optic nerve axon transection in mice (119). Consistent with this are the finding from Kupersmith et al (75) who examined both optic nerve MRI and OCT and found no correlation between optic nerve lesion proximity to the globe and early GCL+IPL thinning.

In this context, it is worth noting again the direct infiltration of the retina with microglia and macrophages (120) found in post mortem MS eyes. These early changes in GCL point to a potential cell body mediated neurodegeneration, or that early functional changes in the optic nerve axons may cause GCL cell damage, even before true axonal loss has occurred in the RNFL.

The potential for a primary retinal pathology in ON, adds complexity to the interpretation of the thickening changes found in the INL, OPL, ONL and IS/OS layers in the outer retina.

Balk et al(86) in the Amsterdam group contend in their cross-sectional study that the thickened INL acts as a “dam” of plasticity protecting the outer retinal layers from any neurodegeneration. One could interpret our longitudinal data slightly differently. It is notable that the thickening of the IS/OS layer correlates with inner retinal layers at 6 months, but not by 12 months. Potentially, this means that these outer segments are initially somehow induced to reactively enlarge by the neurodegeneration in the inner retinal layers, and subsequently re-organise to conform back to their pre-inflammatory thickening. In this scenario, the progressive thickening observed in the INL would be in turn reactive to this re-organisation, rather than a ‘dam’ preventing any change in the outer retina.

It is possible that the changes in the outer retina are not inflammatory, and are a mechanical expansion in response to increased vitreomacular traction pulling the newly thinned inner retina, towards the centre of the eye. This is supported by the fact that whilst the segmented outer retinal layers change configuration from 6 to 12 months (INL expanding, IS/OS contracting) the total macular thickness is fairly static. Further support can be pulled from the finding that the IS/OS segment has a significant negative correlation with GCL at 6 months which is lost by 12 months. It could be inferred that the gap left by a thinning GCL is initially filled by an expanded IS/OS that subsequently secedes and the INL mechanically expands to fill the space created. However, detailed analysis of OCT in patients with microcystic macular oedema in the INL following inflammatory ON has shown no evidence of vitreomacular traction contributing (133). Furthermore, the strength of the INL correlation with GCL does not appear to change from 6 to 12 months.

A further possibility is that the dynamic outer retinal changes are driven either as a consequence of inflammatory mediated cell death in the GCL layer, or by direct inflammation in these outer retinal layers. In post mortem MS eyes, intra-retinal

inflammatory cells did not reach beyond the INL (120), however uveal and perivenous inflammation with breakdown of the blood-retinal barrier is a known clinical and pathological manifestation of MS (48). The IS/OS segment, which contains the retinal pigment epithelium, is the most anatomically and physiologically connected retinal layer to the uveal tract, it is possible that a direct reaction to this is responsible for the dynamic findings observed. Furthermore, experimental models of ON have shown evidence of apoptosis in the ONL. It may be that our in vivo findings in OCT represent reactive oedema in response to cell death of photoreceptors following ON, or a reactive oedema to the neurodegeneration in the inner retina mediated by activated microglial cells which have been found in experimental models (119).

3.5.3 Limitations

Attempting to secure a pathophysiological explanation for the changes noted on OCT highlights one of the key limitations of OCT studies including this chapter. With OCT we are studying changes in thickness of layers of cell types based on our apriori knowledge of the cellular arrangement of the retina rather than studying cell types directly. One challenge for example is defining the role of Muller cells (the retinal glial cells) in our dynamic changes, as these cells are positioned from the external limiting membrane to the internal limiting membrane, Thus they could influence the changes found in any of the retinal layers from the mRFNL to the ONL or indeed also in the IS/OS layer due to their adjacent anatomical position.

Moreover, it is possible that diseased retina has a dynamic change in reflectivity of near infra red light, thus affecting OCT - derived thickness that is not necessarily a change in true layer thickness or a change in cell number.

Whilst the data has been shown through study of our repeatability measurements to be robust, clearly as with any imaging modality there is the potential for measurement error to affect results.

3.5.4 Conclusion

This chapter confirms that there is neurodegeration in the inner retinal layers in our cohort in line with widely reported findings from other cohorts. It also shows that most of the variability in LCVA that is explained by OCT is driven by neurodegeneration in the GCL. This data shows that significant INL swelling occurs over a one year timecourse, and that the IS/OS layer shows a dynamic change over the course of a year following optic neuritis.

In the next chapter we go on to assess whether the identified neurodegeneration in the inner retina can account for downstream neurodegeneration in the posterior visual pathways.

4 Chapter 4. Using diffusion tensor imaging to assess transsynaptic neurodegeration in the visual system following ON

In the previous chapter we explored neurodegeneration at a retinal level following ON and also showed that further analysis of the retinal layers did not reveal any effect of amiloride.

However, a key finding in early clinical evidence of amiloride was its effect in arresting rate of decline in diffusion measures of white matter integrity (29). Therefore, in the ACTION trial MRI imaging was collected at each timepoint to evaluate the effect of amiloride on white matter in the brain. Despite failing to find an effect on retinal measures following ON, it remains of interest to determine whether a difference between groups can be found in measures of white matter integrity.

Moreover, collecting longitudinal data on both the white matter of the brain, and detailed retina data in OCT, allowed longitudinal assessment of anterograde transsynaptic neurodegeneration in the optic radiations (OR) in response to presynaptic neurodegeneration in the retinal ganglion cells.

4.1.1 Diffusion MRI and white matter integrity

Intrinsically the diffusion of water molecules is isotropic. In tissue, diffusion is restricted by tissue structures, ie white and grey matter cell membranes. In the absence of diffusion, the signal following a 180 degree spin echo pulse (S0e) would be the same as the initial signal (S0). However, in the presence of diffusion, due to

the multi-directionality of water molecules, there is some signal loss between S0 and S0e. We can label this signal loss the diffusion coefficient (D) which is also determined by the "b" value which related to our encode and decode (diffusion) gradient strength and gradient duration during our spin echo, thus S=S0e-bD. The S0 can be calculated from acquiring signal with b=0 image (ie no gradients). By applying diffusion gradients in different directions, we can encode information on the different amount of diffusion in different orientations. This allows us to calculate a diffusion tensor for each voxel, composed of eigen vectors describing diffusion orientation and and eigenvalues describing the amount of diffusion along the eigenvalue.

From the diffusion tensor we can derive the value of diffusion in the principal diffusion direction (the first eigenvalue) in a voxel - the axial diffusivity (AD). We can also ascertain the average of the diffusion transverse to the principal diffusion direction, by calculating the mean of eigenvalues the second and third eigen vectors, this is termed radial diffusivity (RD). With these values we can also calculate the fractional anisotropy of a voxel, that is, the degree of variance between the three eigenvalues. A high FA means that diffusion of water molecules is highly restricted along one direction - as found in unidirectional white matter tracts. In the context of MS, a fall in FA can be interpreted as being due to axonal loss, but may also be influenced by a loss of myelin in fibre bundles (134). Indeed the relationship between reduced myelination and reduced FA has been found in combined post mortem DTI and pathology studies (135, 136). Moreover, in the second study, it was found that the association between reduced myelin and axonal loss, rather than axonal loss itself, in fact explained an initial association between reduction in FA and axonal loss (136).

Separate analysis of AD and RD can inform on which metrics are contributing to a change in FA. Based on animal models of mice with congenitally poor CNS myelination, RD increases have been demonstrated to be sensitive to pathologically

confirmed poor myelination (137), with AD being unaffected. Thus, it has been reasonably inferred that AD reductions reflect axon loss and not myelin loss. In human MS populations RD increases and FA decreases are a consistent finding (138), however AD reductions are often not found. One notable exception is a study of paediatric MS (139) (mean age 15 years), which found both increased RD and decreased FA and AD in comparison with healthy, controls in non-lesioned white matter. Lack of change in AD in later, chronic MS patients can be explained by the extensive cytopathological changes occuring not just in the damaged and repairing neuro-axonal unit in such populations, but also in supporting cells, notably microglia. Indeed, one post mortem DTI /pathology study found that diffusivity scalar correlations in non-lesioned white matter correlated with activated microglia, and not axonal count or myelin count.

Thus, from DTI we can derive diffusivity scalars, FA, AD and RD. Whilst the precise cellular changes underpinning changes in these scalars cannot be precisely delineated invivo, it can be reasonably inferred that they inform on tissue white matter integrity. Moreover, in an early CIS population such as that of the ACTION trial, we have an opportunity to asses such scalars without the potential confounds of long term complex changes in neuro-axonal remyelination and repair mechanisms that have been postulated contribute to, and confound the interpretation of, these values in chronic disease cohorts (140). In the context of the visual system following ON, these values can be used as surrogate biomarkers of white matter integrity and thus transsynaptic neurodegeneration across the LGN.

4.1.2 Anterograde transsynaptic neurodegeneration

Neurodegeneration is a key pathological process leading to disability in MS(141). However, the downstream contribution of discrete relapses to remote

neurodegeneration via transsynaptic processes remains unclear. Pathologically, the visual pathways have been studied in the optic nerves, tracts and LGN in post mortem MS brains, and evidence of selective post-syntaptic loss of parvocellular layers in the LGN (58). Pathological studies correlating beyond the LGN to the OR are lacking. Animal models however are supportive of transsynaptic neurodegeneration along the visual pathways following ON transection (142). Electron microscopy in animal models of the synapse between the optic tract and LGN following ON transection has shown alterations of post-synaptic dendrites, and potentially toxic “seepage” of material from the degenerating pre-synaptic ON axon (143, 144). Given this post mortem and experimental evidence of transsynaptic neurodegeneration following injury to the visual system, OCT and DTI are useful ways to assess whether transsynaptic neurodegeneraiton can be captured in vivo.

4.1.3 Existing DTI evidence for transsynaptic neurodegeneration following ON

Cross-sectional evidence for transsynaptic neurodegeneration comparing patients with a previous history of ON and controls has been found to be mixed. One group, studying patients at 1.5 Tesla have found reduced FA in ON patients compared to controls, though this was mainly shown to be dependent on lesions in the OR (145, 146)– however, this is the only group to report such a relationship between lesion volume and white matter integrity in the OR in ON patients. This group found an isolated association with nasal pRNFL and contralateral AD, but no correlation with FA or RD. Another 1.5T study did find differences in curvature of the OR in tractography, but not differences in FA (147). A more recent study of 15 patients with a history of ON compared to controls did show a reduction in FA tractography derived mean FA measures at 3 Tesla (148). However, this was not related to pre-synaptic neurodegeneration as measured by multifocal PVEP in this study.

Two longitudinal assessments of the OR following ON have been published, both performed at 1.5 Tesla. One data set, recently published, found that FA was significantly reduced over time in a longitudinal follow up of 28 ON patients over one year using probabilistic tractography (149). There was found to be a correlation between optic nerve atrophy on MRI and the FA changes in the OR. However, in the supplementary data, the authors showed that the there was in fact no significant difference in the rate of change in FA between the ON group and the control group. A further study of 38 patients scanned at 0, 6 and 12 months showed that the rate of reduction in FA in the OR was significantly more in ON patients compared to controls. However, compared to their own baseline FA values there was no significant change in FA or other diffusivity scalar over time in the ON patients (150). A borderline significant correlation with pRNFL reduction was found for AD reduction in the non-lesioned sub-group of patients. Both of these studies found no correlation with lesion volume and OR diffusivity scalar changes.

4.2 Aims

Given the differing findings and lack of previous correlation with OCT data in the existing literature on transsynaptic neurodegeneration, In this chapter my aims were to;

- Assess for an effect of amiloride in whole brain diffusion measures and in a region of interest analysis in the OR
- Assess for an effect over time in whole brain diffusion measures and in a region of interest analysis in the OR
- Assess for correlations between pre-synaptic neurodegeneration in the retina - as measured by OCT derived macular GCL volume, and post-synaptic measures of white matter integrity in the OR, over time.

4.3 Methods

4.3.1 Scan acquisition - OCT

OCT data was collected and analysed as described in chapter 2

4.3.2 Scan acquisition – MRI

All scans were collected on a Siemens Verio 3 tesla MRI scanner with a 32 channel head coil.

DTI: 60 diffusion directions with B-value 1500 and 5 volumes with no diffusion weighting, TR 8900ms, TE 91.2 ms, FOV 192 x 192mm, voxel-size 2.0x2.0x2.0mm, 64 slices, 1 average. Acquisition time = 9min 56 secs. Additional no diffusion weighting imaging single EPI with the same dimensions acquired in the opposite (PA) direction for scan pre-processing. (acquisition time = 0:36) .

Structural Imaging: 3 dimensional MPRAG sequence with voxel size 1x1x1mm, TR 2040ms, TE 4.7ms, 1 average. (acquisition time = 5m 56s)

Sequences for lesion detection PD: 2 dimensional spin echo, 90 slices, slice thickness 1.1mm, voxel size 0.9 x 0.9 mm, FOV 220 x 99mm, TR 10960ms, TE 11ms, 1 average. (acquisition time = 5 mins 08 secs)

Flair: 2 dimensional turbo spin echo 48 slices, slice thickness 3mm, TE 73.0ms, TR 9000ms, voxel size 0.9x0.9. 1 average. PD: 2 dimensional turbo spin echo, 48 slices, slice thickness 3mm, voxel size 0.5x0.5mm, FOV 220x220mm, TR 3000ms, TE 18ms, 1 average. (acquisition time = 4mins 14 secs)

4.3.3 Image processing - whole brain analysis

First, whole brain diffusion measures were used to assess differences between amiloride and placebo groups. Voxelwise statistical analysis of the FA data was carried out using Tract-Based Spatial Statistics (TBSS) (151), part of the FMRIB software library (FSL) (152). First, FA images were created by fitting a tensor model to the raw diffusion data using the FRMIB diffusion toolbox (FDT), and then brain-extracted using BET (153). An example subject FA map is shown in figure 4.1 All subjects' FA data were then aligned into a common space using the non linear registration tool FMRIB non linear registraton tool (FNIRT) (154), which uses a b-spline representation of the registration warp field (155). Next, the mean FA image was created and thinned to create a mean FA skeleton which represents the centres of all tracts common to the group. Each subject's aligned FA data was then projected onto this skeleton and the resulting data fed into voxelwise cross-subject statistics. For some analyses, lesion maps were created for patients with white matter lesions, and entered as a nuisance regressor into the final model so that lesioned voxels would be disregarded in the statistical comparisons over time.

AD is automatically produced as a tensor map by FDT in native subject diffusion space. Thus, for groupwise analysis of AD using TBSS, the same transformations into standard diffusion space used for FA were applied to AD images, and the same mean FA skeleton mask was used to apply voxelwise statistic on AD at the centre of the white matter tracts.

RD maps were produced using FSL maths by calculating the mean of the second and third eigenvalues for each voxel. These native subject space 3D scans were then transformed into the standard space TBSS map as for AD and voxelwise statistics applied.

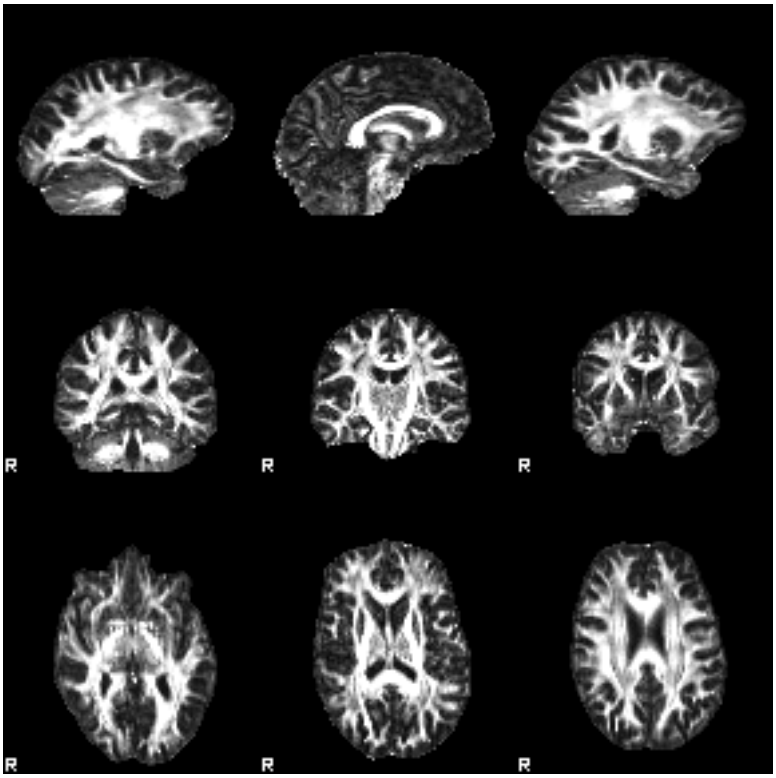

Figure 4.1. Example brain extracted FA map from a single subject produced by FDT

4.3.4 Scanner change

During the course of the study, the original Siemens 3T Verio scanner in the FMRIB centre was upgraded, however the same model of scanner with the same head coil was available in the AVIC centre and the study was continued on it. Nevertheless an assessment was made of the two scanners by assessing an unrelated samples T-test between the AVIC and FMRIB centre scanners at the 6 month timepoint which had the most even spread of scans between the two scanners.

4.3.5 Crossing fibres analysis

In order to increase the interpretability of the diffusivity scalar measures obtained with TBSS in crossing-fibre regions, TBSS was performed also on scalars associated

with a specific direction of fibres in each voxel. The model applied assumed that two fibre populations existed for each voxel.

After the pre-processing steps, common to the previous TBSS analyses, partial volume estimates for fibre orientations 1 and 2 (F1 and F2 respectively) were calculated in each voxel for each subject using the FSL tool bedpost X (156, 157). F1 and F2 were reassigned within subject at each voxel in order to ensure consistency across voxels, such that adjacent voxels had the same label assigned to the same fibre population. Then, F1 and F2 were reassigned again in order to ensure that orientations were consistent across subjects. Both these steps were accomplished using the “tbss_x” software, part of FSL (158).

4.3.6 Horizontal Flipping

Approximately 50% of optic nerve fibres cross at the chiasm from each optic nerve (159), meaning that whilst we are studying unilateral disease in the eye, the effects in the posterior visual pathways should be equally bilateral . Nevertheless, in order to fully exclude the possibility of a unilateral effect in the posterior visual pathways dependent on the laterality of the affected eye, analyses were performed with brain scans flipped horizontally using the fsl command fslswapdim, so that all affected eyes were aligned on the right hand side (22 patients were flipped from left to right). This was done after FDT was applied and diffusion tensor images created. A separate mean FA skeleton was created for the flipped scans and the same design matrices were applied for statistical analysis. Analyses using the horizontally flipped data are referred to as “flipped”, the original unflipped data is referred to as the “native” analyses hereafter.

4.3.7 Lesion masking

Given the large number of scans with lesions, a semi-automated method was used with a beta version of FSL brain intensity abnormality classification algorithm (BIANCA) (160). A training set was created using the baseline scans of all patients with lesions (n= 24), the training set consisted of a manual mask created in PD space, the T1 and FLAIR images were then registered to this space. When calculating the automated masks the BIANCA tool took into account information from all 3 structural images when subsequently deciding on lesioned and non-lesioned voxels for the automated mask using a k-nearest neighbour algorithm. Each scan's own manual mask was not used for training in creating an automated mask.

BIANCA is beta software, thus final edits were made to each mask, and all three timepoints were reviewed together in order to ensure that lesions were consistently masked at each timepoint if present, to ensure that changes in lesion detection sensitivity did not influence the result of the effect over time. In particular, all areas of "caps and bands" at the anterior and posterior horns of the lateral ventricles were removed (161).

Lesion masks were then transformed into standard space using FNIRT, (154)and binarised at a threshold of 0.3 using FSL maths. For non-lesioned patients, a blank standard space mask was used.

4.3.8 Lesioned and non-lesioned patients analysis

One of the key limitations of lesion masking is that it only masks the part of the white matter tract that is lesioned, and does not take into account any downstream effects of lesion on the white matter tracts (162). In this data set around half of the patients

had no white matter lesions. Therefore patients with and without lesions were analysed as separate groups to assess if the presence of lesions affected the results. All pre-processing was identical in sub group analysis as in the whole group. Separate mean FA maps and mean FA skeletons were produced for both the lesioned and non-lesioned groups.

4.3.9 Assessing the effect of Amiloride in TBSS

Voxelwise differences between the amiloride and placebo group were assessed using an unrelated samples t-test design matrix and the permutation tool *Randomise* in FSL (163). This was performed for the cross-sectional data at each timepoint for 6 and 12 months, with both native and flipped space. Each cross-sectional timepoint analysis had a separate mean FA map and FA skeleton composed of only those scans involved in each analysis.

In addition, each patient's FA skeleton aligned to the standard space template in TBSS at baseline was subtracted from both the 6 month scans, and the difference in FA between the two timepoints was spatially represented using FSLmaths. The resulting “difference” maps for each subject were then merged into a 4 dimensional group file, and an unrelated samples t-test could be run on this data, thus assessing whether treatment with amiloride had an effect on the change in FA over time. The same analysis was performed for 12 month data. These analyses were also run both with native and flipped diffusion data. For these longitudinal analyses, a TBSS mean FA and mean FA skeleton derived from all scans at all timepoints was used.

All analyses were run with age and sex as nuisance regressors, and analyses were performed separately with and without lesion masks as additional nuisance regressors.

4.3.10 Longitudinal statistics for whole brain diffusion scalar statistics (FA, AD, RD, F1, F2)

Voxelwise differences over time were assessed in a repeated measures ANOVA design matrix using the permutation tool *Randomise* in FSL (163). An exchangeability block was used to ensure permutation testing only occurred within subject, respecting the repeated measures structure of the data. The statistics were corrected for multiple comparisons across voxels (family wise error) and spatial clustering support was used to verify areas of significance using threshold-free cluster enhancement (TFCE) in FSL (164). Age, sex and treatment group (amiloride or placebo) were included in the design matrix as nuisance regressors. F-tests were initially inspected with a significant p value of 0.05. Each ANOVA had 6 individual t-tests (base > 6 months, 6 months > base, base > 12 months, 12 months > base, 6 > 12 months, 12 > 6 months), therefore for t-tests only voxels with a p value of ≤ 0.01 were considered significant.

4.3.11 Region of interest (ROI) analysis - the optic radiations.

4.3.11.1 Data processing

Optic radiations (OR) were identified based on the method recently published by Kolbe et al (150). Using the standard space FA skeleton produced with this data, I manually identified the same regions of the OR that were analysed in their publication (figure 4.2). Use of the TBSS skeleton meant we continued to analyse the centre of the tracts in this ROI analysis - the areas with the highest FA where changes over time and across group were likely to be most robust.

Figure 4.2. OR ROI marked out for use in this chapter (top panel, in red, superimposed on green mean FA skeleton thresholded at 0.2). In the bottom panel, the OR ROI used in Kolbe et al are shown. Z slices refer to MNI co-ordinates of the standard space mean FA maps shown for both studies.

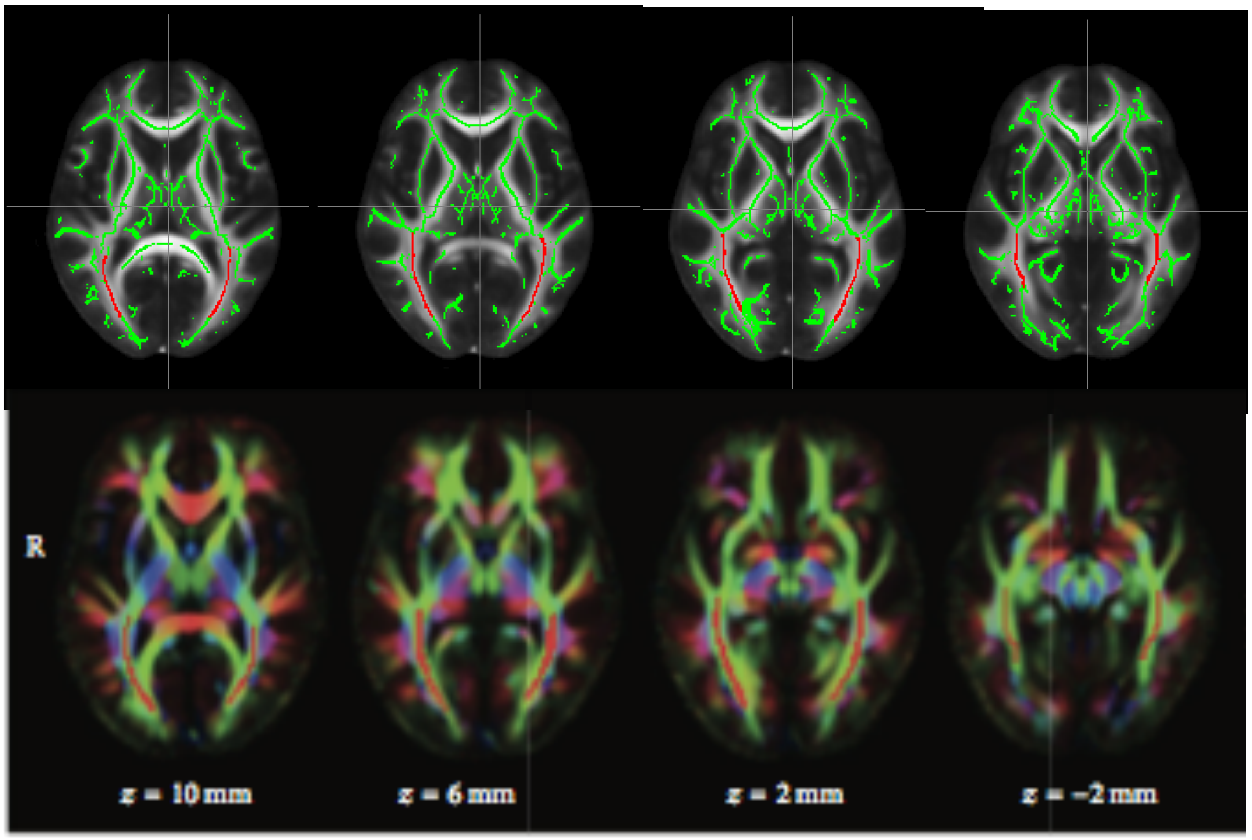

ROI masks were then transformed into the native diffusion space using FNIRT, and mean FA, AD and RD values were extracted from the masked area using FSLmaths. These values were then applied in IBM SPSS version 22 for all of the statistical tests described below.

4.3.11.2 Amiloride vs Placebo

To compare between amiloride and placebo groups independent samples t-tests were used cross-sectionally for 6 and 12 months, for all diffusivity scalars (FA, AD,

RD). If the data was non-parametric an Independent Samples Mann-Whitney U test was used.

In addition, the value of 6 month minus baseline was calculated for each subject's FA skeleton using FSL maths, and the difference between amiloride and placebo groups was calculated with the appropriate test unrelated samples t-test as above. This was repeated for AD and RD. The same was done for 12 months minus baseline for all three diffusivity scalars.

Analyses were performed for whole group, and for lesioned and non lesioned patients, and performed for the combined mean FA of both optic radiations and separately for right and left. This led to a total of 108 separate comparisons.

4.3.11.3 Longitudinal change

Longitudinal change over time in FA values was assessed using either an ANOVA or in the case of non-parametric data with a related samples Friedman's analysis of variance by ranks. Again analyses were performed for whole group, and for lesioned and non lesioned patients, and performed for the combined mean of both optic radiations and separately for right and left for each diffusivity scalar.

4.3.11.4 Correlation with OCT

The value of 6 months minus baseline GCL volume was calculated and this was correlated separately with 6 months minus baseline FA, AD and RD values. The same analysis was done for 12 months minus baseline values. If both variables were parametric, a Pearson's correlation coefficient was calculated, if either variable's distribution was non-parametric a Spearman's rho correlation was calculated. For 12 month's data, analyses were performed for whole group, and for lesioned and non

lesioned sub-groups. The combined mean of both optic radiations and separate means for right and left OR were correlated with GCL for each diffusivity scalar. Although this did result in multiple comparisons (27 correlations in total), there is considerable covariance due to the derivation of FA from AD and RD and from the anatomical relation of the constituent optic radiations, therefore p values were not corrected for multiple comparisons.

4.4 Results

4.4.1 Effect of Scanner

No significant difference was found between the AVIC group (n=13) and the FMRIB group (n=30) at the 6 month timepoint on an unrelated samples t-test of whole brain TBSS results (p0.425)

4.4.2 Effect of Amiloride

None of the whole brain TBSS analyses showed any significant differences between the amiloride and placebo groups. (figure 4.3 and table 4.1)

Figure 4.3. Schematic showing total number of whole brain TBSS FA comparisons made to assess for a drug effect of Amiloride (12 separate t-tests, A-L).

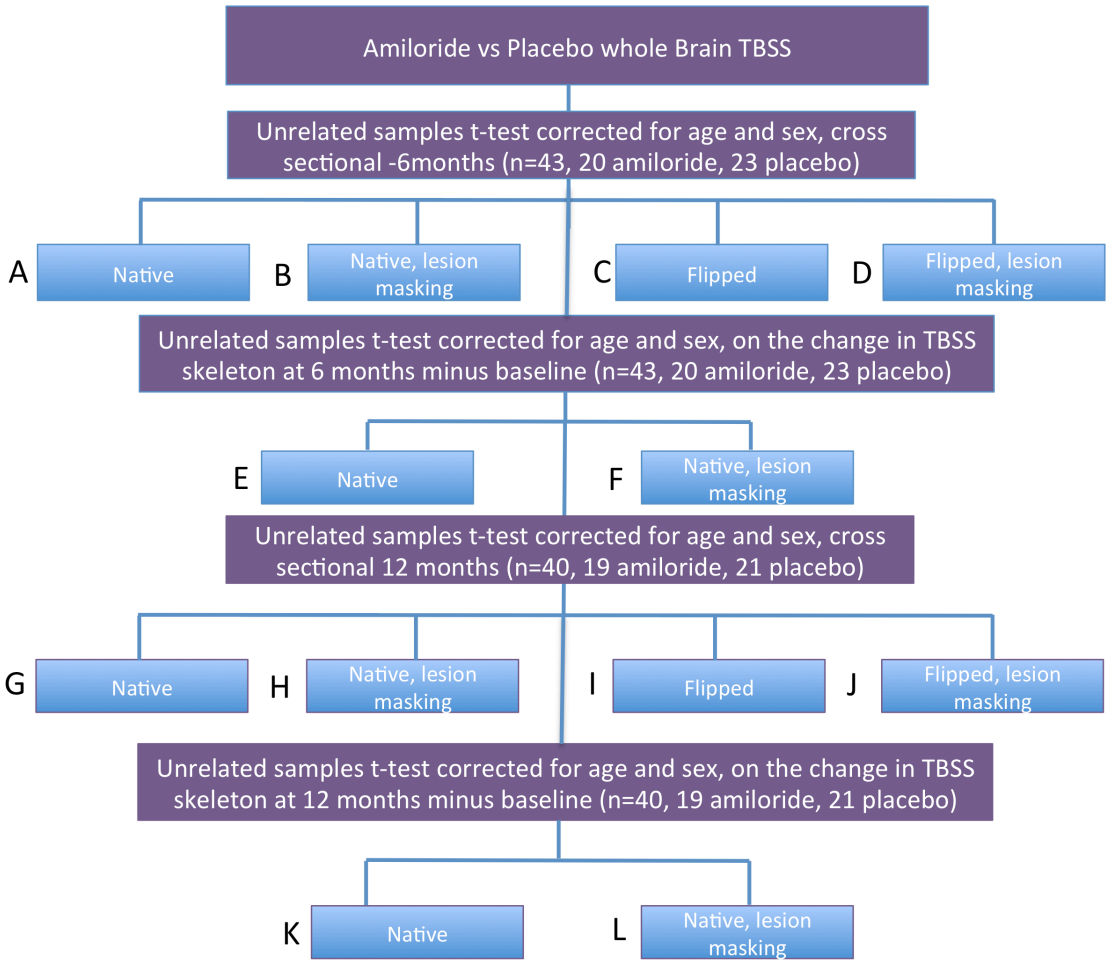

Table 4.1. Unrelated samples t-test of the comparisons in figure 1, corrected for age and sex

	p		p
A	0.203797	G	0.168249
B	0.25813	H	0.190265
C	0.246617	I	0.152292
D	0.210866	J	0.134114
E	0.37666	K	0.657241
F	0.183397	L	0.421531

In the OR ROI analysis of differences between amiloride and placebo groups, of the 108 comparisons performed, 2 results showed a signficant difference

between amiloride and placebo groups. The raw value for mean AD in the right optic radiation in cross-sectional analysis of the 6 and 12 month timepoints in the non-lesioned sub-group analysis (n=18), the amiloride group having a 5% smaller AD than the placebo group at both timepoints (p 0.014 for both). However, when assessing for differences in the change in AD in this subgroup of patients in the Right OR, there was no significant difference found between amiloride and placebo groups. Given the number of comparisons being made and the lack of support from the corresponding analyses, it seems likely that this is a result of multiple comparisons being made and does not represent a significant difference between groups.

Thus, it was concluded there was no effect from amiloride in the data, and when assessing for differences over time the whole group was analysed.

4.4.3 Whole brain TBSS analysis

The initial analysis of whole brain FA was performed separately for the native data with masks and without masks and the flipped data with and without masks.

F-tests from a repeated measures ANOVA assessing the effects of time in all 4 types of analysis are shown in figure 4.4, and the minimum p values are shown in table 4.2. The results of these analyses showed that the addition of lesion masks and flipping of the data did not significantly alter the pattern of results on the F-test, with all 4 types of analysis showing areas of significant change in relation to timepoint.

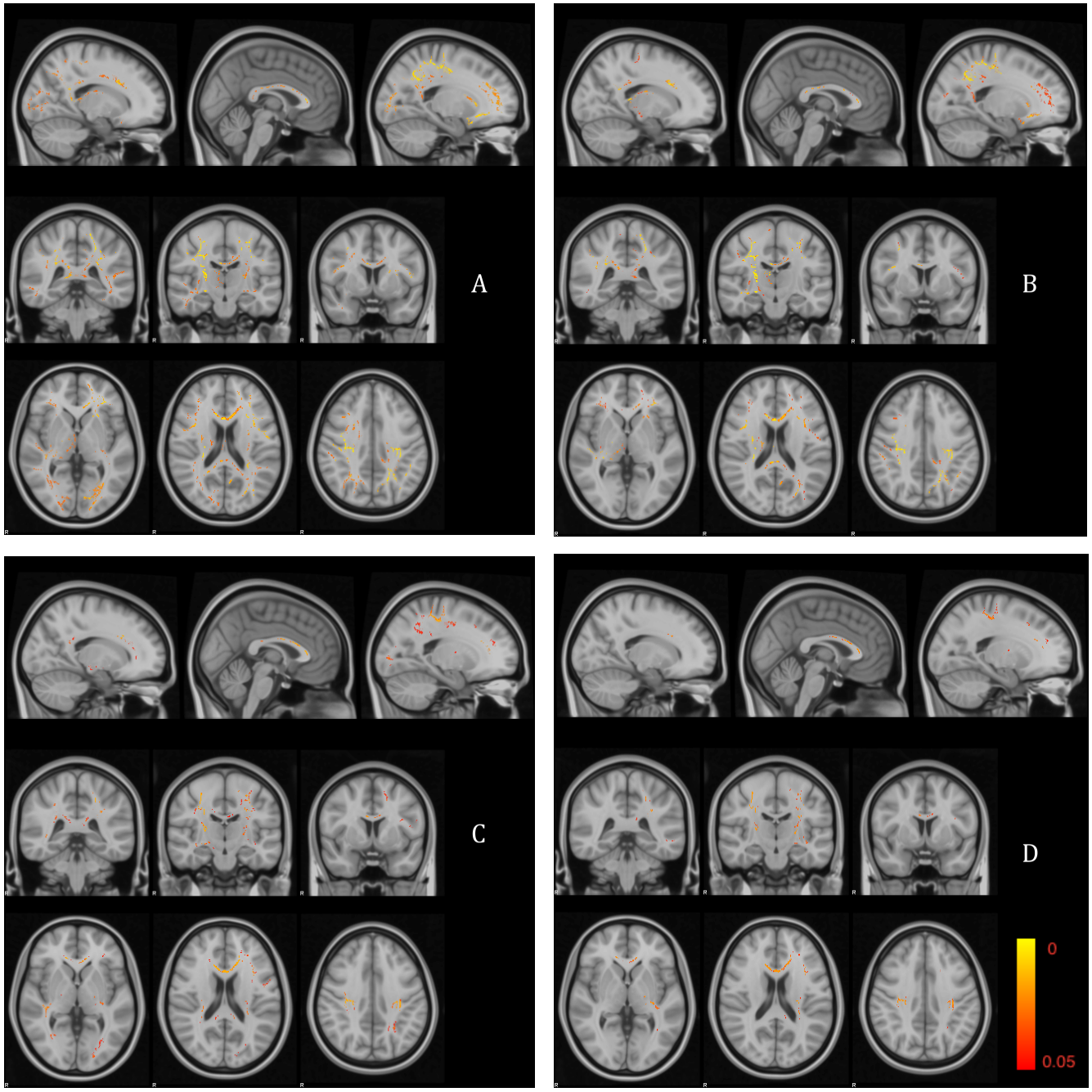

Figure 4.4 The effect of flipping the data and lesion masking the FA data on significant clusters in TBSS repeated measures ANOVA of the effect of timepoin on FA. In each panel the overall effect of time (the F-test on the ANOVA) is shown, thresholded at p ≤ 0.05 on TFCE corrected outputs. A = native data with n lesion masking. B= Native data with lesior masking. C=Flipped data with no lesion masking, D= flipped data with lesion masking.

	Native	Native, with lesion masks	Flipped	Flipped, with lesion masks	Lesions only (n= 22)	No lesions (n=18)	Flipped, Lesions only (n=22)	Flipped,no lesions (n=18)
F-test - any affect of time (p)	**0.000201**	**0.000201**	**0.002019**	**0.002019**	**0.007877**	0.284185	**0.051505**	0.146637
6 months > baseline (p)	0.373864	0.297516	0.386992	0.329832	0.547768	0.135528	0.706322	0.158756
Baseline > 6 months (p)	0.218542	0.251868	0.220157	0.258534	0.162795	0.304585	0.181377	0.195314
12 months > baseline (p)	**0.005857**	**0.004241**	**0.012725**	**0.007069**	0.09594	0.092911	0.099576	0.133307
Baseline > 12 months (p)	**0.008685**	**0.006665**	**0.013129**	**0.018582**	0.105837	**0.025853**	0.102	**0.026055**
12 months > 6months (p)	0.15714	0.107453	0.327207	0.253484	0.116138	0.776813	0.111695	0.611594
6 months > 12 months (p)	0.367401	0.192486	0.516865	0.514846	0.592204	0.22965	0.68572	0.406383

Table 4.2, Repeated measures ANOVA assessing the effect of time on FA between the 0, 6 and 12 month timepoints (n=40), and the constituent pairwise analyses. The smallest p value is shown for each and significant values of p < 0.05 are highlighted in bold. The pattern remains the same regardless of which input is used in all patients. (flipped, unflipped, with or without lesion masking) However splitting into lesioned and non-lesioned patients reduces the power to detect change.

Analysis was also performed on the lesioned and non-lesioned subgroups (table 4.2), however neither of these analyses showed any interpretable significant result - the F-test was significant with no significant t-tests in the non-lesioned patients, and in the lesioned patients the F-test was not significant, rendering the borderline significant pairwise test non-robust (12 months greater FA than baseline p 0.03).

Given the extensive computational demands of adding lesion masks to such a large dataset with long analysis times (several days) and the inherent problems with lesion masking discussed above, subsequent analysis of AD and RD and crossing fibres analysis was performed in native space without lesion masks on the whole group of patients.

4.4.4 Changes in Diffusivity scalars over time

Clusters significant on F-test at the 0.05 level corrected for multiple comparisons across voxels from an ANOVA over time corrected for age and sex are shown for FA, AD and RD. All three scalars showed significant differences over time across multiple brain regions, including in the optic radiations (figure 4.5).

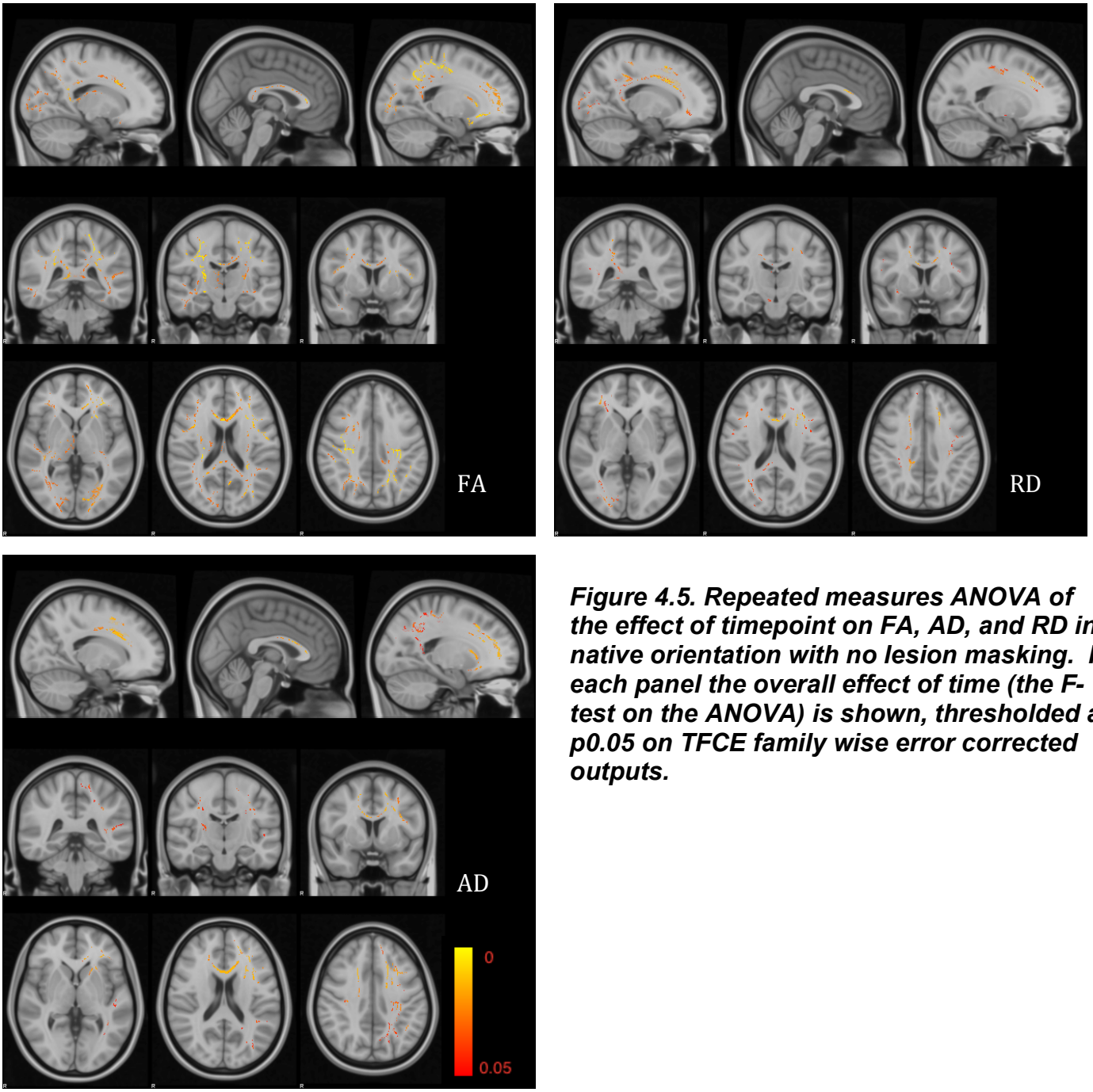

Figure 4.5. Repeated measures ANOVA of the effect of timepoint on FA, AD, and RD in native orientation with no lesion masking. In each panel the overall effect of time (the F-test on the ANOVA) is shown, thresholded at p0.05 on TFCE family wise error corrected outputs.

Pairwise analysis, with the significance threshold raised to $p \leq 0.01$, showed significant clusters in areas where 12 months FA, AD and RD were significantly higher than at baseline as displayed in figure 4.6. The surviving area for FA was a small cluster at the crossover between the superior longitudinal fasciculus and the corticospinal tract. AD showed more widespread areas of increase over time (including the corpus callosum, left cortico-spinal tract and superior longitudinal fascicle), but these were accompanied by increases in the

corpus callosum in RD, resulting in no significant increase in FA over 12 months in this region.

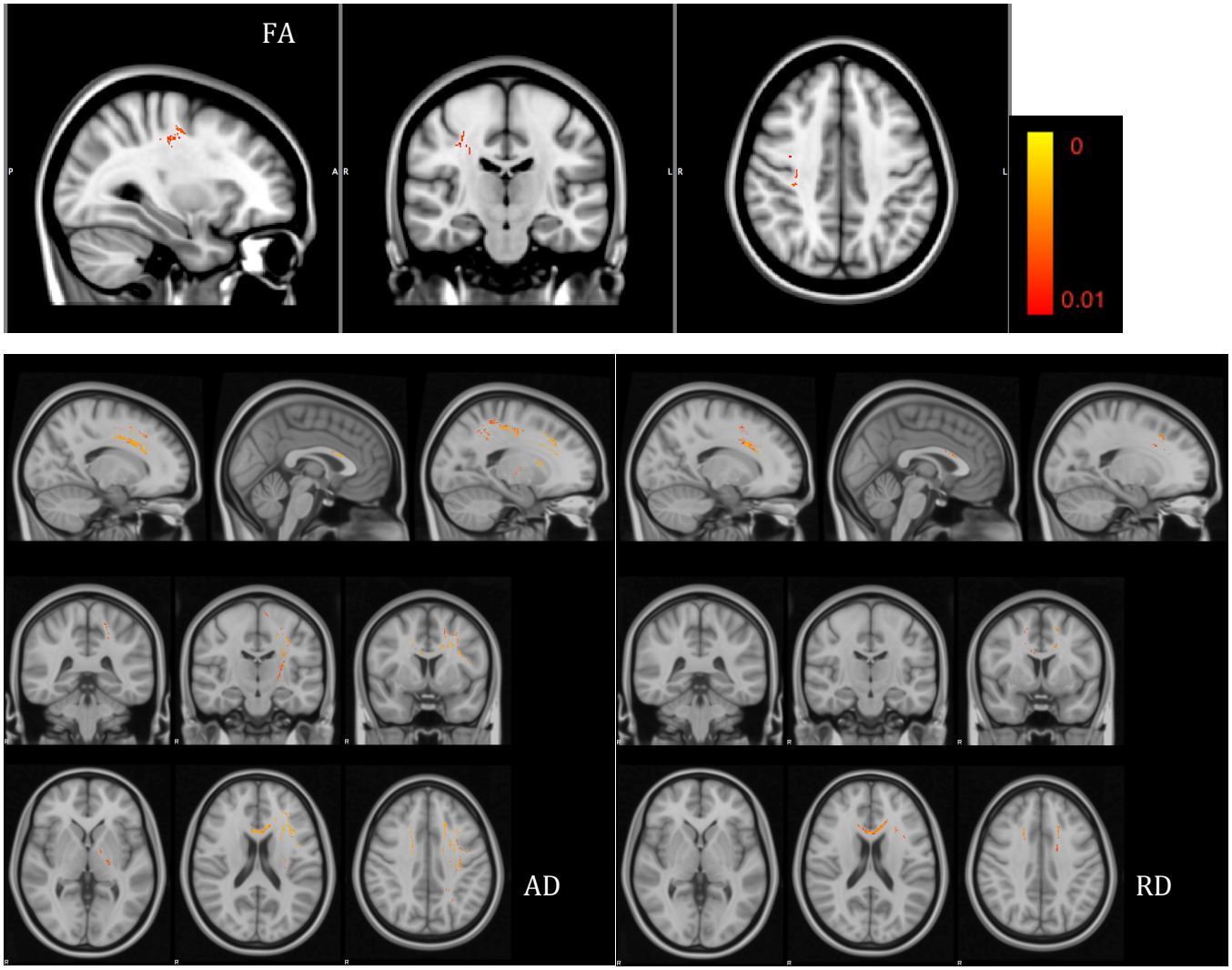

Figure 4.6 Pairwise analysis from ANOVA of effect of time (corrected for age, sex and treatment group), displaying areas where values at 12 months were higher than baseline. In view of multiple comparisons, significance value of p ≤ 0.01 was set on TFCE family wise error corrected outputs. Only a small cluster in an area of crossed fibers survived in FA (cross over between superior longitudinal fasciculus and cortico-spinal tract). More widespread changes are observed in AD and RD.

In the pairwise analysis of areas with lower diffusivity scalars at 12 months compared to baseline, both FA and AD had small significant clusters. (Figure 4.7) In FA this was in the right corpus callosum, and in AD there were some small clusters around the right occipito frontal fascicle and the corpus callosum. There were no significant changes in this pairwise analysis in RD, however the areas of RD that increased over time in the corpus callosum are consistent with the fall over time in FA.

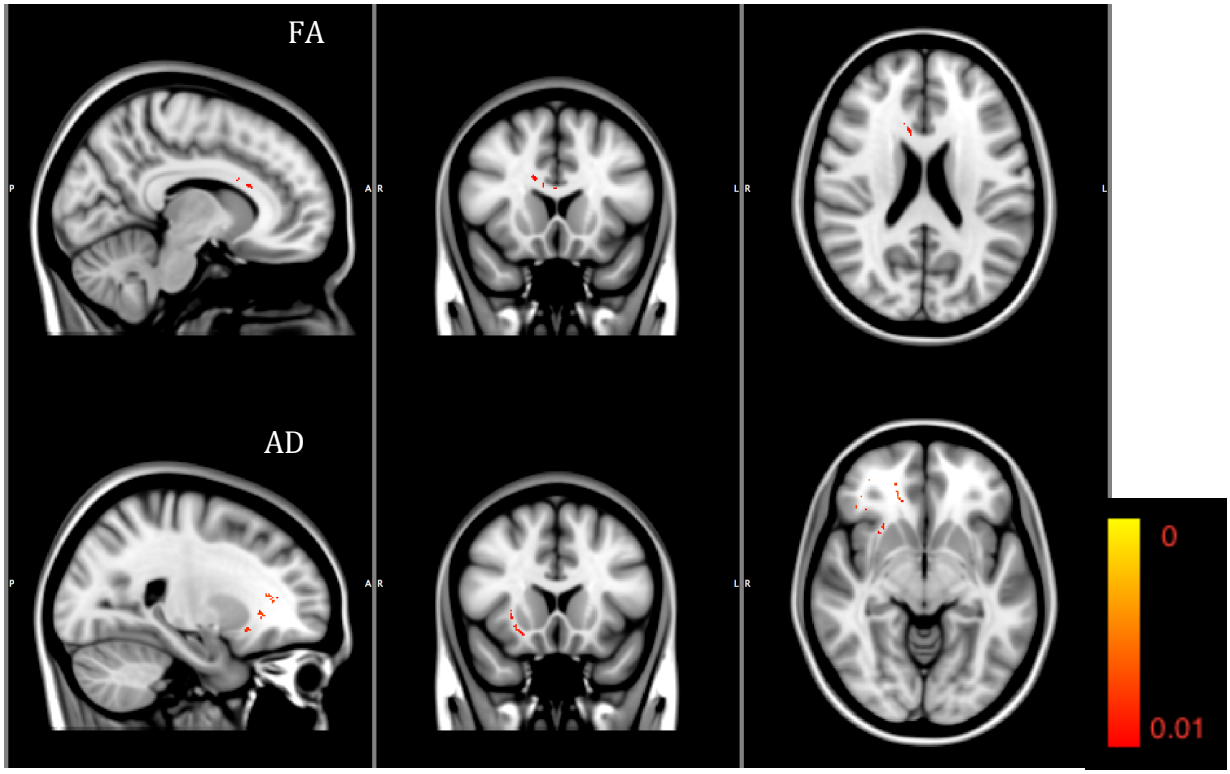

Figure 4.7 Pairwise analysis from ANOVA of effect of time (corrected for age, sex and treatment group), displaying areas where values at 12 months were lower than baseline. In view of multiple comparisons, significance value of p ≤ 0.01 on TFCE family wise error corrected outputs. In FA a reduction in FA was shown in the corpus callosum, in AD reduction was shown in the right superior occipito-frontal fascicle and subcortical frontal white matter. No clusters in RD survived to this level of significance.

AD had a small cluster in the left corpus callosum that increased from 6 months to 12 months (not shown) but otherwise the pairwise analyses did not show any significant changes between baseline and 6 months or between 6 and 12 months.

4.4.5 Crossing Fibres analysis

Crossing fibres analysis did not reach significance in any voxel in the F-test ANOVA over time in either the first or second diffusion direction (p 0.117 and p 0.503 respectively, not shown).

4.4.6 Region of Interest (ROI) analysis in the optic radiations (OR)

4.4.7 Changes over time

A repeated measures ANOVA of FA, AD and RD over time did not show a significant change over time in any of the whole group analyses. In the sub group analysis of the lesioned patients there were no significant changes over time. In the sub group analysis of the non-lesioned patients, there was one significant F-test in analysis of AD in the left optic radiation (p 0.033) driven by a pairwise analysis showing that there was a significant drop in AD between 0 and 6 months, but no other differences between 0 and 12 and 6 and 12 months (Figure 4.8).

Figure 4.8 Change in diffusivity scalars over time in OR ROI analysis. Error bars represent 95% confidence intervals of the mean

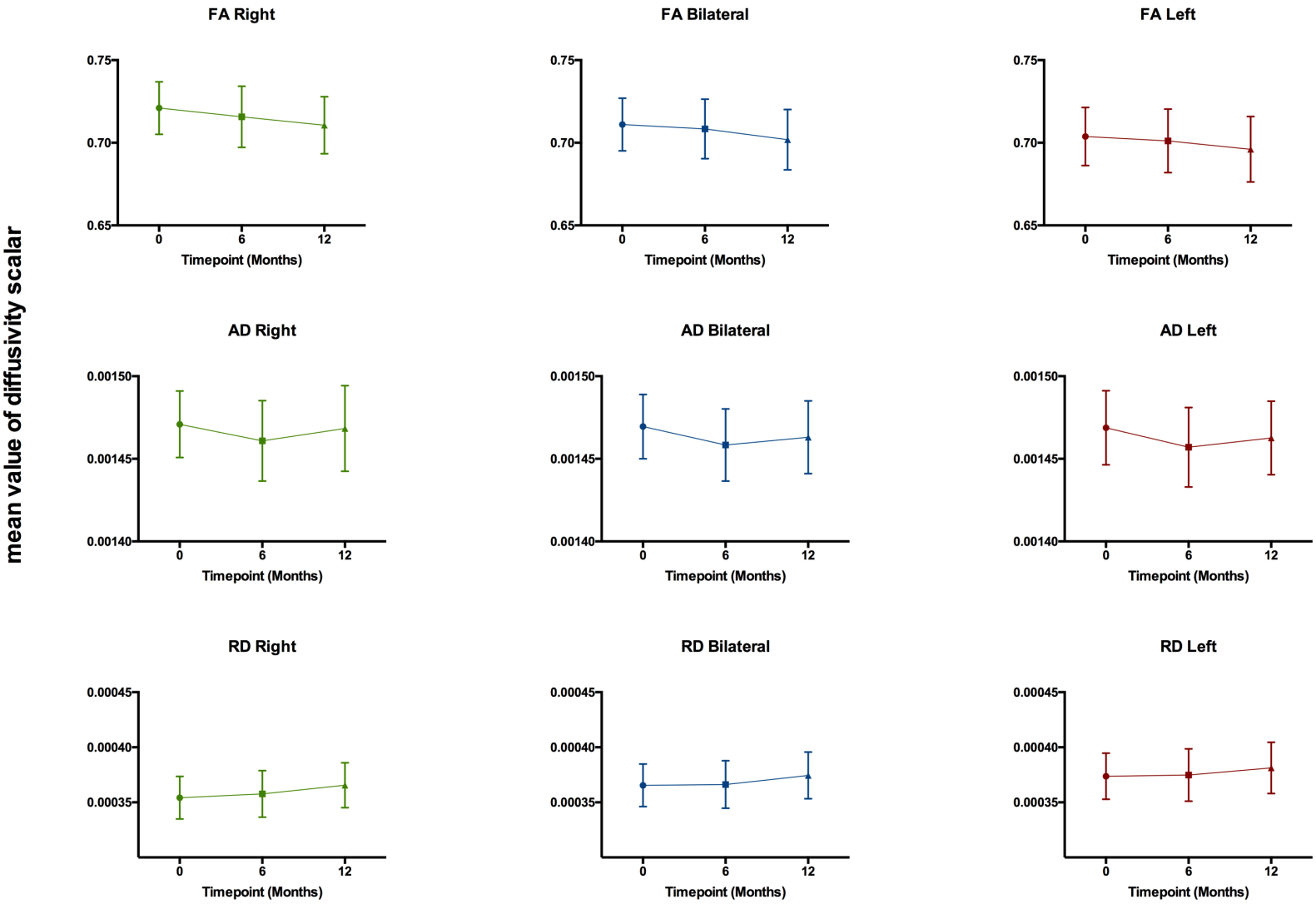

4.4.8 Correlations

Change in diffusivity scalars over time had several significant correlations with change in GCL volume on OCT. The whole group correlations at 6 months are shown in table 3a and for 12 months in table 3b. Correlations strengthened at 12 months compared to 6 months. In the whole group, FA correlations were found bilaterally, right and left (figure 4.9) and a corresponding negative correlation was found in bilateral and right RD (figure 4.10). In the sub group analysis of lesioned and non lesioned patients 1 out of 9 correlations were significant to the $p < 0.05$ level in each - right FA in lesioned patients and bilateral RD in non-lesioned patients (Figures 4.11 and 4.12).

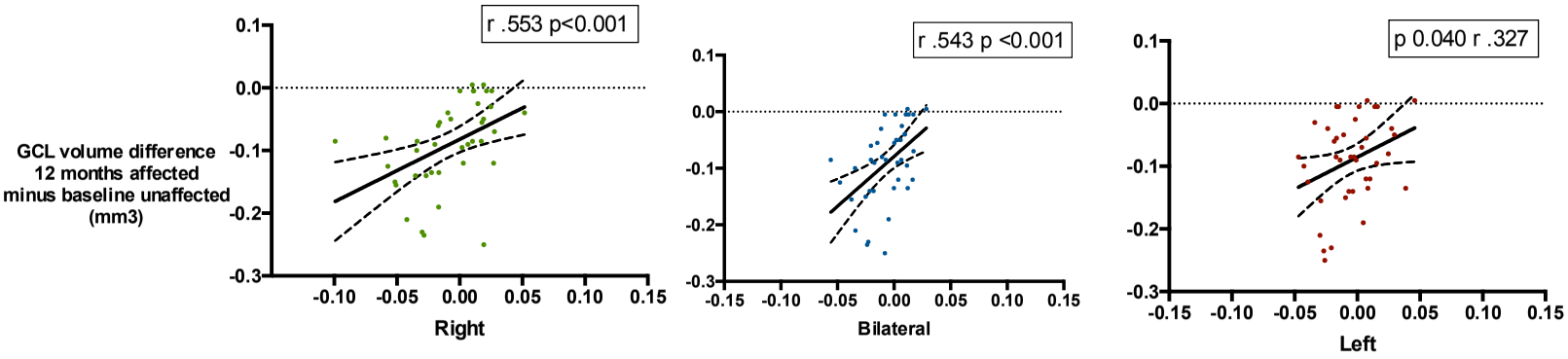

Figure 4.9. Correlations between GCL volume change on OCT and change over tir in FA of OR RC analysis. Straig lines represent the best fit line correlation, an the curved line represent the 95% confidenc interval of the linear correlati

Diffusivity Scalar		*Bilateral FA*	*Right FA*	*Left FA*	*Bilateral AD*	*Right AD*	*Left AD*	*Bilateral RD*	*Right RD*	*Left RD*
6 months (n=43)	r value (spearmans)	.333*	.473**	0.22	0.235	0.259	0.063	0.191	-.373*	-0.196
	Sig. (2-tailed)	0.029	0.001	0.156	0.129	0.093	0.687	0.221	0.014	0.208
12 months (n=40)	r value (spearmans)	.553**	.543**	.327*	0.185	0.159	0.178	-.496**	-.531**	-0.297
	Sig. (2-tailed)	0	0	0.04	0.253	0.326	0.273	0.001	0	0.063

Tables 4.3. Correlation co-efficients between G volume change on OCT and change in diffusivit scalars at 6 months (A) and 12 months (B)

Figure 4.10. Correlations for whole group at 12 months beween GCL on OCT and change in remaining diffusivity scalars (AD and RD). Significant correlations are shown boxed above the respective scatter plot. Straight lines represent the best fit linear correlation, and the curved lines represent the 95% confidence interval of the linear correlation

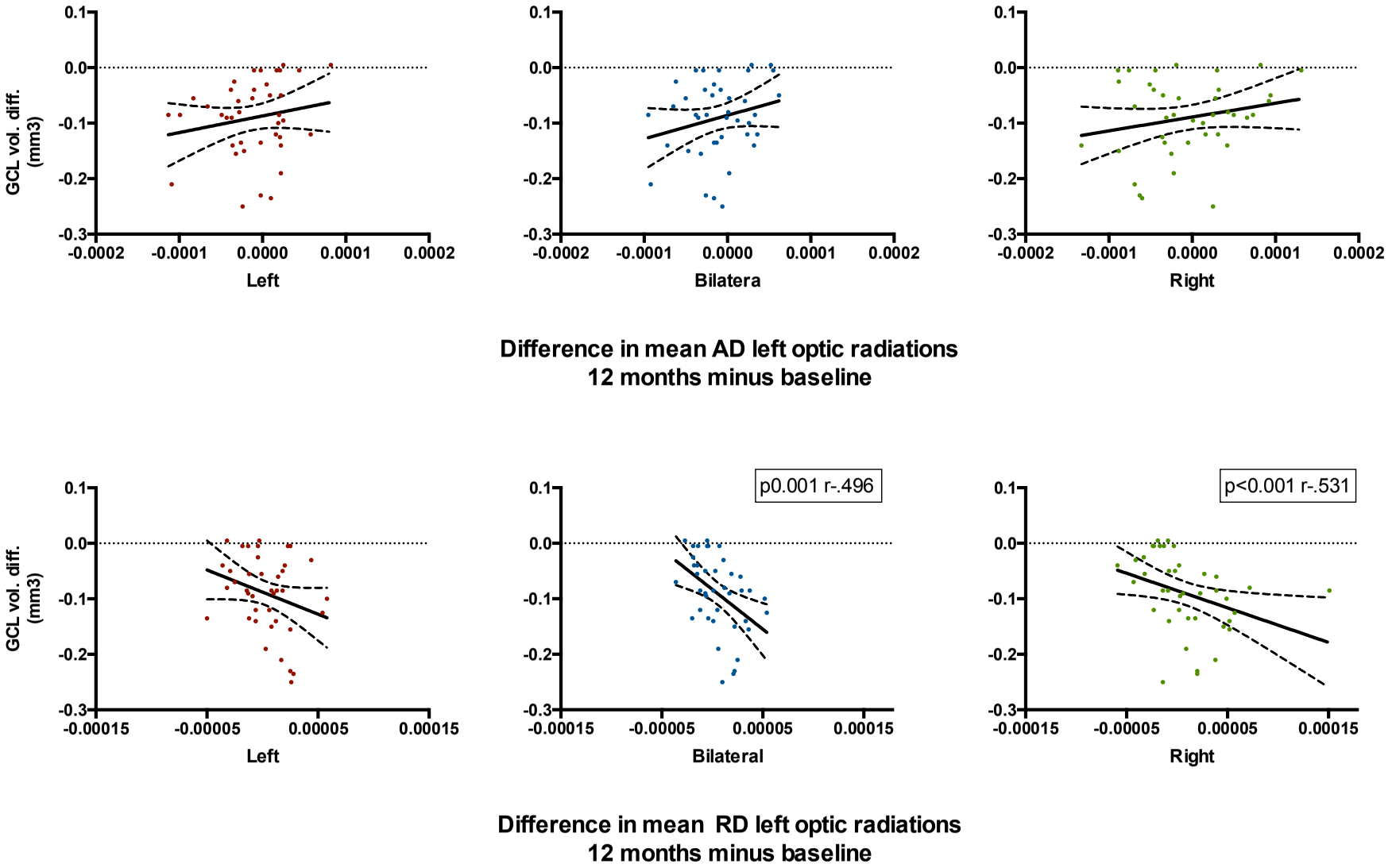

Figure 4.11. Correlations for non lesioned only sub group (n=18) at 12 months beween GCL on OCT and change in diffusivity scalars (AD and RD). Significant correlations are shown boxed above the respective scatter plot. Straight lines represent the best fit linear correlation, and the curved lines represent the 95% confidence interval of the linear correlation

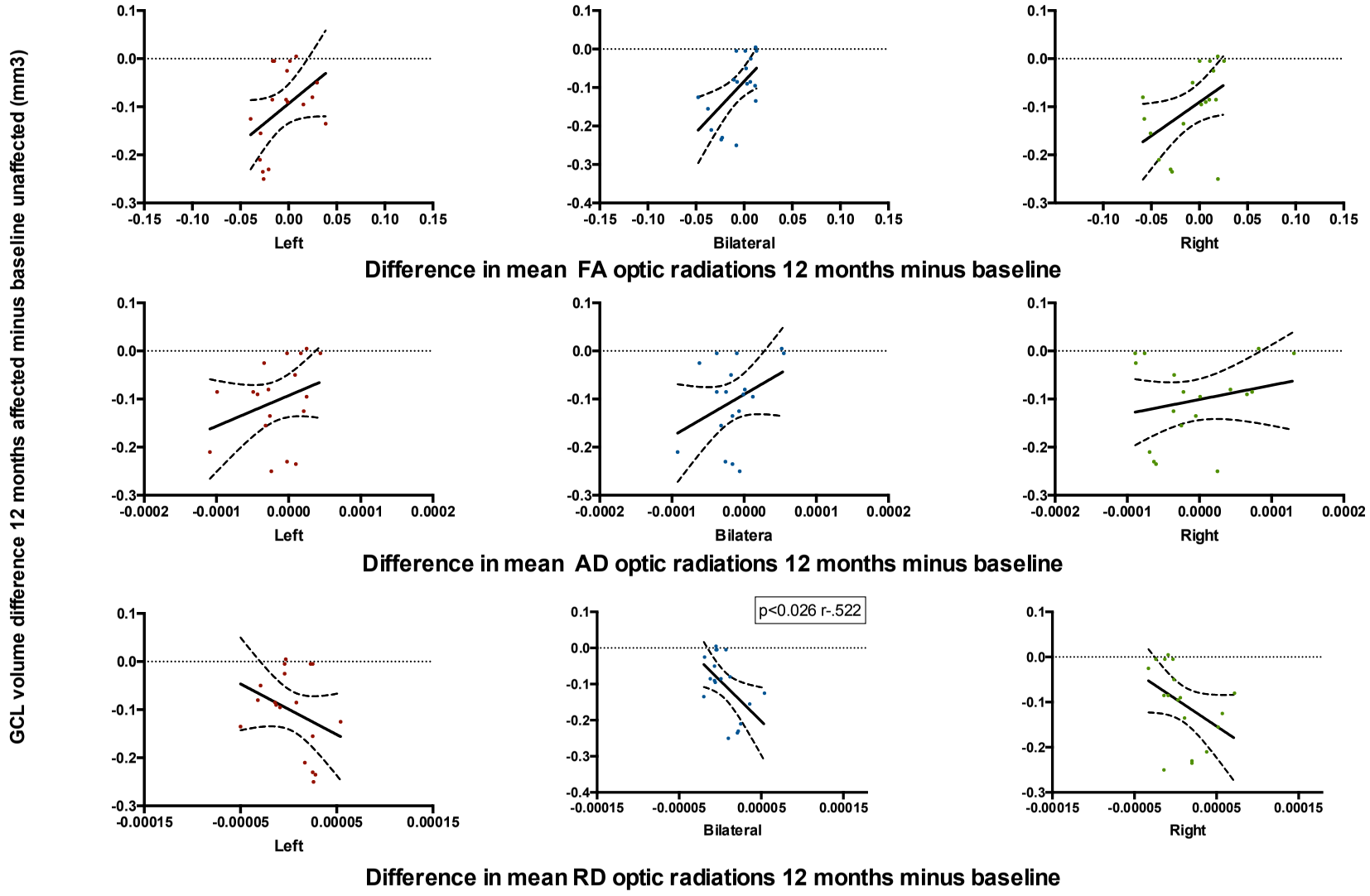

Figure 4.12. Correlations for lesioned only sub group (n=22) at 12 months beween GCL on OCT and change in diffusivity scalars (AD and RD). Significant correlations are shown boxed above the respective scatter plot. Straight lines represent the best fit linear correlation, and the curved lines represent the 95% confidence interval of the linear correlation

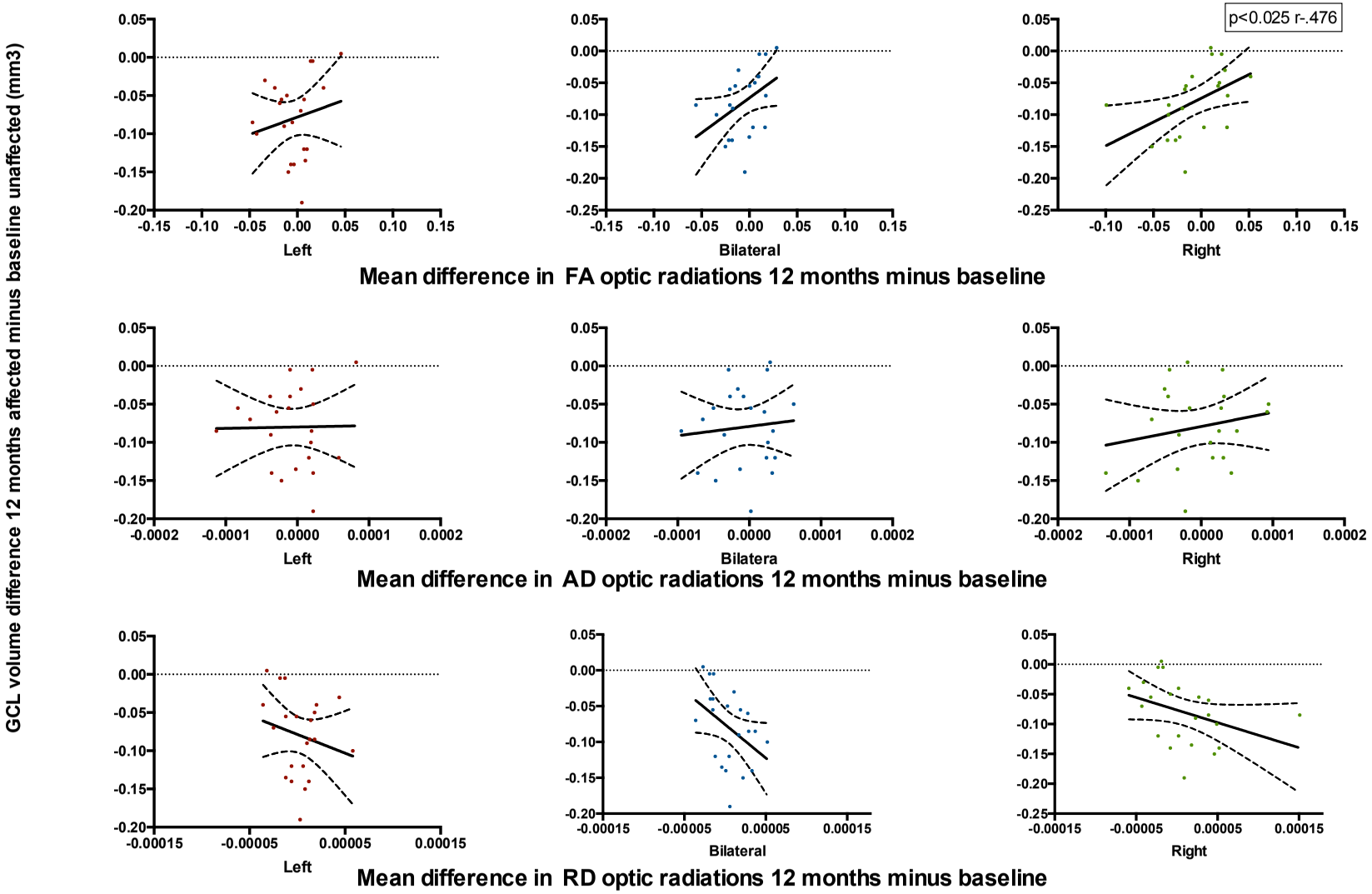

4.5 Discussion

This is the first longitudinal study of optic radiation DTI and GCL volume on OCT. It shows strong correlation between damage over time in the anterior visual pathway following optic neuritis, and change over time in the postsynaptic optic radiations in metrics of white matter integrity. These correlations strengthened between the 6 and 12 month timepoints, suggesting an evolving relationship of transsynaptic neurodegeneration. In isolation, this result suggests that transsynaptic neurodegeneration occurs in anatomically relevant areas of the posterior visual pathways following optic neuritis.

However, the data as a whole reveals a somewhat less clear picture.

The results of the whole brain analysis are less succinct. Whilst the overall comparison did show an effect of time on the whole brain diffusivity scalars, the direction and anatomical location of the changes were not as expected apriori - they did not show reduced white matter integrity in the OR.

One unexpected finding was that the ANOVA over time was driven in part by numerous regions appearing to show increased FA, and therefore an increase in white matter integrity over time, between 0 and 12 months following optic neuritis. However these changes fell in regions where white matter fibres of different orientation crossed over – crossing fibre regions. For example, there was a significant increase in FA in the region where the corticospinal tract crosses the superior longitudinal fasciculus in the right hemisphere. The model of a single tensor for a voxel which contains multiple fibre orientations is problematic in interpretation,

thus the initial TBSS results are difficult to interpret in these regions. This was further explored by applying a model with two fibre orientations to the whole brain data, however this analysis failed to show significance in the ANOVA over time in either fibre orientation.

It is possible that beyond the technical explanation of crossed fibre areas giving results that are hard to interpret, that the increase in FA could be driven by a biological mechanism. In particular the superior longitudinal fasciculus is an area that is integral to the ventral stream and has been found to be linked to motion perception (165). Motion perception, though not tested in the ACTION trial, has been shown to be a domain of vision that has a sustained deficit after other visual domains have improved (166). There is some evidence that the ventral stream, which includes the superior longitudinal fasciculus, is not fully mature until the fourth decade of life (167). Thus, while by no means conclusive, the possibility that our FA findings relate to some degree of adaptive structural plasticity in response to ON remains, and that in the superior longitudinal fasciculus there is an increase in white matter integrity.

A clear finding from the whole brain analysis however, is that contrary to the pre-analysis hypothesis, no significant change over time was found in the optic radiations. Furthermore, whilst there was a trend for a reduction in FA over time in the OR, this did not reach significance in this dataset. This may reflect a powering effect, however it is interesting to note that other regions - chiefly the corpus callosum, did show a reduction in FA over time in this study.

The reduction in corpus callosum could be explained by the fact that it is the largest white matter tract in the brain, with good fibre coherence, making it highly amenable to study with the single tensor model in DTI. Given we were studying mainly CIS patients who were at risk of developing MS, a fall in white matter integrity in this

region could be representative of the global neurodegenerative process in such a cohort (168), reflected in an area of high sensitivity. Moreover CIS patients have been shown to have identifiable atrophy of the corpus callosum as early as one year in longitudinal studies (169).

Another potential reason for the paucity of change in diffusivity scalars in the OR over the 12 month follow up period, could be the contribution of *cortico* geniculate fibres that provide *efferent* connections from the cortex to LGN. Such fibres are thought to have a role in enhancing receptive field properties of LGN cells, and increasing the gain of reticulogeniculate transmission and synchronising network activity in a stimulus specific manner (170). Such fibres are thought to account for a large proportion of OR fibres between the cortex and LGN, and may affect the rate at which transsynaptic neurodegeneration would be evident in an analysis such as this.

4.5.1 Limitations

The contribution of white matter lesions to these findings is not certain. Sub-group analysis of non-lesioned patients was likely to be underpowered to detect these findings, as subgroup analysis of both groups, lesioned and non-lesioned patients, resulted in a non-significant ANOVA in the former, and no significant pairwise tests in the latter. The addition of white matter lesion masking did not appear to alter the results of the whole brain analysis for FA. It may be that the limited change from lesion masking in this longitudinal dataset is due to a limited contribution to groupwise trends from individual subjects heterogenously located lesions with differing degrees of change in diffusivity scalars over one year. However, due to the computational cost and uncertain benefit of the lesion masking technique it was not pursued for further analysis.

Whilst TBSS is the leading method of analysing diffusion data which is highly automated and therefore reduces user bias and increased reproducibility, there are limitations inherent to its use. The major limitation relates to areas where more than one tract with different fibre orientations intersect, as discussed above (171). However it is important to remember that both the TBSS and ROI analysis in this chapter depend on registrations to standard space, derived from control data, that can be imprecise for individual subject anatomy. In the ROI analysis this was limited by choosing the TBSS defined central (peak FA) fibres from OR tract, in an area in standard space known to be dominated by OR. However, this did mean I ignored sections of OR proximal to the LGN that curve postero-medially and are hard to separate from other fibres. User intensive seed and target based probabilistic tractography may have increased the area of OR that could be analysed. However, even with such techniques, the anterior curved portion of the OR is often not analysed in reported studies due to unreliability, and for group analysis, registration steps are still required (145). Nevertheless, the previous study that did find a significant change over time in FA in a linear mixed effects model over 12 months following ON (without OCT data) used a seed and target approach (149).

In addition, whilst a 12 month follow up period of longitudinal data is useful, transsynynaptic neurodegeneration is likely to be an ongoing phenomenon over several years, as has been shown for retrograde degeneration in RNFL from lesions in the visual cortex (172). Cross-sectional studies of the OR in ON patients have concluded that whilst diffusivity scalars show reduced white matter integrity in patients with a previous history of ON, the changes correlate with volume OR white matter lesions, rather than OCT metrics - suggesting that wallerian degeneration from white matter lesions in MS can mask transsynaptic neurodegeneration. In NMO patients, who albeit are likely to have severe optic neuritis, the confounds of lesions and global neurodegeneration are less prominent. Such patients have been found to

have marked reductions in FA cross-sectionally across whole brain FA measures, compared to controls (173). The data in this chapter shows some evidence of a trend in reduction of OR FA within one year, and a correlation with neurodegeneration in the visual system in a longitudinal dataset. However more prolonged longitudinal follow up would be useful in determining the long term contribution and outcome from transsynaptic neurodegeneration.

4.6 Conclusions

In this study, for the first time, the longitudinal degree of loss of DTI-measures of white matter integrity in the OR correlate with OCT measures of longitudinal neurodegeneration following optic neuritis, which suggests process transsynaptic neurodegeneration following ON. Whole brain DTI measures of white matter integrity show more complex longitudinal changes following ON, with cautious evidence of secondary visual areas showing an increase in white matter integrity following ON, which is a potential sign of adaptive plasticity following optic neuritis. Further work is required to assess the role of white matter lesions in these changes, the long term change in the OR beyond 12 months, and to confirm the relation of the secondary visual changes to visual function following optic neuritis.

5 Chapter 5. Longitudinal Changes in Resting State FMRI following optic neuritis

In this chapter we explore how resting functional connectivity (FC) changes over in the visual system, and assess if this relates to the degree of retinal neurodegeration and visual recovery.

5.1.1 Functional MRI (fMRI) - the blood oxygen level dependent (BOLD) response.

Functional MRI (fMRI) is an integral tool in neuroscience to probe brain activity in experimental and pathological conditions (174). FMRI is based on detecting the blood oxygen level dependent (BOLD) response in the brain (175) in response to stimuli.To assess the BOLD response whole brain, T2* weighted images are collected sequentially forming 4 dimensional datasets, and changes in signal intensity during a task or stimulus are compared with those collected at rest. When an area of the brain is metabolically active, vasodilation occurs, initially increasing the flow of deoxygentated blood. This contains paramagnetic deoxyhaemoglobin, which results in reduced MRI signal, thereafter, an influx of oxygenated blood containing diamagnetic oxyhaemoglobin, resulting in an increased MR signal. Measured fluctuations in this T2* weighted signal are then analysed across the brain.

5.1.2 Resting state fMRI

In addition to task related changes in BOLD signal, fluctuation in the BOLD signal whilst subjects are studied at rest have consistently been identified in fMRI data (176). These networks of activation in the “resting state” have been shown to anatomically correspond to activation networks in task-based fMRI (177).

Activation in the medial parietal , bilateral inferolateral parietal and ventromedial frontal cortices are some of the most consistent and strongest networks identified in the resting state and they are termed the “default mode network” (178). Peri-calcarine, medial occipital and lateral occipital cortex activation, are also readily identifiable networks in the resting state. These correspond both to areas known to be related to vision and that respond to visual stimulation on fMRI (56, 177) and are termed visual resting state networks. Thus, resting state functional MRI (RSfMRI), can be used as an alternative to task-based fMRI in order to assess changes in FC in domains of function, such as vision, under experimental and pathological conditions.

This strategy of studying FC at rest has several advantages over a task-based paradigm. On a practical level, it does not involve additional instructions or equipment for patients, which makes it less complicated to perform for patients undergoing an acute and distressing event. It also speeds up acquisition which allows us to maximise the use of time in the scanner. Furthermore, performance of tasks is variable across subjects, particularly in patient groups who may be at risk of cognitive impairment, and this can confound the results of task-based MRI.

5.1.3 Functional plasticity in ON and previous RSfMRI studies in ON.

A number of studies have demonstrated that patterns of activation differ in MS and ON patients compared to controls in stimulus and task-based fMRI, suggesting that such patients undergo functional plasticity. This is particularly evident in higher and extra striate visual areas (179-181) . Early functional plasticity in the lateral occipital complex has been shown to convey an improved visual recovery (182), but otherwise, the adaptive advantage of increased FC appears uncertain.

Moreover, FC changes within resting state brain networks, and whether they are adaptive or maladaptive following optic neuritis, are less fully elaborated, and do not have longitudinal studies reported. Whilst all published studies have identified abnormalities in resting state networks compared to controls, all are cross-sectional, using different analysis techniques, and the nature of the abnormalities has differed - some studies have shown increased FC in visual networks whilst others have shown reduced FC following ON. Furthermore, studies assessing correlations between OCT changes in the pRNFL have failed to show a clear relationship between the degree of damage in the retina and the degree of variance in FC within study groups.

Whilst in one study (183) OCT pRNFL correlated with the degree of reduced intra-hemispheric connection between the right and left visual cortices, these were early patients (mean 50 days post ON) and thus, these results may have been confounded by pRNFL swelling. Using a seed-based approach analysing areas of connectivity with V1 in the striate cortex, this data also showed reduced FC in the ON group compared to healthy controls (183). In a separate cross-sectional analysis of MS patients with a history of ON compared to those without, increased FC was found in the peristriate visual cortex in the former, however no correlation with OCT pRNFL was found (184). Other studies have found differences in the medial visual component in MS patients (a quarter of whom had a history of ON) and controls, and correlations in this area cross-sectionally between RSfMRI FC in the same network and visual processing speed in the MS group (185). Another group studied ON patients in whole brain RSfMRI parameters and found widespread differences between ON and healthy controls (77, 186).

5.2 Aims

In the previous chapter, whole brain analysis of diffusion measures showed some evidence of increased white matter integrity in secondary visual areas, and reduction in white matter integrity in the OR dependent upon neurodegeneration in the retina following ON. In chapter 3, 2.5% LCVA was shown to be highly correlated with GCL volume on OCT, but GCL volume did not explain the entire variance in LCVA (R^2 0.33). Moreover, adding other retinal layers to a multiple linear regression model failed to increase the explained variance in LCVA. Given the longitudinal resting state data collected in this study afforded not only the opportunity to look for functional neuroplasticity in RSfMRI, but also to examine the adaptive or maladaptive nature of those changes in the context of clinical and OCT data in the same patients, my aims in this study were;

- To assess for an effect of amiloride in resting state FC
- To assess for change over time in FC in visual resting state networks, default mode networks, and a control network (sensory/auditory network)
- To assess whether changes in FC correlated with visual function as assessed by 2.5% LCVA
- To assess whether changes in FC correlated with neurodegeneration as assessed by GCL volume on OCT
- To assess whether the variance in correlation between GCL volume on OCT and 2.5% LCVA, could be explained by changes in FC in RSfMRI.

5.3 Methods

5.3.1 OCT acquisition and processing and visual testing

OCT and 2.5% LCVA data was acquired and processed as described in chapter 2

5.3.2 MRI scan acquisition

All scans were collected on a Siemens Verio 3 tesla MRI scanner with a 32 channel head coil.

Structural Imaging. The same 3 dimensional described in chapter 4 (MPRAG sequence with voxel size 1x1x1mm, TR 2040ms, TE 4.7ms, 1 average, acquisition time = 5m 56s) was used.

Functional MRI - BOLD signal detection for resting state data. During resting state acquisition, participants were in the the MRI scanner and asked to “close your eyes and think of nothing”. We acquired an axial 2 dimensional echo planar imaging (EPI) sequence in an AP orientation, with 3mm slices and a voxel size of 3.0x3.0x3.0mm. Repetition time was 2410ms and echo time was 30ms. 44 slices were acquired, 1 average FOV 192x192x192mm. Acquisition time was 5 mins 16 seconds resulting in 128 EPI scans being acquired. In addition a fieldmap scan was acquired with two echo times (TR 477ms TE1 5.19ms TE2 7.65ms). An example 3D file from the 4D EPI acquisition from a single subject is given in figure 5.1

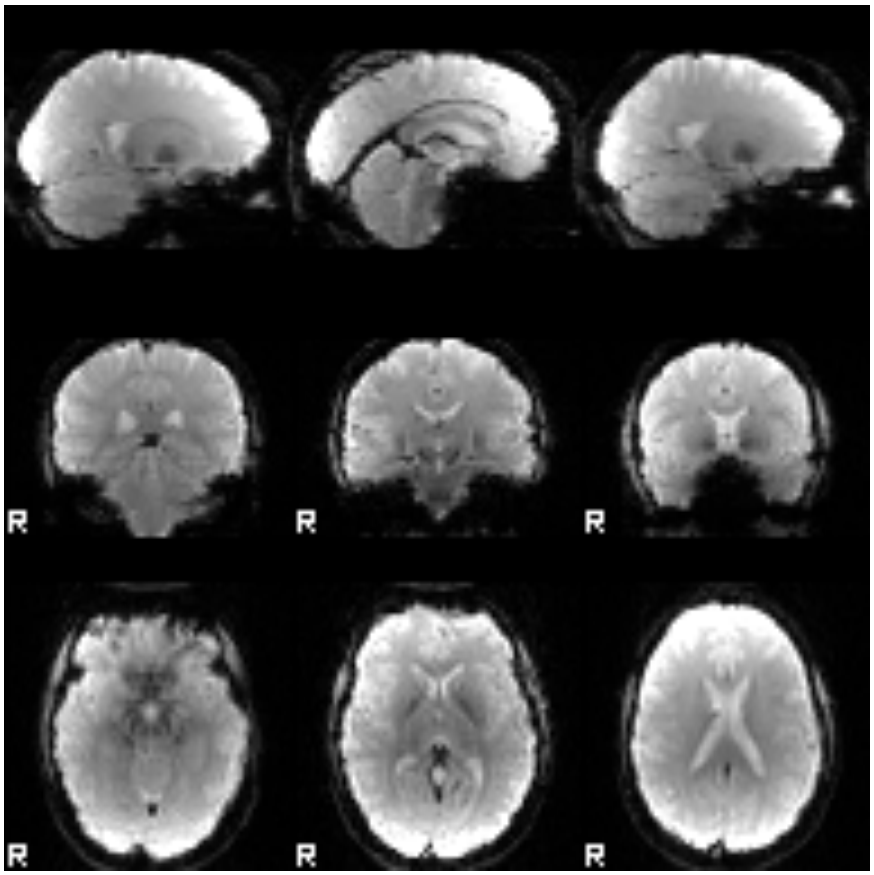

Figure 5.1 example EPI data from a single subject post fieldmap unwarping

5.3.3 Functional MRI pre-processing and group level analysis

All scans were processed using the FSL tool MELODIC (Multivariate Exploratory Linear Optimized Decomposition into Independent Components) (176, 187). The analysis seeks to identify independent components in the resting state data. Initially, at a single subject level, each FMRI time series is decomposed into independent components. The sum of each of these components are equal to the original data. Some of these components will be derived from noise - eg subject head motion or motion and field disturbance from cardiac and respiratory cycles, alongside signal from resting state activity. Fortunately, most of the components driven by noise follow a gaussian distribution in their frequencies - ie are normally distributed, random and unstructured. By contrast most of the true signal components are non-

gaussian in the distribution of their frequency – ie do not follow the normal distribution, are structured and create signal due to a biological process. Therefore in independent component (IC) analysis, we can separate the signal into potential components, and those that are most non-gaussian are most likely to represent the underlying data (188). At the single subject level the number of independent components was unrestricted.

Prior to performing group analysis we used the FSL FIX tool which removes noise components from each subject's FMRI time series before entering into the group level analysis (189, 190). This required training data that is best derived from manual review of subjects in the dataset rather than using standard training sets which are vulnerable to artefact from use of different scanners and different scan settings. The aim of this is to reduce the contribution of noise to the pre-processed fMRI data and therefore use more signal for analysis.

I created a data-specific training set by manually reviewing the independent components from 10 randomly selected subjects (2 at baseline, 4 at 6 months and 3 at 12 months) and labelled components as either true resting state signal or as noise eg motion artefact, or physiological (cardiac and respiratory, white matter, CSF) noise. I assigned these labels on the basis of reviewing the time series, temporal power map and spatial map for each component in the training sets. This was then fed into FIX. Following this, each subject then had a new 4D echo planar imaging file which had been "cleaned" of noise and was registered to the standard space MNI template.

Following the first level analysis, the subjects were then temporally concatenated - (meaning that each FMRI timeseries was placed after the other). In order to achieve

this, subjects FMRI data was registered into standard 2mm MNI space using FNIRT (154), after the post-FIX structural data had been registered to the subjects own structural T1 image using FLIRT (191, 192). Following this concatenation the entire multi-subject data set was deconstructed to 25 components, a similar dimensionality reported in key resting state papers (176, 177). At the group level, I also tested increasing the number of components to 35 components, however this resulted in a number of components being split, and the networks were not as recognisable as those at 25. Of the networks produced, those that were included in analysis are shown in figures 5.2 and 5.3

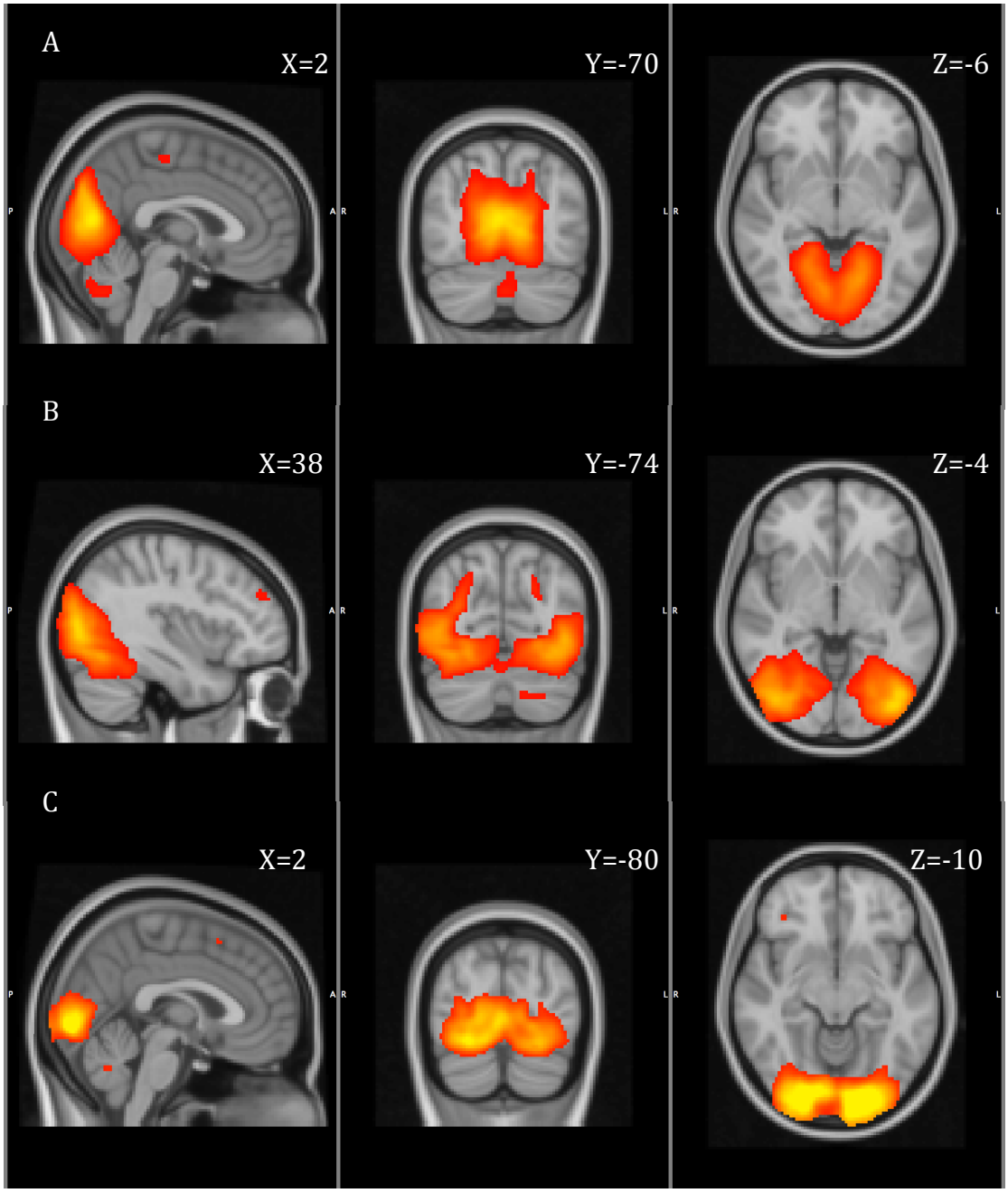

Figure 5.2. The three visual components identified from a 25 component group ICA, derived from 125 scans (39 patients at 0, 6 at 12 months, and additional 4 patients at 0 and 6 months only). Component A, medial visual network. Component B, lateral visual network. Component C, occipital pole visual network. MNI x, y and z co-ordinates are displayed.

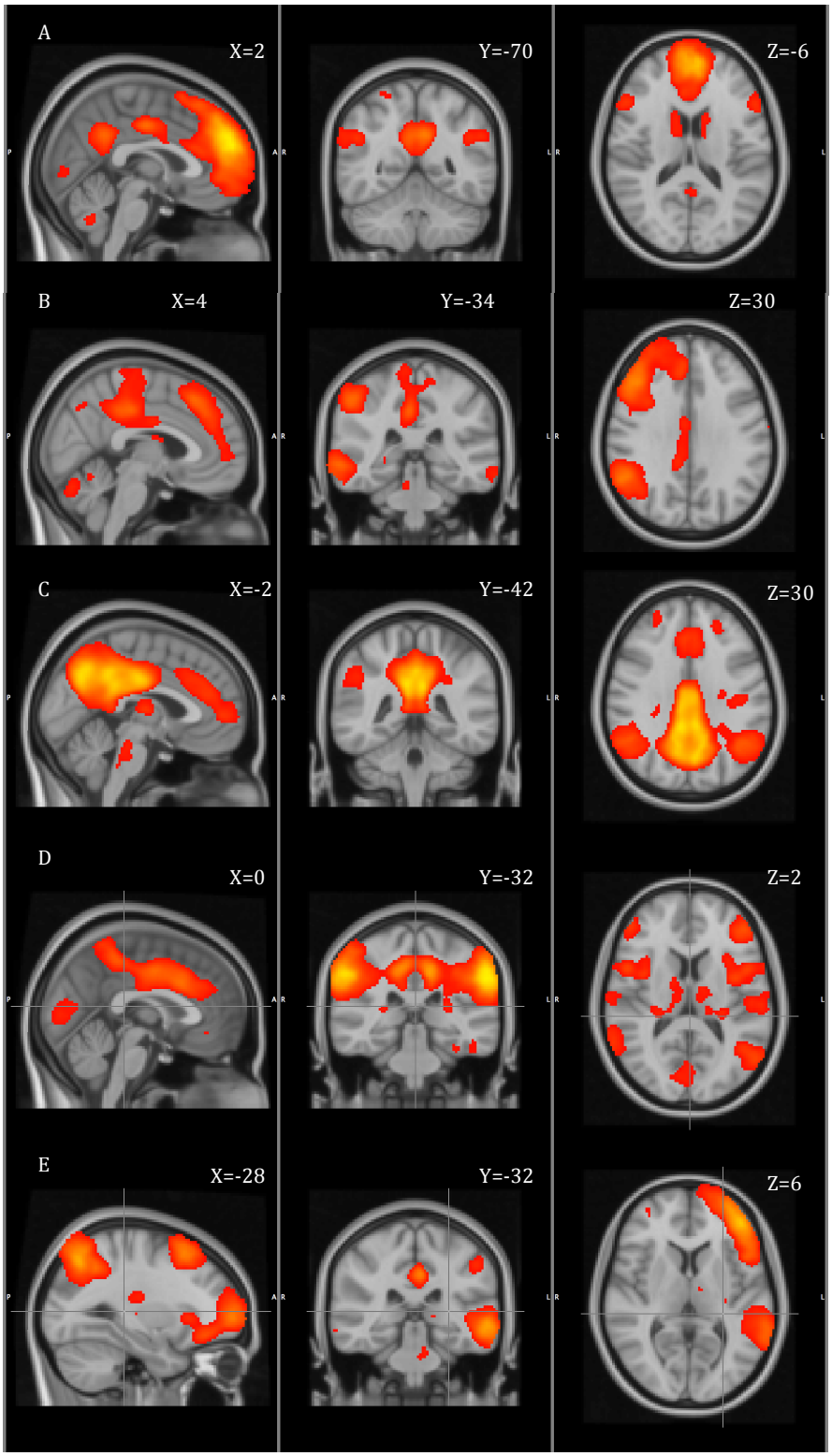

Figure 5.3. Non visual components from the 125 scan group ICA. A Executive control network. B Right frontoparietal. C Default mode network. D Mixed sensory and auditory network. E Left frontoparietal network. MNI x, y and z co-ordinates are displayed.

For all further analyses, networks created by using all scans at all timepoints were taken as the reference networks for group statistics when assessing differences between amiloride and placebo groups, and when assessing for correlations between the resting state data and visual, and retinal imaging parameters.

The FSL statistical tool *dual regression* was then used. The set of spatial maps from the group-average analysis was used to generate subject-specific versions of the spatial maps, and associated timeseries, using dual regression (193, 194). First, for each subject, the group-average set of spatial maps is regressed (as spatial regressors in a multiple regression) into the subject's 4D space-time dataset. This results in a set of subject-specific timeseries, one per group-level spatial map. Next, those timeseries are regressed (as temporal regressors, again in a multiple regression) into the same 4D dataset, resulting in a set of subject-specific spatial maps, one per group-level spatial map. Each subject's resulting spatial map has slightly different areas of activation to the group map, reflecting the degree of connectivity in that individual. Thus we can then test for differences in groups, and look for correlations between RSN data and clinical and OCT data using FSL's *randomise* permutation-testing tool.

5.3.3.1 Comparing amiloride and placebo groups

An unrelated samples t-test was performed separately for 6 months and 12 months between the placebo and amiloride groups using dual regression technique, incorporating *randomise* with 5000 permutations, corrected for age and sex. For this and all analyses described in this chapter using *dual regression* and *randomise,* the statistics were corrected for multiple comparisons across voxels (family wise error) and spatial clustering support was used to verify areas of significance using threshold-free cluster enhancement (TFCE) in FSL (164).

In addition, for each subject, running dual regression meant that for each IC of interest, there was a subject and timepoint specific map of activation (stage 2 of dual regression), each registered to standard space. Using FSL maths, the longitudinal change in connectivity between timepoints could be calculated by subtracting these maps at 6 or 12 month map from the baseline map. This calculated statistical map is hereafter referred to as the “difference” map, and it represented the change in areas of activation between the two timepoints, and allowed me to compare the change in the two groups over time in the GLM, using *randomise* with 5000 permutations, corrected for age and sex.

5.3.3.2 Assessing change over time

Dual regression with *randomise* was again used to assess for change over time in selected ICs, and family wise error corrcted TFCE was again used to correct for multiple comparasons across voxels. A design matrix for an ANOVA was composed which included exchangeability block as in chapter 4, to ensure permutation testing only occurred within subject, respecting the repeated measures structure of the data.

As per chapter 4, F-tests on ANOVA were initially inspected with a significant p value of 0.05. Each ANOVA had 6 individual t-tests (base > 6 months, 6 months > base, base > 12 months, 12 months > base, 6 > 12 months, 12 > 6 months), therefore for t-tests only voxels with a p value of ≤ 0.01 were considered significant.

5.3.3.3 Correlating resting state data with LCVA, OCT data and residual of correlation between OCT and GCL

The retinal measure chosen for correlation was again OCT derived GCL volume, consistent with the previous chapter. The visual measure chosen for correlation with

RSN change was 2.5% LCVA, given that it was found to have a strong correlation with GCL volume in chapter 3. For each, the input into correlation with difference maps were the difference between the unaffected fellow eye at baseline and the visual or OCT measure at 6 or 12 months. Then, I attempted to assess if the "additional" variability in vision, not explained by GCL volume, could be explained by changes in RSN FC. For this, the standardised residual was extracted for each subject from the best fit in a linear regression of the change at 6 or 12 months affected eye, minus unaffected eye at baseline between 2.5% LCVA, and GCL volume on OCT. This residual value was then used as the input for a further regression with change from in RSN FC. This variable is referred to hereafter as the "residual".

OCT, visual and residual variables were correlated with the difference maps using *randomise*, and spatial maps of correlation between the variable and the IC were produced. Correlations were initially run uncorrected, but later corrected for age and sex. Only the visual networks were selected for these analyses, however, due to the number of comparisons being made (3 variables, 3 visual ICs, two timepoints), a significance threshold for clusters was set at $p \leq 0.01$.

5.3.3.4 Assessing for motion artefact

One concern regarding longitudinal change in RSfMRI networks is that motion artefact is not spread evenly across timepoints. At the baseline timepoint when patients are having their first MRI not long after a new diagnosis of ON, more subject movement in the scanner due to anxiety could be provoked than at follow up timepoints where the subject is more familiar with trial procedures.

Motion artefact was identified and corrected in pre-processing by two methods. Inherent to the MELODIC pipeline is the FSL MCFLIRT (192) motion correction tool which corrects for subject motion between slices using FLIRT. Furthermore, as part of the FIX de-noising of data (189, 190) further motion artefact was removed. The likely presence of motion artefact affecting BOLD signal can be assessed by the DVAR value (195). VAR refers to the variance in the root mean squared (RMS) signal change across the brain, and the D refers to the temporal derivative of this value in the 4D data set. Thus, the DVAR calculates the change in variance in signal intensity across the whole brain between timepoints. Uncorrected head motion between volumes would contribute to a high DVAR value.

Following FIX and MELODIC de-noising of the data, using a pre-prepared matlab script, DVAR values were averaged for the whole time series for each subject at each timepoint. DVAR values for each timepoint were then reported to assess the amount of motion artefact left in the data. Values of greater than 20 in DVAR are suggested to reflect a high degree of motion artefact (196). To assess for significant change over time in this indicative statistic of motion artefact, values were fed into a related samples Friedman's analysis of variance due to the non parametric distribution of the 6 month DVAR values on Shapiro Wilk testing of distribution. This was performed in IBM SPSS v 22.0

5.4 Results

5.4.1 Motion parameters

Mean DVAR results from each timepoint were less than 20 (regarded as a threshold for a "high" DVAR (196) for all groups and were fairly consistent (15.77, baseline,

16.84, 6 months, 16.67, 12 months). Contrary to the apriori expectation there was a higher DVAR at 12 months, suggesting a slight increase in motion artefact at 12 months. A subsequent Friedman's ANOVA analysis did show that there was a significant effect of time on DVAR (p 0.018) and this was driven by the difference between baseline and 12 months on pairwise analysis (p 0.005).

5.4.2 Effect of Amiloride

The medial visual network did show a cluster that had significantly less connectivity in the amiloride group at 6 months, this was significant at the 0.05 level (p = 0.0201), however, this was not in a grey matter area (posterior corpus callosum). Furthermore, an unrelated samples t-test of the change from 0 to 6 months showed no significant differences between groups (peak voxel p value =0.461), suggesting there was no significant difference in the change in FC in this visual network between groups. No other 12 or 6 month comparisons in the visual networks showed any difference between the amiloride or placebo groups.

Therefore the data were analysed as a whole group. For further analyses however, treatment group, along with sex and age was added as a nuisance regressor

5.4.3 Effect of time

Initially, ANOVA over time was run on the visual networks (3 networks), the default mode networks (4 networks) and the sensory/auditory network (total of 8 networks). On F test only the 3 visual networks had highly significant changes over time, and none of the non-visual networks had significant changes over time.

Table 5.1 Peak p value in a repeated measures ANOVA assessing the effect of time on FC in 8 selected networks

Network	Peak p value on F-test of ANOVA (Significant at 0.05)
Medial visual	**0.000807**
Executive control	0.068673
Lateral visual	**0.000201**
Right frontoparietal	0.689962
Main default mode network	0.238336
Occipital visual	**0.000201**
Mixed sensory and auditory network	0.178348
Left frontoparietal	0.123611

Significant clusters over time in F-test are shown in Figure 5.4 (medial visual network) , 5.5 (lateral visual network) and 5.6 (occipital pole visual network). For the medial and occipital pole visual networks the only pairwise t-test that was significant was that examining areas of greater FC at 12 months than baseline. In the lateral visual network, there was also a large cluster of increased FC between 0 and 12 months, but also a small cluster that showed increased FC from 6 to 12 months.

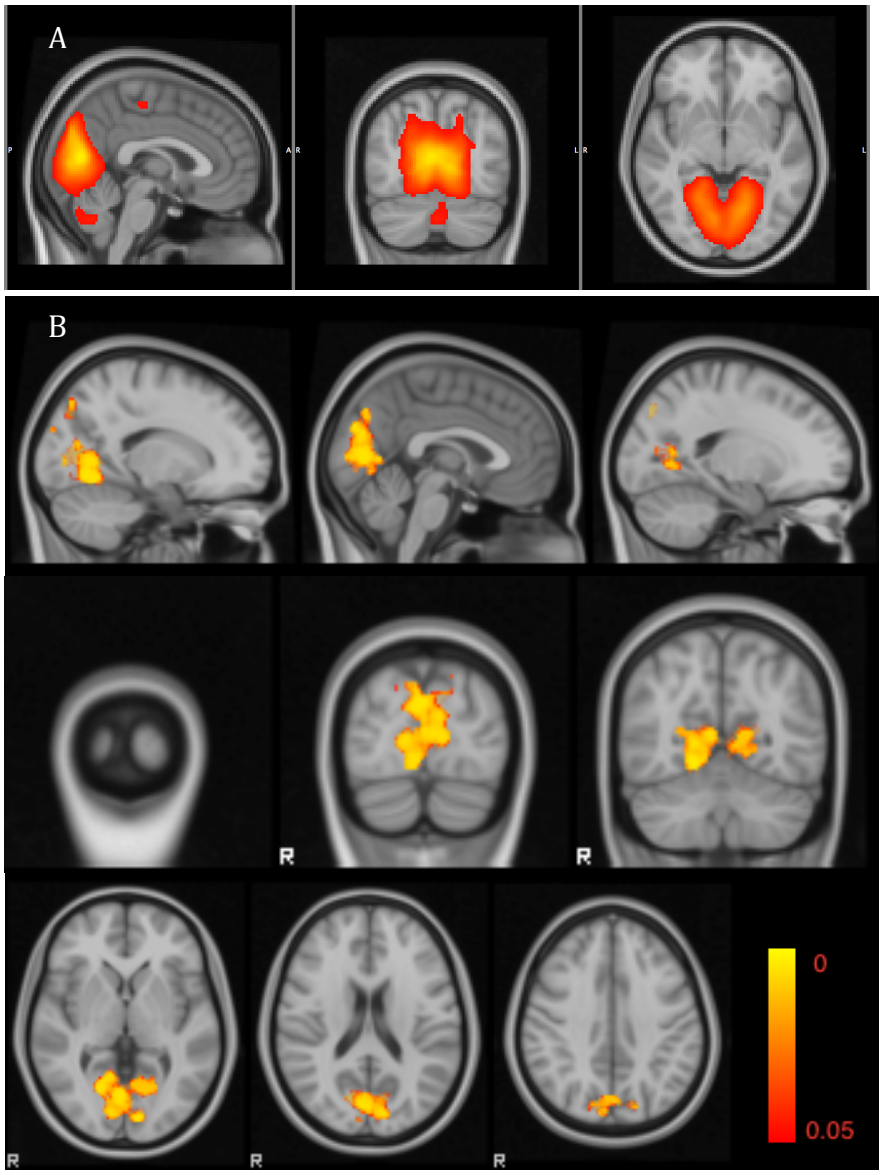

Figure 5.4. Output from ANOVA of affect of time on the medial visual resting state network, corrected for age, sex and treatment group.
A – Medial visual component from group ICA for reference.

B – F test showing any effect of time on medial visual resting state network combining all three timepoints (0,6 and 12 months), thresholded at p ≤0.05 on TFCE family wise error corrected output.

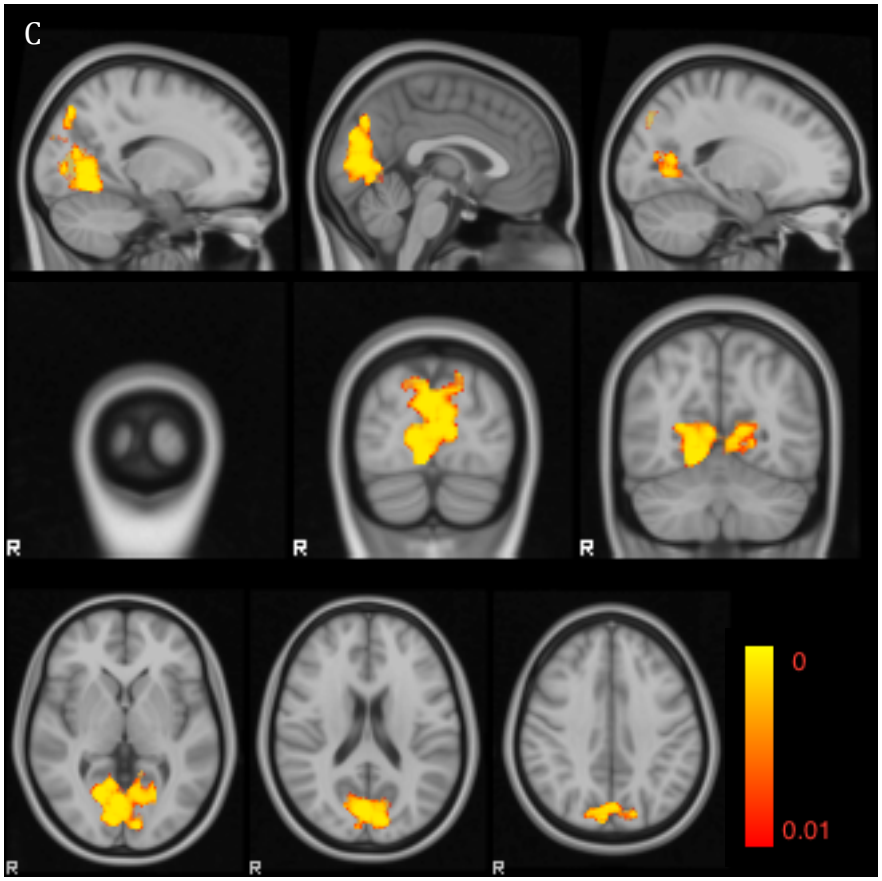

C – Increase in functional connectivity from 0 to 12 months. This was the only pairwise analysis that remained significant at a threshold of p ≤0.01 on TFCE family wise error corrected output, raised in view of multiple pairwise comparisons.

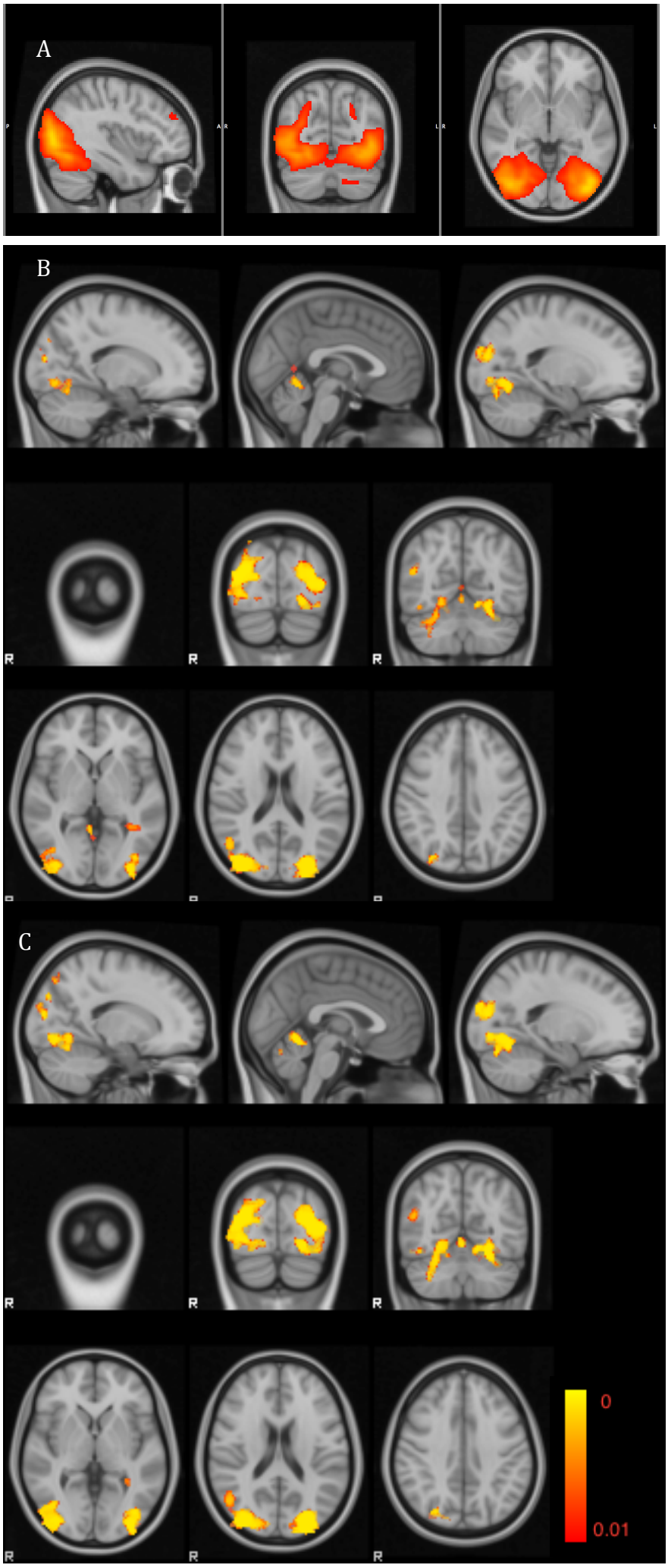

Figure 5.5. Output from ANOVA of affect of time on the lateral visual resting state network, corrected for age, sex and treatment group.

A – Lateral visual component from group ICA for reference.

B – F test showing any effect of time on medial visual resting state network combining all three timepoints (0,6 and 12 months), thresholded at p ≤0.05 on TFCE family wise error corrected output

C – Increase in functional connectivity from 0 to 12 months.

D – Increase in functional connectivity from 6 to 12 months. C &D thresholded for significance at p ≤0.01 on TFCE family wise error corrected output, raised in view of multiple pairwise comparisons.

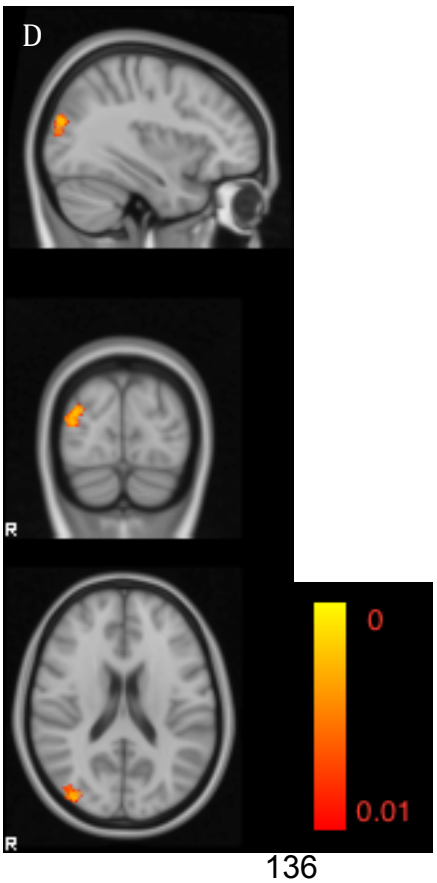

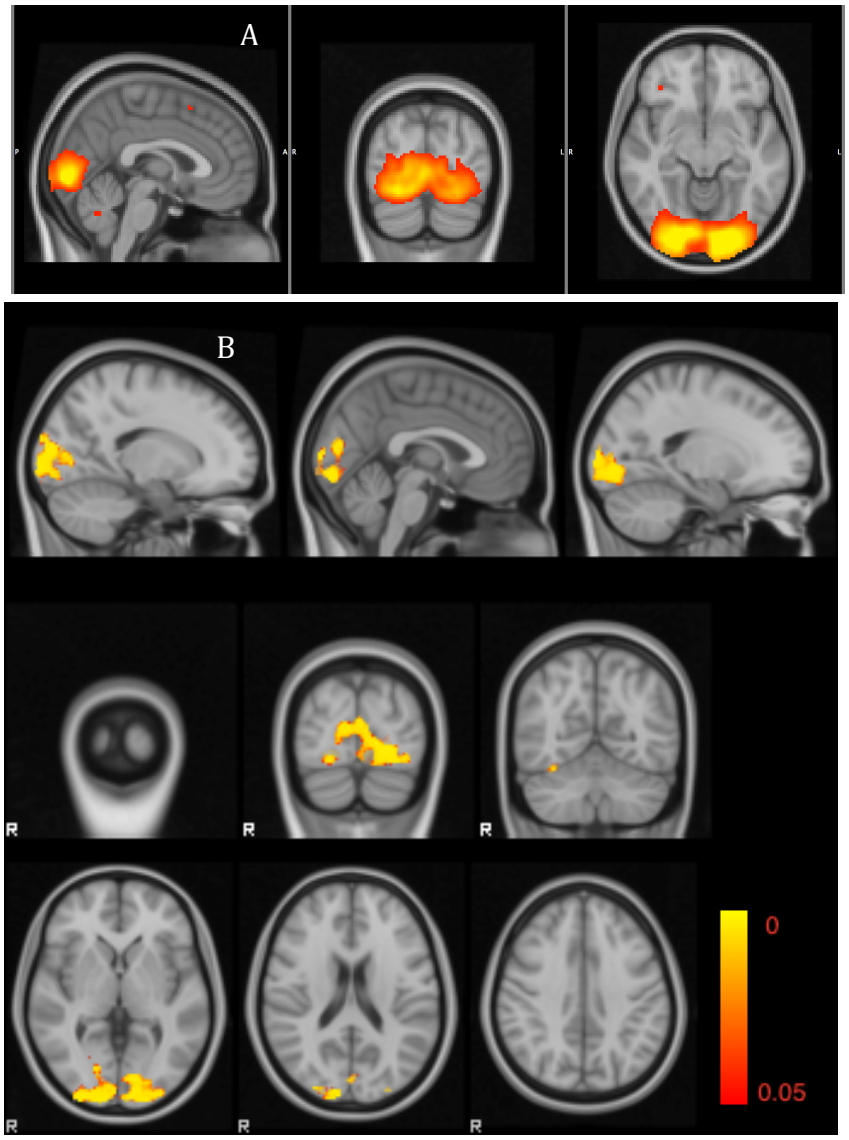

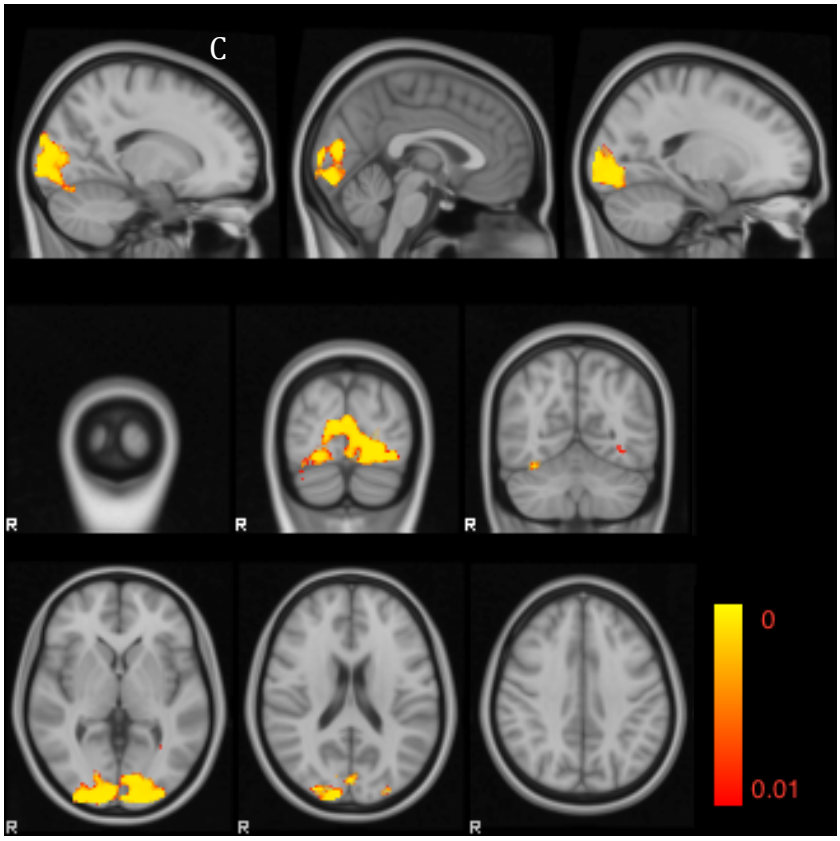

Figure 5.6. Output from ANOVA of affect of time on the occipital pole visual resting state network, corrected for age, sex and treatment group.

A – Lateral visual component from group ICA for reference.

B – F test showing any effect of time on medial visual resting state network combining all three timepoints (0,6 and 12 months), thresholded at p ≤0.05 on TFCE family wise error corrected output

C – Increase in functional connectivity from 0 to 12 months. This was the only pairwise analysis that remained significant at a threshold of p ≤0.01 on TFCE family wise error corrected output, raised in view of multiple pairwise comparisons.

5.4.4 Correlations with GCL volume and 2.5% LCVA

There were no significant correlations between the change in 2.5% LCVA and the change in visual network FC at either the 6 or 12 month timepoint

5.4.5 Correlations with *residuals*

None of the correlations between the change in visual network FC correlated with the residual between the best fit line of a regression between GCL difference and LCVA difference. At the 6 months timepoint however, the occipital pole network was just below threshold for significance, and prior to correction for age and sex, there were some areas of significant correlation. These are shown in figure 5.7

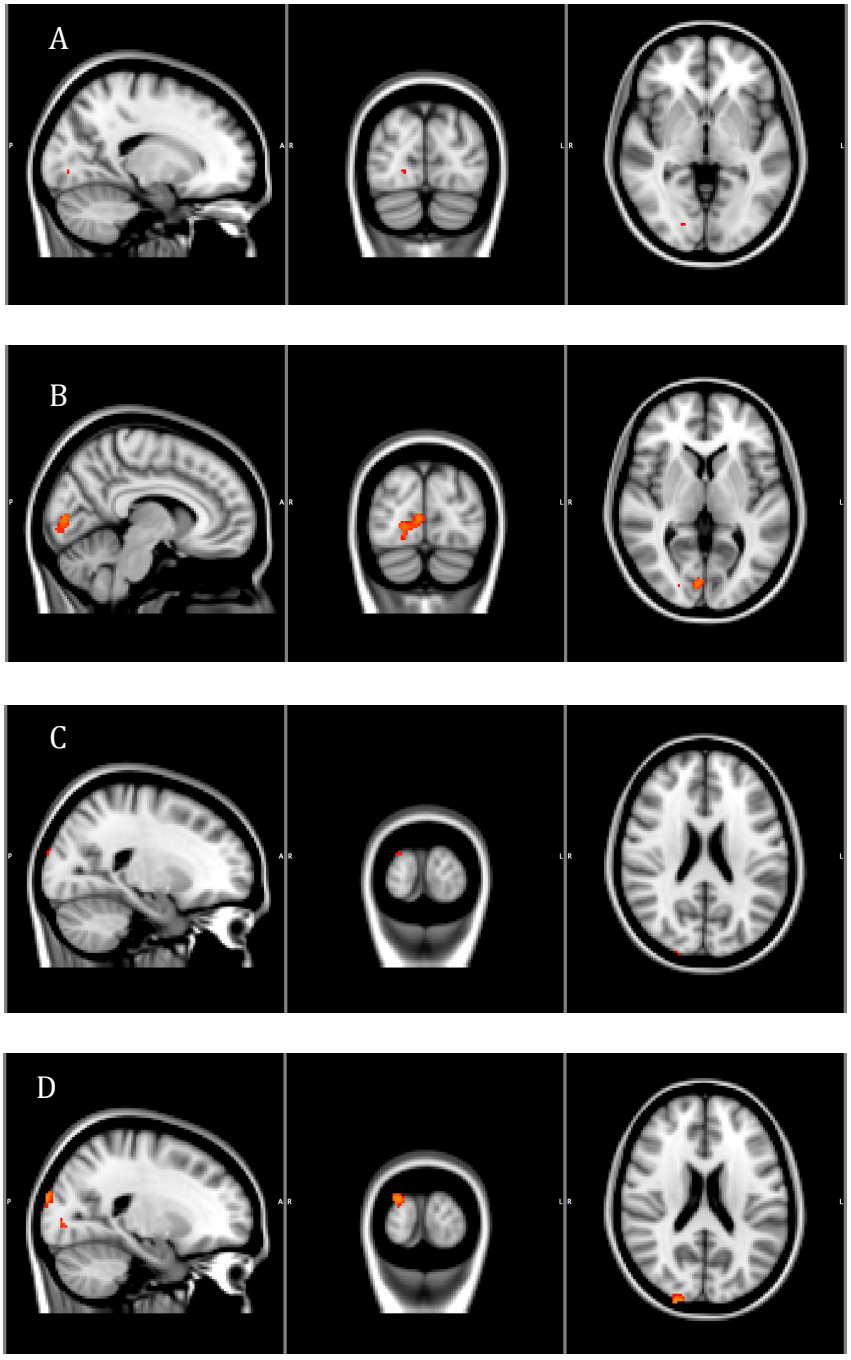

Figure 5.7, results of the correlation between the standardized residuals of a linear regresson between LCVA and GCL volume, and the occipital pole network before correction for age and sex. Functional connectivity correlated in right V1 (thresholded at (A) p ≤ 0.01, (B) p ≤ 0.02. Correlation in right V2 (C) p ≤ 0.01, (D) p ≤ 0.02 on TFCE family wise error corrected output.

When corrected for age and sex the peak significance voxel reduced to p 0.021 on TFCE family wise error corrected output, which was in V1

5.5 Discussion

This is the first longitudinal study of RSfMRI in acute ON with an extended follow up period. It has shown marked increase in FC in all three visual resting state networks identified, particularly between baseline and 12 months. By contrast, no significant change was found in any of the constituent networks in the DMN or the sensory network. Thus, there is clear evidence that FC in RSfMRI visual networks is significantly altered over time following ON, and that this is driven by an increase in FC at 12 months compared to baseline.

However, the implications of these changes in RSfMRI in relation to the clinical severity of ON and visual function post ON remain elusive. Contrary to the apriori hypothesis, there was no correlation between change in GCL volume and change in visual network FC. Furthermore, there was no correlation between 2.5% LCVA and change in visual network FC. An additional hypothesis tested was that the variability in 2.5% LCVA not explained by GCL volume may be explained by changes in RSfMRI. This analysis approached significance at 6 months in the occipiatal pole (peri-calcarine) network as displayed in figure 5.7. However, this lost significance with correction for age and sex, and lacked any correlation at 12 months, the point at which there was greatest change FC over time. It is possible this reflects a non-linear relationship in the dynamc processes involved in cortical functional plasticity in response to de-afferentation. However, it remains difficult based on this data to confidently conclude whether these changes are adaptive or maladaptive.

One reason for a lack of correlation with visual function could be the choice of 2.5% LCVA as the input for correlation analysis. Whilst LCVA is a clinically relevant measure of vision, and sensitive to retinal neurodegeneration following optic neuritis, it is not a complete measure of visual function and visual recovery following optic

neuritis. In stimulus based fMRI, reductions in BOLD signal response have correlated with visual acuity following ON for monocular stimulation. However, this is readily explained by a reduced neuronal input in stimulating a more severely damaged eye, and does not necessarily inform about cortical plasticity (197). fMRI response to stimulus in extra-striate regions has correlated with the degree of optic nerve injury and visual acuity in baseline fMRI following ON, but not with follow up MRI scans(180). Aside from visual acuity and contrast sensitivity, deficits in motion perception have been found to be particularly affected following ON even when recovery of VA and LCVA has occurred, and is accompanied by ongoing reduction in fMRI response, even at one year following optic neuritis(166). Whether changes in RSfMRI FC are an adaptive response in higher visual functioning such as in motion perception following ON remains to be assessed.

Corrections were made in pre-processing for motion artefact using the FSL tools FIX and MCFLIRT, however, the residual role of motion in the data is worth reflecting on. Whilst there was a significant change in DVAR scores between 0 and 6 months, reassurance can be drawn from the low mean DVAR in each timepoint (all <20). Furthermore, initially 8 networks were tested for change over time in ANOVA, and only the visual networks had significant F tests. Motion artefact is known to preferentially affect voxels further from the central pivot at which head motion occurs, maximally at the anterior frontal cortex (198). This area matches with the executive control network (A in figure 5.2) and if head motion accounted for the change over time in the visual networks, a change in this network would be expected also. The lack of effect over time in that network, further suggests that the increase in FC in the visual networks is related to a true signal change.

The exclusivity of the findings to the visual networks and not to the DMN is of interest. A previous cross-sectional study found that a CIS population (2 of 14 of

whom were ON) had found increased FC in all the DMN networks we explored, but not in the visual resting state network (199) compared to RRMS and healthy controls. The differing findings in our study with a uniformly ON and primarily CIS population (only 2 /40 patients had an MS diagnosis at entry to our study) suggest that the changes found in the visual networks demonstrate cortical adaption specific to the de-afferentation experienced from ON.

Elucidation of the significance of the changes in RSfMRI would be enhanced by the addition of a healthy control group, in particular in exploring with more certainty whether the DMN differs longitudinally in ON patients versus controls. However the data presented here was set up initially to assess the effect of amiloride on RSfMRI following ON. Again, whilst there was a small cluster at 6 months that showed difference in the amiloride group in one visual network, subsequent analysis of difference of the change over time between groups showed no significant findings. Combined with the finding that the difference was in a white matter area, this is likely to be a chance result, and the data was analysed as a whole group on the basis there was no significant effect from amiloride.

5.5.1 Conclusion and future directions

This data has demonstrated longitudinal change from baseline to recovery in optic neuritis exclusively in visual networks and not in the default mode networks. Whilst this does demonstrate neuro plasticity following an insult to the anterior visual system, the functional consequences and adaptive nature of this change in connectivity could not be concluded in this work, from assessing either retinal neurodegeneration or low contrast visual acuity. Future work would relate such resting state changes to a healthy control group, and also assess whether the

variations in other visual domains, such as motion perception, are related to degree of change in FC in the visual resting state networks .

6 Chapter 6. Conclusions and future directions

This thesis has evaluated neuroprotection through a clinical trial of amiloride in ON, and subsequently given a detailed analysis of retinal changes following ON. From there, transsynaptic neurodegeneration was assessed through DTI in the OR, and neuroplasticity was explored through RSfMRI. The key findings are summarised below. Thereafter, these are interpreted in light of the research questions posed in chapter 1, and future directions for the research presented in this thesis are then explored.

6.1 Key Findings

In chapter 2, a phase II randomised controlled trial of amiloride 10mg vs placebo in acute ON was conducted and the findings were as follows;

- There was no neuroprotective benefit found from amiloride in the primary outcome measure of pRNFL on GDx, or on any of the secondary outcome measures.

- In one secondary outcome measure, PVEP P100 time to peak, there was a significant prolongation (worsening) in the amiloride treated group.

- Detailed analysis revealed early neurodegeneration in the GCIPL of affected eyes, which correlated with the time of OCT from onset of symptoms. Thus, one contributor to the lack of effect of amiloride on neuroprotection on ON in this trial, could be that the window of time where neuroprotective therapies will be effective is shorter than was anticipated when the trial was set up.

In chapter 3 the longitudinal change in macular retinal layers over one year following ON were explored in detail, and the findings were as follows;

- Analysing the peri-foveal macular volumes in retinal layers was shown to have a high reliability on testing of repeated measures. This data in this thesis compared favourably to published data.

- This was this first longitudinal study to show that significant swelling in the INL following ON develops over 12 months, and is not significantly thickened by 6 months compared to baseline, though it is swollen compared to the unaffected fellow eye.

- In the IS/OS segments of photoreceptors, there was a dynamic swelling in the retina, which in our data peaks at the 6 months timepoint, and regressed back to baseline at the 12 month timepoint. This confirms the findings of other groups, however, this is the largest cohort to find such a dynamic change to this degree of segmentation, and the temporal evolution of this change differed somewhat from a previous study, in which this finding had lost significance at 6 months.

- In line with previous studies, the macular total retinal thickness, GCL, RNFL, IPL and OPL, all show thinning from baseline to 6 months, with no significant change between 6 and 12 months.

- The longitudinal change in thickness in total macular thickness and mRNFL, GCL and IPL layers significantly correlated with the change in HCVA and LCVA both at 1.25% and 2.5% at 6 and 12 months. At 6 months there was a

significant correlation between these visual measures and ONL and IS/OS, however, this was not present at 12 months, reflecting the dynamic change in these layers. By 12 months the INL correlated with LCVA. In a multiple regression model, most of the variability in LCVA could be explained by GCL volume, and addition of other retinal layers did not appear to strongly influence the variability explained by the model.

- This is the first longitudinal dataset to correlate PERG N95 amplitude with retinal layers, r values are higher than in a previously published cross-sectional dataset and we show a correlation with the INL and PERG for the first time.

- Analysis of retinal layers show strong correlations between changes in layers. These are particularly striking in the positive correlations found in the change in the inner retinal (mRNFL, GCL and IPL) layers, but there are also highly significant negative correlations between the drop in inner retinal thickness and the gain in INL and ONL thickness. Notably, the IS/OS shows weak, though significant, negative correlations at 6 months with the inner retinal layers, but these have disappeared by 12 months, reflecting the dynamic changes in this outer layer.

- Amiloride was not found to have affected longitudinal change in any retinal layers

In chapter 4, changes in whole brain diffusion measures of white matter integrity were assessed over time following ON. In addition, for the first time, macular OCT GCL layer was correlated longitudinally with changes in the OR, to assess for transsynaptic neurodegeneration. The findings were as follows:

- A correlation was found between damage over time in the anterior visual pathway following optic neuritis (measured by OCT GCL volume), and change over time in the postsynaptic OR in metrics of white matter integrity (FA, and RD). These correlations increased between the 6 and 12 month timepoints, suggesting an evolving relationship of transsynaptic neurodegeneration.

- Whilst there was a trend in an ANOVA over time for a reduction in the mean FA in the OR, this did not reach significance.

- Whole brain analysis did not show a change in the OR over time. Instead increases over time in FA were shown in the superior longitudinal fasciculus and reductions in FA were shown in the corpus callosum and the frontal white matter. However, the whole brain changes notable in the superior longitudinal fasciculus are in areas of crossed white matter fibers, complicating the interpretability of diffusivity scalars derived from a single tensor model.

- These whole brain changes were further explored with crossed fibers analysis assessing for changes in the principal and secondary diffusion direction in an attempt to assess the effect of crossed fibers contributing to this finding. However, this analysis failed to reach significance. Thus, it remains possible that the increases in FA in the superior longitudinal fasciculus reflect neuroplasticity in secondary visual areas.

- Amiloride was not found to have an effect on any whole brain or OR diffusion scalars.

In Chapter 5, neuroplasticity was assessed by utilising longitudinal RSfMRI to assess FC in visual networks and in the default mode networks. The findings were as follows:

- There were widespread changes over time in all three visual networks (the medial visual network, the lateral visual network, and the occipital pole visual network) and no significant changes in any other networks that were assessed (4 default mode networks and one sensory network included as a control)

- In all three networks these changes were primarily driven by an increase in FC from baseline to 12 months following ON. In the lateral visual network there was also a significant increase in functional connectivity over time between 6 and 12 months.

- The adaptive implications for this increase in FC were assessed by looking at correlations between the change in FC in visual networks from 0 to 6 months and 0 to 12 months and the corresponding change in GCL volume and 2.5% LCVA. However these correlations did not reach significance.

- A further assessment was to test whether variability in LCVA not explained by GCL (the residual variance), could be explained by changes in FC in visual resting state networks. This correlation was of borderline significance at 6 months in a small cluster around V1, but was not significant at 12 months.

- Amiloride was concluded not to have an effect on RSfMRI FC.

6.2 Interpretation of Key findings

The key findings can be interpreted in light of the research questions posed in chapter 1.

Is ASIC channel blockade via amiloride neuroprotective in ON?

In this thesis, ASIC channel blockade via amiloride was not found to be neuroprotective in ON. However, as we have seen above, the ACTION trial showed that neurodegeneration is an early phenomenon in ON and thus it may be that our long window of recruitment (up to 28 days) affected our ability to assess this.

Can our understanding of the temporal evolution of retinal changes following ON be enhanced by assessing OCT longitudinally, how do these changes influence visual outcomes, and this ameliorated by amiloride?

This thesis has shown a comparatively large dataset and explored the temporal evolution of changes in retinal layers in ON. It has supported the recent finding of dynamic changes in the IS/OS segment following ON and enhanced our understanding of the temporal evolution of this change. Furthermore it has provided the missing link between existing cross-sectional data showing INL swelling following ON, and the lack of INL swelling in longitudinal studies that have previously run to 6 months in smaller sample sizes. Amongst the retinal layers, most of the variability in visual function, as measured by LCVA, is explained by GCL volume. The retinal changes following ON do not appear to be influenced by amiloride.

Is transynaptic neurodegeneration present in the posterior visual pathways following ON and this ameliorated by amiloride?

The findings in chapter 4 support the presence of anterograde transsynatpic neurodegeration to a degree. The relationship between pre-synaptic neurodegeneration in the form of GCL volume change and OR diffusivity scalars, FA and RD were robust, and strengthened from 6 to 12 months.

However, change in the OR on whole brain TBSS analysis was lacking. This could be due to reduced sensitivity to OR change at a whole brain level, likely to be dominated by large and unidirectional white matter tracts such as the corpus callosum, or due to compensatory change in white matter integrity in retrograde efferent corticogenuclate fibers.

In addition, unexpectedly there was an increase in FA in some areas relevant to higher visual processing. This finding highlights that white matter integrity can reflect neuroplasticity in the white matter tracts in addition to neurodegeneration. It may be that neuroplastic responses in white matter connections to higher visual areas are also initiated in response to the primary insult. However, on a whole brain level, the issue of crossed fibers confounding these results should encourage caution in these findings, as extensively discussed in chapter 4. Amiloride was not found to affect any change in measures of white matter integrity.

Is there evidence of neuroplasticity in the visual cortex following ON, and is this influenced by amiloride?

Chapter 5 does show marked increases in FC over time in the visual networks on RSfMRI. As explored in the chapter, the adaptive nature of these changes could not be conclusively elucidated.

The cluster of voxels in V1 in the occipital pole network that were of borderline significance when assessing for the residual variance in LCVA not explained by OCT was a tantalising finding at 6 months. Whilst not conclusive of FC in RSfMRI being an adaptive response, it could be explained by increased in FC being related to visual recovery, but that that relationship could be non-linear over time.

Whilst the implications of this increase in FC to clinical and visual recovery were not clearly extracted in this data, the increase in FC is nevertheless a robust and novel finding in this thesis. A biological mechanism for this change is strongly supported by the finding that increases in FC were highly significant in the visual networks and not significant in other networks tested. The clusters of significance were large and were located in cortical areas highly relevant to vision.

6.3 Future directions

6.3.1 Amiloride in MS and clinical trial design in ON

As we have seen, this trial failed to show an effect of amiloride. Whilst this is suggestive of a lack of effect of amiloride, one key reason for a lack of effect could be the prolonged recruitment time in our trial. Thus, a key recommendation from this data is that future therapeutic trials should have as short a window between symptoms and inclusion as possible. Of great interest therefore is that a further trial of amiloride in ON is in progress (200) and aims to recruit within 10 days of ON. An ongoing phase III trial of erythropoietin also aims to recruit within 10 days (201).

In addition to trials in ON, the phase IIb MS-SMART trial in SPMS is ongoing (202) and this includes an amiloride arm. Should the results of the MS-SMART trial conflict with the lack of effect in the trial described in this thesis, this will give further insight into how clnical trials in ON translate into MS. It may be that acute inflammatory events such as ON have an adequately divergent pathophysiology from progressive MS, to require different therapeutic targets.

There was a signal from the secondary outcome measures in the ACTION trial described in this thesis, that amiloride may have had a detrimental effect on recovery of the P100 time to peak, which could be a reflection of amiloride impeding remyelination following ON. This was an unexpected result given laboratory evidence that amiloride preserved myelination through blockade of the ASIC. Further basic science research evaluating the role of ASIC and its effects on myelin and oligodendrocytes in CNS inflammatory disease, could help interpret these findings.

Furthermore, with regard to trial design in ON, I would recommend that future researchers are selective in visual outcomes in clinical trials. Outcomes such as visual field and colour vision, whilst long established investigations in clinical trials, suffer from being time consuming, and highly affected by patient fatigue. Researchers planning future clinical trials should consider limiting the number of investigations to those that are most high yield such as LCVA, to improve trial efficiency.

6.3.2 Retinal layer change following ON

In our data IS/OS thickening peaked at 6 months and regressed back to baseline at 12 months. Whilst this dynamic change in the IS/OS segment has been found by

other groups to some extent, as we have seen, these have had either a less precise segmentation (129) or a smaller sample size with shorter follow up (127) than our study. A longer study, with more frequent OCT scanning, perhaps even every week or two in the early stages of ON, would be optimal to refine our understanding of the trajectory of retinal changes following ON. However, ensuring consistent follow up in such a trial would be a challenge in achieving an adequate sample size.

6.3.3 Transsynaptic neurodegeneration

Current longitudinal studies on transsynaptic neurodegeration in the OR following ON, including this data, are limited to 12 months following ON (149, 150). However, transsynaptic neurodegeneration may take longer to evolve than within that timescale. Therefore, if possible, further longitudinal follow up with re-scanning at 2 and even 3 years would add further information on the temporal evolution of changes in diffusivity scalars in the OR following ON, and whether they continue to relate to OCT findings.

Differing analysis techniques have been applied by multiple groups to diffusion MRI in the OR following ON. A collaborative approach, with data sharing and unified technique would be of benefit. This could enhance our understanding of how significant a contribution transsynaptic neurodegeneration from a discrete relapse such as ON makes to the global neurodegenerative trend seen in MS. The technique used in this thesis, based on TBSS, is highly automated, and thus lends itself to reduced bias and handling large datasets (in this thesis, the analysis included 120 scans).

Data sharing and increased sample size would also allow a more meaningful comparison of lesioned and non-lesioned ON patients The sub group analysis of these patients in this thesis in chapter 4 appeared to suffer from a lack of power. Such an analysis may be a preferable way to assess and counter the effect of lesions on diffusivity scalars, over the alternative of lesion masking techniques. As we have explored in chapter 4, such techniques do not necessarily take into account the downstream effect of lesions in normal appearing white matter remote to a lesion from wallerian degeneration.

6.3.4 Neuroplasticity

Concurrent with the above, the findings in chapter 4 of increases in FA over time in white matter tracts relevant to higher visual processing in the dorsal stream (the superior longitudinal fasciculus) may represent neuroplasticity in response to ON. Further analysis with tractography of the superior longitudinal fasciculus may help to refine the registration based technique in this thesis. Furthermore, data sharing or replication of this technique in a different dataset may also help refine this result and more firmly establish whether white matter integrity increases in white matter relevant to higher visual processing following ON.

Whilst the findings in chapter 5 show marked increases in FC over time, the question of whether the adaptive significance of these changes remains difficult to extrapolate from this data. Whilst the trend for a correlation in a relevant visual area (the occipital pole network, located at V1) at 6 months with the amount the variance in the correlation between 2.5% LCVA and GCL suggested this was an adaptive response, other analyses at 6 and 12 months did not substantiate this. Addition of additional visual parameters which have been shown to be preferentially affected in ON, such

as motion perception, may help resolve the uncertainty over the adaptive nature of this change.

Furthermore, the lack of finding any change in the networks identified as part of the default mode network in chapter 5 is of interest, and counter to previous findings in cross-sectional studies. It may be that the addition of a healthy control group to a longitudinal analysis of RSfMRI following ON shows further changes in FC in resting state networks other than the visual networks.

6.4 General Conclusions

The work described in this thesis was designed to test the effect of ASIC blockade via amiloride as a neuroprotective agent in ON. Whilst this apriori hypothesis was not supported by the data in this thesis, it has provided a number of important insights into clinical trails design and ON.

This thesis has shown that going forward, early timing of intervention is critical to assessing neuroprotective therapies in ON. Against a background of ongoing trials of amiloride in ON and MS, this the work described in this thesis takes an important role in the ongoing translational journey of this CNS therapeutic target.

Alongside these insights into neuroprotection, the work in this thesis has enhanced our broader understanding of clinical trial design in ON and of the changes in the visual system following ON.

The visual system is a structurally eloquent CNS system suited to multimodal techniques to explore the relationship between presynaptic anterior visual system

and the postsynaptic posterior visual system. The work contained in this thesis has capitalised on this. A detailed analysis of the changes over time in the retina following ON has been shown with novel findings of the temporal evolution of these changes and how they relate to existing cross-sectional data. Following on from this it has shown that these relate to changes in the postsynaptic white matter, supporting the concept that transsynaptic neurodegeneration contributes to neuronal loss in MS.

In addition this work has shown neuroplasticity in the visual cortex over time following ON. This was not shown to directly relate to retinal neurodegeneration or clinical recovery. However, the striking changes in resting FC following ON give a strong launchpad for further exploration of the adaptive role of cortical plasticity following ON for future researchers, and patients.

7 Publications arising from this thesis

7.1 In Press

Mckee, J.B., Elston, J., Evangelou, N., Gerry, S., Fugger, L., Kennard, C., Kong, Y., Palace, J. And Craner, M., 2015. Amiloride Clinical Trial In Optic Neuritis (ACTION) protocol: a randomised, double blind, placebo controlled trial. *BMJ open,* **5**(11), pp. e009200-2015-009200.

7.2 Under Review

Mckee, J.B., Cottrial CL., Epps S., Elston, J., Evangelou, N., Gerry, S., Kennard, C., Kong, Y., Koelewyn , A., Kueker, W., Palace, J. And Craner, M Amiloride does not protect retinal nerve fibre layer thickness in optic neuritis in a phase 2 randomised controlled trial.

7.3 Conference Proceedings

7.3.1 Oral Presentations

European Committee for treatment and research in Multiple Sclerosis (ECTRIMS), London. McKee JB, CL Cottrial, Elston J, Gerry S, Evangelou N, Fugger L, Kennard C, Koelewyn A, Kong Y, Palace J, Craner M *Amiloride does not protect retinal nerve fibre layer thickness following acute optic neuritis; result from a phase II, double blind, randomised controlled trial* September 2016

Scottish Ophthalmological Club, Glasgow. McKee JB, CL Cottrial, Elston J, Epps S, Evangelou N, Fugger L, Kennard C, Palace J, Craner M *Retinal ganglion cell volume correlates with pattern electroretinogram in acute optic neuritis.* September 2015

Oxford Ophthalmological Congress, Oxford. McKee JB, CL Cottrial, Elston J, Epps S, Evangelou N, Fugger L, Kennard C, Palace J, Craner M *Retinal ganglion cell volume correlates with pattern electroretinogram in acute optic neuritis.* July 2015

Medical Ophthalmology Society UK, Birmingham. 2015 McKee JB , Elston J, Evangelou N, Fugger L, Kennard C, Palace J, Craner M *Assessment of ganglion cell layer volume in acute optic neuritis shows early neurodegeneration* March 2015

Medical Ophthalmology Society UK, London. McKee JB , Elston J, Evangelou N, Fugger L, Kennard C, Palace J, Craner M *The Amiloride Clinical Trial in Optic neuritis (ACTION trial): Trial paradigm and baseline data* March 2014

7.3.2 Poster Presentations

British Society for Clinical Electrophysiology of Vision (BRISCEV), Oxford. *Retinal ganglion cell volume correlates with pattern electroretinogram in acute optic neuritis.* September 2015

European Neuro-Ophthalmology Society (EUNOS) Meeting, Ljubljana, Slovenia. McKee JB, CL Cottrial, Elston J, Evangelou N, Fugger L, Kennard C, Palace J, Craner M *Retinal ganglion cell volume correlates with pattern electroretinogram in acute optic neuritis.* June 2015

European Committee for treatment and research in Multiple Sclerosis (ECTRIMS) Boston, USA. McKee JB, Elston J, Evangelou N, Fugger L, Kennard C, Palace J, Craner M (joint meeting with American Society) *Multimodal clinical trial paradigm to assess neuroprotection in optic neuritis: baseline data* October 2014

8 References

1. Karampampa K, Gustavsson A, Miltenburger C, Eckert B. Treatment experience, burden and unmet needs (TRIBUNE) in MS study: results from five European countries. Mult Scler. 2012 June 1,;18(2):7-15.

2. Miller DH, Altmann DR, Chard DT. Advances in imaging to support the development of novel therapies for multiple sclerosis. Clinical Pharmacology & Therapeutics. 2012 Apr;91(4):621-34.

3. Stys PK, Zamponi GW, van Minnen J, Geurts JJ. Will the real multiple sclerosis please stand up? Nature Reviews Neuroscience. 2012 Jul;13(7):507-14.

4. Polman CH, Reingold SC, Banwell B, Clanet M, Cohen JA, Filippi M, et al. Diagnostic criteria for multiple sclerosis: 2010 Revisions to the McDonald criteria. Ann Neurol. 2011 -2;69(2):292-302.

5. Barkhof F, Bruck W, De Groot C,J.A., Bergers E, Hulshof S, Geurts J, et al. Remyelinated lesions in multiple sclerosis: magnetic resonance image appearance. Arch Neurol. 2003 Aug;60(8):1073-81.

6. Filippi M, Rovaris M, Rocca MA, Sormani MP, Wolinsky JS, Comi G. Glatiramer acetate reduces the proportion of new MS lesions evolving into "black holes". Neurology. 2001 Aug 28,;57(4):731-3.

7. Hauser SL, Oksenberg JR. The Neurobiology of Multiple Sclerosis: Genes, Inflammation, and Neurodegeneration. Neuron. 2006 -10-05;52(1):61-76.

8. Kuhlmann T, Lingfeld G, Bitsch A, Schuchardt J, Bruck W. Acute axonal damage in multiple sclerosis is most extensive in early disease stages and decreases over time. Brain. 2002 Oct;125:2202-12.

9. Compston A, Coles A. Multiple sclerosis. Lancet. 2008 Oct 25;372(9648):1502-17.

10. Henderson APD, Barnett MH, Parratt JDE, Prineas JW. Multiple sclerosis: Distribution of inflammatory cells in newly forming lesions. Ann Neurol. 2009 December 1,;66(6):739-53.

11. DeLuca GC, Williams K, Evangelou N, Ebers GC, Esiri MM. The contribution of demyelination to axonal loss in multiple sclerosis. Brain. 2006 /06;129(6):1507-16.

12. Dendrou CA, Fugger L, Friese MA. Immunopathology of multiple sclerosis. Nat Rev Immunol. 2015 print;15(9):545-58.

13. Raffel J, Gafson AR, Dahdaleh S, Malik O, Jones B, Nicholas R. Inflammatory Activity on Natalizumab Predicts Short-Term but Not Long-Term Disability in Multiple Sclerosis. PLOS ONE. 2017 Jan 12,;12(1):e0169546.

14. Shirani A, Zhao Y, Karim ME, Evans C, Kingwell E, Van Der Kop ML, et al. Association between use of interferon beta and progression of disability in patients with relapsing-remitting multiple sclerosis. JAMA - Journal of the American Medical Association. 2012 18 Jul 2012;308(3):247-56.

15. Goodin DS, Jones J, Li D, Traboulsee A, Reder AT, Beckmann K, et al. Establishing Long-Term Efficacy in Chronic Disease: Use of Recursive Partitioning and Propensity Score Adjustment to Estimate Outcome in MS. PLOS ONE. 2011 Nov 30,;6(11):e22444.

16. Coles AJ, Cohen JA, Fox EJ, Giovannoni G, Hartung H, Havrdova E, et al. Alemtuzumab CARE-MS II 5-year follow-up Efficacy and safety findings. Neurology. 2017 -08-23:10.1212/WNL.0000000000004354.

17. A Bermel,Robert, Inglese M. Neurodegeneration and inflammation in MS The eye teaches us about the storm. Neurology. 2013 January 1,;80:19-20.

18. Friese MA, Craner MJ, Etzensperger R, Vergo S, Wemmie JA, Welsh MJ, et al. Acid-sensing ion channel-1 contributes to axonal degeneration in autoimmune inflammation of the central nervous system. Nat Med. 2007 Dec;13(12):1483-9.

19. Stys PK. General mechanisms of axonal damage and its prevention. J Neurol Sci. 2005 6/15;233(1–2):3-13.

20. Beraud E, Viola A, Regaya I, Confort-Gouny S, Siaud P, Ibarrola D, et al. Block of neural Kv1.1 potassium channels for neuroinflammatory disease therapy. Ann Neurol. 2006 Nov;60(5):586-96.

21. Bittner S, Bauer MA, Ehling P, Bobak N, Breuer J, Herrmann AM, et al. The TASK1 channel inhibitor A293 shows efficacy in a mouse model of multiple sclerosis. Experimental Neurology. 2012 December 1,;238(2):149-55.

22. Lo AC, Black JA, Waxman SG. Neuroprotection of axons with phenytoin in experimental allergic encephalomyelitis. Neuroreport. 2002 Oct 28,;13(15):1909-12.

23. Raftopoulos R, Hickman SJ, Toosy A, Sharrack B, Mallik S, Paling D, et al. Phenytoin for neuroprotection in patients with acute optic neuritis: a randomised, placebo-controlled, phase 2 trial. The Lancet Neurology. 2016 3;15(3):259-69.

24. Smith KJ, Lassmann H. The role of nitric oxide in multiple sclerosis. The Lancet Neurology. 2002 8;1(4):232-41.

25. Vergo S, Craner MJ, Etzensperger R, Attfield K, Friese MA, Newcombe J, et al. Acid-sensing ion channel 1 is involved in both axonal injury and demyelination in multiple sclerosis and its animal model. Brain. 2011 Feb;134(Pt 2):571-84.

26. Cadiou H, Studer M, Jones NG, Smith ES, Ballard A, McMahon SB, et al. Modulation of acid-sensing ion channel activity by nitric oxide. Journal of Neuroscience. 2007 Nov 28;27(48):13251-60.

27. Waldmann R, Champigny G, Bassilana F, Heurteaux C, Lazdunski M. A proton-gated cation channel involved in acid-sensing. Nature. 1997 Mar 13;386(6621):173-7.

28. Benos DJ. Amiloride: a molecular probe of sodium transport in tissues and cells. Am J Physiol. 1982 Mar;242(3):131-45.

29. Arun T, Tomassini V, Sbardella E, de Ruiter MB, Matthews L, Leite MI, et al. Targeting ASIC1 in primary progressive multiple sclerosis: evidence of neuroprotection with amiloride. Brain. 2013 Jan;136(Pt 1):106-15.

30. Barkhof F, Calabresi PA, Miller DH, Reingold SC. Imaging outcomes for neuroprotection and repair in multiple sclerosis trials. Nature Reviews Neurology. 2009 May;5(5):256-66.

31. Beck RW, Gal RL, Bhatti MT, Brodsky MC, Buckley EG, Chrousos GA, et al. Visual function more than 10 years after optic neuritis: experience of the optic neuritis treatment trial. Am J Ophthalmol. 2004 Jan;137(1):77-83.

32. Optic Neuritis Study G. Multiple sclerosis risk after optic neuritis: final optic neuritis treatment trial follow-up. Arch Neurol. 2008 Jun;65(6):727-32.

33. Sisto D, Trojano M, Vetrugno M, Trabucco T, Iliceto G, Sborgia C. Subclinical visual involvement in multiple sclerosis: a study by MRI, VEPs, frequency-doubling perimetry, standard perimetry, and contrast sensitivity. Invest Ophthalmol Vis Sci. 2005 Apr;46(4):1264-8.

34. Friese MA, Schattling B, Fugger L. Mechanisms of neurodegeneration and axonal dysfunction in multiple sclerosis. Nat Rev Neurol. 2014 Apr;10(4):225-38.

35. Pau D, Al Zubidi N, Yalamanchili S, Plant GT, Lee AG. Optic neuritis. Eye. 2011 Jul;25(7):833-42.

36. Costello F, Hodge W, Pan YI, Eggenberger E, Coupland S, Kardon RH. Tracking retinal nerve fiber layer loss after optic neuritis: a prospective study using optical coherence tomography. Multiple Sclerosis. 2008 Aug;14(7):893-905.

37. Beck RW, Cleary PA, Anderson MM,Jr, Keltner JL, Shults WT, Kaufman DI, et al. A Randomized, Controlled Trial of Corticosteroids in the Treatment of Acute Optic Neuritis. N Engl J Med. 1992 February 27,;326(9):581-8.

38. Beck RW, Cleary PA. Optic neuritis treatment trial. One-year follow-up results. Arch Ophthalmol. 1993 Jun;111(6):773-5.

39. Storoni M, Pittock SJ, Weinshenker BG, Plant GT. Optic neuritis in an ethnically diverse population: higher risk of atypical cases in patients of African or African-Caribbean heritage. J Neurol Sci. 2012 Jan 15;312(1-2):21-5.

40. Hickman SJ, Ko M, Chaudhry F, Jay WM, Plant GT. Optic Neuritis: An Update Typical and Atypical Optic Neuritis. Neuroophthalmology. 2008 01/01; 2015/05;32(5):237-48.

41. Kapoor R, Miller DH, Jones SJ, Plant GT, Brusa A, Gass A, et al. Effects of intravenous methylprednisolone on outcome in MRI-based prognostic subgroups in acute optic neuritis. Neurology. 1998 January 01;50(1):230-7.

42. Golnik KC. Infectious optic neuropathy. Semin Ophthalmol. 2002 Mar;17(1):11-7.

43. Kidd D, Burton B, Plant GT, Graham EM. Chronic relapsing inflammatory optic neuropathy (CRION). Brain. 2003 Feb;126:276-84.

44. Waters PJ, Pittock SJ, Bennett JL, Jarius S, Weinshenker BG, Wingerchuk DM. Evaluation of aquaporin-4 antibody assays. Clin Exp Neuroimmunol. 2014 Oct;5(3):290-303.

45. Suhs KW, Hein K, Sattler MB, Gorlitz A, Ciupka C, Scholz K, et al. A randomized, double-blind, phase 2 study of erythropoietin in optic neuritis. Ann Neurol. 2012 Aug;72(2):199-210.

46. Cadavid D, Balcer L, Galetta S, Aktas O, Ziemssen T, Vanopdenbosch L, et al. Efficacy Analysis of the Anti-LINGO-1 Monoclonal Antibody BIIB033 in Acute Optic Neuritis: the RENEW Trial. Neurology. 2015 April 06;84(14 Supplement):Supplement (P7.202).

47. Balcer LJ, Miller DH, Reingold SC, Cohen JA. Vision and vision-related outcome measures in multiple sclerosis. Brain. 2015 Jan;138(Pt 1):11-27.

48. Kerrison JB, Flynn T, Green WR. RETINAL PATHOLOGIC CHANGES IN MULTIPLE SCLEROSIS. Retina. 1994;14(5):445-51.

49. Esfahani MR, Harandi ZA, Movasat M, Nikdel M, Adelpour M, Momeni A, et al. Memantine for axonal loss of optic neuritis. Graefes Arch Clin Exp Ophthalmol. 2012 Jun;250(6):863-9.

50. Trip SA, Schlottmann PG, Jones SJ, Kallis C, Altmann DR, Garway-Heath DF, et al. Scanning laser polarimetry quantification of retinal nerve fiber layer thinning following optic neuritis. Journal of Neuro-Ophthalmology. 2010 Sep;30(3):235-42.

51. Syc SB, Saidha S, Newsome SD, Ratchford JN, Levy M, Ford E, et al. Optical coherence tomography segmentation reveals ganglion cell layer pathology after optic neuritis. Brain. 2012 Feb;135(Pt 2):521-33.

52. Costello F. The afferent visual pathway: designing a structural-functional paradigm of multiple sclerosis. Isrn Neurology Print. 2013;2013:134858.

53. Schiller PH, Tehovnik EJ. The Retina. In: *Vision And The Visual System* Oxford University Press; 2015.

54. Berg JM, Tymoczko JL, Stryer L, Freeman WH. Photoreceptor Molecules in the Eye Detect Visible Light. In: Biochemistry. 5th Edition. W H Freeman; 2002.

55. Schiller PH, Tehovnik EJ. The Midget and Parasol Systems. In: *Vision And The Visual System* Oxford University Press; 2015.

56. Snell RS, Lemp MA, Snell RS, Lemp MA. The Visual Pathway. In: Clinical Anatomy of the Eye. Blackwell Science Ltd,.; 1997. p. 379-412.

57. Schiller PH, Tehovnik EJ. The Lateral Geniculate Nucleus. In *Vision And The Visual System* : Oxford University Press; 2015.

58. Evangelou N, Konz D, Esiri MM, Smith S, Palace J, Matthews PM. Size-selective neuronal changes in the anterior optic pathways suggest a differential susceptibility to injury in multiple sclerosis. Brain. 2001 Sep;124(Pt 9):1813-20.

59. Jeffries AM, Killian NJ, Pezaris JS. Mapping the primate lateral geniculate nucleus: A review of experiments and methods. J Physiol Paris. 2014 -2;108(1):3-10.

60. Gennari F. Francisci Gennari Parmensis medicinae doctoris collegiati De peculiari structura cerebri nonnullisque ejus morbis: paucae aliae anatom. observat. accedunt. Parmae: Parma : Ex Regio Typographeo(IS), Bodoni, Giambattista; 1782.

61. Schiller PH, Tehovnik EJ. The Striate Cortex. In: *Vision And The Visual System* Oxford University Press; 2015.

62. Goodale MA, Milner AD. Separate visual pathways for perception and action. Trends Neurosci. 1992;15(1):20-5.

63. Cloutman LL. Interaction between dorsal and ventral processing streams: Where, when and how? Brain and Language. 2013 November 1,;127(2):251-63.

64. Goodale MA. Transforming vision into action. Vision Research. 2011 July 1,;51(13):1567-87.

65. Haak KV, Beckmann CF. Objective analysis of the topological organization of the human cortical visual connectome suggests three visual pathways. Cortex. 2018 /01/01;98:73-83.

66. Weiner KS, Grill-Spector K. Neural representations of faces and limbs neighbor in human high-level visual cortex: Evidence for a new organization principle. Psychol Res. 2013;77(1):74-97.

67. Galletti C, Fattori P. The dorsal visual stream revisited: Stable circuits or dynamic pathways? Cortex. 2018 January 1,;98:203-17.

68. Hutchison RM, Gallivan JP. Functional coupling between frontoparietal and occipitotemporal pathways during action and perception. Cortex. 2018 January 1,;98:8-27.

69. Zatorre RJ, Fields RD, Johansen-Berg H. Plasticity in gray and white: neuroimaging changes in brain structure during learning. Nat Neurosci. 2012 April;15(4):528-36.

70. Cense B, Chen TC, Park BH, Pierce MC, de Boer JF. Thickness and birefringence of healthy retinal nerve fiber layer tissue measured with polarization-sensitive optical coherence tomography. Invest Ophthalmol Vis Sci. 2004 Aug;45(8):2606-12.

71. Reus NJ, Zhou Q, Lemij HG. Enhanced imaging algorithm for scanning laser polarimetry with variable corneal compensation. Invest Ophthalmol Vis Sci. 2006 Sep;47(9):3870-7.

72. Mai TA, Reus NJ, Lemij HG. Structure-function relationship is stronger with enhanced corneal compensation than with variable corneal compensation in scanning laser polarimetry. Invest Ophthalmol Vis Sci. 2007 Apr;48(4):1651-8.

73. Parisi V, Manni G, Spadaro M, Colacino G, Restuccia R, Marchi S, et al. Correlation between morphological and functional retinal impairment in multiple sclerosis patients. Invest Ophthalmol Vis Sci. 1999 Oct;40(11):2520-7.

74. Frohman EM, Dwyer MG, Frohman T, Cox JL, Salter A, Greenberg BM, et al. Relationship of optic nerve and brain conventional and non-conventional MRI measures and retinal nerve fiber layer thickness, as assessed by OCT and GDx: A pilot study. J Neurol Sci. 2009 7/15;282(1–2):96-105.

75. Kupersmith MJ, Mandel G, Anderson S, Meltzer DE, Kardon R. Baseline, one and three month changes in the peripapillary retinal nerve fiber layer in acute optic neuritis: relation to baseline vision and MRI. J Neurol Sci. 2011 Sep 15;308(1-2):117-23.

76. Wojtkowski M, Leitgeb R, Kowalczyk A, Bajraszewski T, Fercher AF. In vivo human retinal imaging by Fourier domain optical coherence tomography. J Biomed Opt. 2002 Jul;7(3):457-63.

77. Huang X, Cai FQ, Hu PH, Zhong YL, Zhang Y, Wei R, et al. Disturbed spontaneous brain-activity pattern in patients with optic neuritis using amplitude of low-frequency fluctuation: a functional magnetic resonance imaging study. Neuropsychiatr Dis Treat. 2015 Dec 16;11:3075-83.

78. Fisher JB, Jacobs DA, Markowitz CE, Galetta SL, Volpe NJ, Nano-Schiavi M, et al. Relation of visual function to retinal nerve fiber layer thickness in multiple sclerosis. Ophthalmology. 2006 Feb;113(2):324-32.

79. Trip SA, Schlottmann PG, Jones SJ, Altmann DR, Garway-Heath DF, Thompson AJ, et al. Retinal nerve fiber layer axonal loss and visual dysfunction in optic neuritis. Ann Neurol. 2005 Sep;58(3):383-91.

80. Costello F, Coupland S, Hodge W, Lorello GR, Koroluk J, Pan YI, et al. Quantifying axonal loss after optic neuritis with optical coherence tomography. Ann Neurol. 2006 Jun;59(6):963-9.

81. Henderson AP, Altmann DR, Trip AS, Kallis C, Jones SJ, Schlottmann PG, et al. A serial study of retinal changes following optic neuritis with sample size estimates for acute neuroprotection trials. Brain. 2010 Sep;133(9):2592-602.

82. Petzold A, de Boer JF, Schippling S, Vermersch P, Kardon R, Green A, et al. Optical coherence tomography in multiple sclerosis: a systematic review and meta-analysis. The Lancet Neurology. 2010 9;9(9):921-32.

83. Tatrai E, Simo M, Iljicsov A, Nemeth J, DeBuc DC, Somfai G. In Vivo Evaluation of Retinal Neurodegeneration in Patients with Multiple Sclerosis. PLOS ONE. 2012 Jan 26,;7(1):e30922.

84. Walter SD, Ishikawa H, Galetta KM, Sakai RE, Feller DJ, Henderson SB, et al. Ganglion Cell Loss in Relation to Visual Disability in Multiple Sclerosis. Ophthalmology. 2012 6;119(6):1250-7.

85. Tewarie P, Balk L, Costello F, Green A, Martin R, Schippling S, et al. The OSCAR-IB consensus criteria for retinal OCT quality assessment. PLoS ONE [Electronic Resource]. 2012;7(4):e34823.

86. Balk LJ, Twisk JW, Steenwijk MD, Daams M, Tewarie P, Killestein J, et al. A dam for retrograde axonal degeneration in multiple sclerosis?. Journal of Neurology, Neurosurgery & Psychiatry. 2014 Jul;85(7):782-9.

87. Oberwahrenbrock T, Weinhold M, Mikolajczak J, Zimmermann H, Paul F, Beckers I, et al. Reliability of Intra-Retinal Layer Thickness Estimates. PLOS ONE. 2015 Sep 8,;10(9):e0137316.

88. Kalloniatis M, Luu C. Visual Acuity. In: Kolb H, Fernandez E, Nelson R, editors. Webvision: The Organization of the Retina and Visual System. Salt Lake City (UT): University of Utah Health Sciences Center; 1995.

89. Ferris FL, Kassoff A, Bresnick GH, Bailey I. New visual acuity charts for clinical research. Am J Ophthalmol. 1982 Jul;94(1):91-6.

90. Frederiksen JL, Larsson HB, Ottovay E, Stigsby B, Olesen J. Acute optic neuritis with normal visual acuity. Comparison of symptoms and signs with psychophysiological, electrophysiological and magnetic resonance imaging data. Acta Ophthalmol (Copenh). 1991 Jun;69(3):357-66.

91. Beck RW, Ruchman MC, Savino PJ, Schatz NJ. Contrast sensitivity measurements in acute and resolved optic neuritis. Br J Ophthalmol. 1984 - 10;68(10):756-9.

92. Balcer LJ, Baier ML, Pelak VS, Fox RJ, Shuwairi S, Galetta SL, et al. New low-contrast vision charts: reliability and test characteristics in patients with multiple sclerosis. Mult Scler. 2000 Jun;6(3):163-71.

93. Baier ML, Cutter GR, Rudick RA, Miller D, Cohen JA, Weinstock-Guttman B, et al. Low-contrast letter acuity testing captures visual dysfunction in patients with multiple sclerosis. Neurology. 2005 Mar 22,;64(6):992-5.

94. Balcer LJ, Baier ML, Cohen JA, Kooijmans MF, Sandrock AW, Nanoâ€“Schiavi ML, et al. Contrast letter acuity as a visual component for the Multiple Sclerosis Functional Composite. Neurology. 2003 11;61(10):1367-73.

95. Optic Neuritis Study G. The clinical profile of optic neuritis. Experience of the Optic Neuritis Treatment Trial. Optic Neuritis Study Group. Arch Ophthalmol. 1991 Dec;109(12):1673-8.

96. Fleishman JA, Beck RW, Linares OA, Klein JW. Deficits in Visual Function after Resolution of Optic Neuritis. Ophthalmology. 1987 /08;94(8):1029-35.

97. Farnsworth D. The Farnsworth-Munsell 100-Hue and Dichotomous Tests for Color Vision. J Opt Soc Am. 1943 Oct;33(10):568-78.

98. Katz B. The dyschromatopsia of optic neuritis: a descriptive analysis of data from the optic neuritis treatment trial. Trans Am Ophthalmol Soc. 1995;93:685-708.

99. Hoyt CS. The Farnsworth-Munsell 100 hue test and optic neuritis. Br J Ophthalmol. 1993 -2;77(2):65.

100. Henderson AP, Altmann DR, Trip SA, Miszkiel KA, Schlottmann PG, Jones SJ, et al. Early factors associated with axonal loss after optic neuritis. Ann Neurol. 2011 Dec;70(6):955-63.

101. Keltner JL, Johnson CA, Spurr JO,Beck RW. Baseline visual field profile of optic neuritis: The experience of the optic neuritis treatment trial. Archives of Ophthalmology. 1993 February 1;111(2):231-4.

102. Cheng H, Laron M, Schiffman JS, Tang RA, Frishman LJ. The Relationship between Visual Field and Retinal Nerve Fiber Layer Measurements in Patients with Multiple Sclerosis. Invest Ophthalmol Vis Sci. 2007 -12;48(12):5798-805.

103. Wall M, Johnson CA, Kutzko KE, Nguyen R, Brito C, Keltner JL. Long- and short-term variability of automated perimetry results in patients with optic neuritis and healthy subjects. Arch Ophthalmol. 1998 Jan;116(1):53-61.

104. Bengtsson B, Olsson J, Heijl A, RootzÃ©n H. A new generation of algorithms for computerized threshold perimetry, SITA. Acta Ophthalmol Scand. 1997 Aug;75(4):368-75.

105. Carter JL. Visual Evoked potentials. In: Rubin DI, Daube JR, editors. Clinical Neurophysiology. Oxford, UK: Oxford University Press.

106. Brusa A, Jones SJ, Plant GT. Long-term remyelination after optic neuritis: A 2-year visual evoked potential and psychophysical serial study. Brain. 2001 March;124(3):468-79.

107. Jones SJ, Brusa A. Neurophysiological evidence for long-term repair of \MS\ lesions: implications for axon protection. J Neurol Sci. 2003;206(2):193.

108. Holder GE. Electrophysiological assessment of optic nerve disease. Eye. 2004 Nov;18(11):1133-43.

109. Pueyo V, Martin J, Fernandez J, Almarcegui C, Ara J, Egea C, et al. Axonal loss in the retinal nerve fiber layer in patients with multiple sclerosis. Multiple Sclerosis. 2008 Jun;14(5):609-14.

110. Bach M, Brigell MG, Hawlina M, Holder GE, Johnson MA, McCulloch DL, et al. ISCEV standard for clinical pattern electroretinography (PERG): 2012 update. Documenta Ophthalmologica. 2013 Feb;126(1):1-7.

111. Holder GE. Pattern electroretinography (PERG) and an integrated approach to visual pathway diagnosis. Progress in Retinal & Eye Research. 2001 Jul;20(4):531-61.

112. Hokazono K, Raza AS, Oyamada MK, Hood DC, Monteiro ML. Pattern electroretinogram in neuromyelitis optica and multiple sclerosis with or without optic

neuritis and its correlation with FD-OCT and perimetry. Documenta Ophthalmologica. 2013 Dec;127(3):201-15.

113. Odom JV, Bach M, Brigell M, Holder GE, McCulloch DL, Tormene AP, et al. ISCEV standard for clinical visual evoked potentials (2009 update). Documenta Ophthalmologica. 2010 Feb;120(1):111-9.

114. Tsakiri A, Kallenbach K, Fuglo D, Wanscher B, Larsson H, Frederiksen J. Simvastatin improves final visual outcome in acute optic neuritis: a randomized study. Multiple Sclerosis. 2012 Jan;18(1):72-81.

115. Kupersmith MJ, Garvin MK, Wang JK, Durbin M, Kardon R. Retinal ganglion cell layer thinning within one month of presentation for optic neuritis. Mult Scler. 2016 Apr;22(5):641-8.

116. Costello F, Pan YI, Yeh EA, Hodge W, Burton JM, Kardon R. The temporal evolution of structural and functional measures after acute optic neuritis. Journal of Neurology, Neurosurgery & Psychiatry. 2015 February 10.

117. Saver JL. Time is brain--quantified. Stroke. 2006 Jan;37(1):263-6.

118. Nikic I, Merkler D, Sorbara C, Brinkoetter M, Kreutzfeldt M, Bareyre FM, et al. A reversible form of axon damage in experimental autoimmune encephalomyelitis and multiple sclerosis. Nat Med. 2011 print;17(4):495-9.

119. Fairless R, Williams SK, Hoffmann DB, Stojic A, Hochmeister S, Schmitz F, et al. Preclinical Retinal Neurodegeneration in a Model of Multiple Sclerosis. The Journal of Neuroscience. 2012 April 18;32(16):5585-97.

120. Green AJ, McQuaid S, Hauser SL, Allen IV, Lyness R. Ocular pathology in multiple sclerosis: retinal atrophy and inflammation irrespective of disease duration. Brain. 2010 Jun;133(Pt 6):1591-601.

121. Cramer SP, Modvig S, Simonsen HJ, Frederiksen JL, Larsson HBW. Permeability of the blood - brain barrier predicts conversion from optic neuritis to multiple sclerosis. Brain. 2015 06/09;138(9):2571-83.

122. Gregory AP, Dendrou CA, Attfield KE, Haghikia A, Xifara DK, Butter F, et al. TNF receptor 1 genetic risk mirrors outcome of anti-TNF therapy in multiple sclerosis. Nature. 2012 Aug 23;488(7412):508-11.

123. Varga BE, Gao W, Laurik KL, Tatrai E, Simo M, Somfai G, et al. Investigating Tissue Optical Properties and Texture Descriptors of the Retina in Patients with Multiple Sclerosis. PLOS ONE. 2015 Nov 30,;10(11):e0143711.

124. Oberwahrenbrock T, Ringelstein M, Jentschke S, Deuschle K, Klumbies K, Bellmann-Strobl J, et al. Retinal ganglion cell and inner plexiform layer thinning in clinically isolated syndrome. Mult Scler. 2013 December 1,;19(14):1887-95.

125. Fernandes DB, Raza AS, Nogueira RG, Wang D, Callegaro D, Hood DC, et al. Evaluation of inner retinal layers in patients with multiple sclerosis or neuromyelitis optica using optical coherence tomography. Ophthalmology. 2013 Feb;120(2):387-94.

126. Esen E, Sizmaz S, Balal M, Yar K, Demirkiran M, Unal I, et al. Evaluation of the Innermost Retinal Layers and Visual Evoked Potentials in Patients with Multiple Sclerosis. Curr Eye Res. 2016 October 2,;41(10):1353-8.

127. Gabilondo I, Martinez-Lapiscina EH, Fraga-Pumar E, Ortiz-Perez S, Torres-Torres R, Andorra M, et al. Dynamics of retinal injury after acute optic neuritis. Ann Neurol. 2015 March 1,;77(3):517-28.

128. Kaushik M, Wang CY, Barnett MH, Garrick R, Parratt J, Graham SL, et al. Inner Nuclear Layer Thickening Is Inversley Proportional to Retinal Ganglion Cell Loss in Optic Neuritis. PLOS ONE. 2013 Oct 3,;8(10):e78341.

129. Al-Louzi OA, Bhargava P, Newsome SD, Balcer LJ, Frohman EM, Crainiceanu C, et al. Outer retinal changes following acute optic neuritis. Mult Scler. 2016 Mar;22(3):362-72.

130. Kaufhold F, Zimmermann H, Schneider E, Ruprecht K, Paul F, Oberwahrenbrock T, et al. Optic neuritis is associated with inner nuclear layer thickening and microcystic macular edema independently of multiple sclerosis. PLoS ONE [Electronic Resource]. 2013;8(8):e71145.

131. Fan Q, Teo YY, Saw SM. Application of advanced statistics in ophthalmology. Invest Ophthalmol Vis Sci. 2011 Aug;52(9):6059-65.

132. Newkirk MR, Gardiner SK, Demirel S, Johnson CA. Assessment of False Positives with the Humphrey Field Analyzer II Perimeter with the SITA Algorithm. Invest Ophthalmol Vis Sci. 2006 /10;47(10):4632-7.

133. Brandt AU, Oberwahrenbrock T, Kadas EM, LagrÃ¨ze WA, Paul F. Dynamic formation of macular microcysts independent of vitreous traction changes. Neurology. 2014 Jul 01,;83(1):73-7.

134. Sbardella E, Tona F, Petsas N, Pantano P. DTI Measurements in Multiple Sclerosis: Evaluation of Brain Damage and Clinical Implications. Mult Scler Int. 2013;2013:671730.

135. Kolasinski J, Stagg CJ, Chance SA, DeLuca GC, Esiri MM, Chang E, et al. A combined post-mortem magnetic resonance imaging and quantitative histological study of multiple sclerosis pathology. Brain. 2012 10/01;135(10):2938-51.

136. Schmierer K, Wheeler-Kingshott C, Boulby PA, Scaravilli F, Altmann DR, Barker GJ, et al. Diffusion tensor imaging of post mortem multiple sclerosis brain. Neuroimage. 2006;35(2):467-77.

137. Song S, Sun S, Ramsbottom MJ, Chang C, Russell J, Cross AH. Dysmyelination Revealed through MRI as Increased Radial (but Unchanged Axial) Diffusion of Water. Neuroimage. 2002 November 1,;17(3):1429-36.

138. Fink F, Klein J, Lanz M, Mitrovics T, Lentschig M, Hahn HK, et al. Comparison of Diffusion Tensor-Based Tractography and Quantified Brain Atrophy for Analyzing Demyelination and Axonal Loss in MS. Journal of Neuroimaging. 2010 October 1,;20(4):334-44.

139. Tillema JM, Leach J, Pirko I. Non-lesional white matter changes in pediatric multiple sclerosis and monophasic demyelinating disorders. Mult Scler. 2012 Dec;18(12):1754-9.

140. Aung WY, Mar S, Benzinger TLS. Diffusion tensor MRI as a biomarker in axonal and myelin damage. Imaging in medicine. 2013;5(5):427-40.

141. Trapp BD, Ransohoff R, Rudick R. Axonal pathology in multiple sclerosis: relationship to neurologic disability. Curr Opin Neurol. 1999 Jun;12(3):295-302.

142. You Y, Gupta VK, Graham SL, Klistorner A. Anterograde degeneration along the visual pathway after optic nerve injury. PLoS ONE [Electronic Resource]. 2012;7(12):e52061.

143. Ghetti B, Horoupian DS, WisÂ´niewski HM. Transsynaptic response of the lateral geniculate nucleus and the pattern of degeneration of the nerve terminals in the Rhesus monkey after eye enucleation. Brain Research. 1972 October 13,;45(1):31-48.

144. Ghetti B, WiÅ›niewski HM. On degeneration of terminals in the cat striate cortex. Brain Research. 1972 September 29,;44(2):630-5.

145. Raz N, Bick AS, Ben-Hur T, Levin N. Focal demyelinative damage and neighboring white matter integrity: an optic neuritis study. Mult Scler. 2015 Apr;21(5):562-71.

146. Raz N, Chokron S, Ben-Hur T, Levin N. Temporal reorganization to overcome monocular demyelination. Neurology. 2013 Aug 20,;81(8):702-9.

147. Ciccarelli O, Toosy AT, Hickman SJ, Parker GJ, Wheeler-Kingshott CA, Miller DH, et al. Optic radiation changes after optic neuritis detected by tractography-based group mapping. Hum Brain Mapp. 2005 Jul;25(3):308-16.

148. Kolbe SC, Marriott M, Walt A, Fielding J, Klistorner A, Mitchell PJ, et al. Diffusion tensor imaging correlates of visual impairment in multiple sclerosis and chronic optic neuritis. Invest Ophthalmol Vis Sci. 2012 Feb;53(2):825-32.

149. Tur C, Goodkin O, Altmann DR, Jenkins TM, Miszkiel K, Mirigliani A, et al. Longitudinal evidence for anterograde trans-synaptic degeneration after optic neuritis. Brain. 2016 Mar;139:816-28.

150. Kolbe SC, van dW, Butzkueven H, Klistorner A, Egan GF, Kilpatrick TJ. Serial Diffusion Tensor Imaging of the Optic Radiations after Acute Optic Neuritis. Journal of Ophthalmology. 2016 07/10;2016:2764538.

151. Smith SM, Jenkinson M, Johansen-Berg H, Rueckert D, Nichols TE, Mackay CE, et al. Tract-based spatial statistics: voxelwise analysis of multi-subject diffusion data. Neuroimage. 2006 Jul 15;31(4):1487-505.

152. Smith SM, Jenkinson M, Woolrich MW, Beckmann CF, Behrens TEJ, Johansen-Berg H, et al. Advances in functional and structural MR image analysis and implementation as FSL. Neuroimage. 2004;23 Suppl 1:208.

153. Smith SM. Fast robust automated brain extraction. Hum Brain Mapp. 2002 November 1,;17(3):143-55.

154. Andersson JLR, Jenkinson M, Smith S. Non-linear optimisation. FMRIB technical report TR07JA1. University of Oxford; 2007.

155. Rueckert D, Sonoda LI, Hayes C, Hill DL, Leach MO, Hawkes DJ. Nonrigid registration using free-form deformations: application to breast MR images. IEEE Trans Med Imaging. 1999 Aug;18(8):712-21.

156. Behrens TEJ, Woolrich MW, Jenkinson M, Johansen-Berg H, Nunes RG, Clare S, et al. Characterization and propagation of uncertainty in diffusion-weighted MR imaging. Magn Reson Med. 2003 Nov;50(5):1077-88.

157. Behrens TEJ, Berg HJ, Jbabdi S, Rushworth MFS, Woolrich MW. Probabilistic diffusion tractography with multiple fibre orientations: What can we gain? Neuroimage. 2007 Jan 01,;34(1):144-55.

158. Jbabdi S, Behrens TEJ, Smith SM. Crossing fibres in tract-based spatial statistics. Neuroimage. 2010 January 1,;49(1):249-56.

159. Foroozan R. Chiasmal syndromes. Curr Opin Ophthalmol. 2003 December;14(6):325-31.

160. Griffanti L, Zamboni G, Khan A, Li L, Bonifacio G, Sundaresan V, et al. BIANCA (Brain Intensity AbNormality Classification Algorithm): A new tool for automated segmentation of white matter hyperintensities. Neuroimage. 2016 November 1,;141:191-205.

161. Barkhof F, Scheltens P. Imaging of white matter lesions. Cerebrovasc Dis. 2002;13 Suppl 2:21-30.

162. Singh S, Dallenga T, Winkler A, Roemer S, Maruschak B, Siebert H, et al. Relationship of acute axonal damage, Wallerian degeneration, and clinical disability in multiple sclerosis. J Neuroinflammation. 2017 Mar 17,;14(1):57.

163. Winkler AM, Ridgway GR, Webster MA, Smith SM, Nichols TE. Permutation inference for the general linear model. Neuroimage. 2014 May 15,;92:381-97.

164. Smith SM, Nichols TE. Threshold-free cluster enhancement: addressing problems of smoothing, threshold dependence and localisation in cluster inference. Neuroimage. 2009 Jan 01,;44(1):83-98.

165. Braddick O, Atkinson J, Akshoomoff N, Newman E, Curley LB, Gonzalez MR, et al. Individual differences in children's global motion sensitivity correlate with TBSS-based measures of the superior longitudinal fasciculus. Vision Res. 2016 Dec 16,.

166. Raz N, Dotan S, Benoliel T, Chokron S, Ben-Hur T, Levin N. Sustained motion perception deficit following optic neuritis: Behavioral and cortical evidence. Neurology. 2011 Jun 14,;76(24):2103-11.

167. Reislev NL, Kupers R, Siebner HR, Ptito M, Dyrby TB. Blindness alters the microstructure of the ventral but not the dorsal visual stream. Brain Struct Funct. 2016 /07;221(6):2891-903.

168. Ozturk A, Smith SA, Gordon-Lipkin E, Harrison DM, Shiee N, Pham DL, et al. MRI of the Corpus Callosum in Multiple Sclerosis: Association with Disability. Mult Scler. 2010 -2;16(2):166.

169. Audoin B, Ibarrola D, Malikova I, Soulier E, Confort-Gouny S, Duong MV, et al. Onset and underpinnings of white matter atrophy at the very early stage of multiple sclerosis--a two-year longitudinal MRI/MRSI study of corpus callosum. Multiple Sclerosis. 2007 Jan;13(1):41-51.

170. Seabrook TA, El-Danaf RN, Krahe TE, Fox MA, Guido W. Retinal Input Regulates the Timing of Corticogeniculate Innervation. The Journal of Neuroscience. 2013 June 12;33(24):10085-97.

171. Bach M, Laun FB, Leemans A, Tax CMW, Biessels GJ, Stieltjes B, et al. Methodological considerations on tract-based spatial statistics (TBSS). Neuroimage. 2014 October 15,;100:358-69.

172. Jindahra P, Petrie A, Plant GT. The time course of retrograde trans-synaptic degeneration following occipital lobe damage in humans. Brain. 2012 Feb;135:534-41.

173. Matthews L, Kolind S, Brazier A, Leite MI, Brooks J, Traboulsee A, et al. Imaging Surrogates of Disease Activity in Neuromyelitis Optica Allow Distinction from Multiple Sclerosis. PLoS One. 2015 Sep 18;10(9):e0137715.

174. Glover GH. Overview of Functional Magnetic Resonance Imaging. Neurosurg Clin N Am. 2011 -4;22(2):133-9.

175. Ogawa S, Tank DW, Menon R, Ellermann JM, Kim SG, Merkle H, et al. Intrinsic signal changes accompanying sensory stimulation: functional brain mapping with magnetic resonance imaging. PNAS. 1992 07;89(13):5951-5.

176. Beckmann CF, DeLuca M, Devlin JT, Smith SM. Investigations into resting-state connectivity using independent component analysis. Philos Trans R Soc Lond B Biol Sci. 2005 May 29;360(1457):1001-13.

177. Smith SM, Fox PT, Miller KL, Glahn DC, Fox PM, Mackay CE, et al. Correspondence of the brain's functional architecture during activation and rest. PNAS. 2009 08;106(31):13040-5.

178. Raichle ME, MacLeod AM, Snyder AZ, Powers WJ, Gusnard DA, Shulman GL. A default mode of brain function. Proc Natl Acad Sci U S A. 2001 Jan 16,;98(2):676-82.

179. Levin N, Orlov T, Dotan S, Zohary E. Normal and abnormal fMRI activation patterns in the visual cortex after recovery from optic neuritis. Neuroimage. 2006 December 1,;33(4):1161-8.

180. Toosy AT, Hickman SJ, Miszkiel KA, Jones SJ, Plant GT, Altmann DR, et al. Adaptive cortical plasticity in higher visual areas after acute optic neuritis. Ann Neurol. 2005 May;57(5):622-33.

181. Toosy AT, Werring DJ, Bullmore ET, Plant GT, Barker GJ, Miller DH, et al. Functional magnetic resonance imaging of the cortical response to photic stimulation in humans following optic neuritis recovery. Neuroscience Letters. 2002 September 27,;330(3):255-9.

182. Jenkins TM, Ciccarelli O, Atzori M, Wheeler-Kingshott CA, Miller DH, Thompson AJ, et al. Early pericalcarine atrophy in acute optic neuritis is associated with conversion to multiple sclerosis. Journal of Neurology, Neurosurgery & Psychiatry. 2011 Sep;82(9):1017-21.

183. Wu GF, Brier MR, Parks CA, Ances BM, Van Stavern GP. An Eye on Brain Integrity: Acute Optic Neuritis Affects Resting State Functional Connectivity. Invest Ophthalmol Vis Sci. 2015 Apr;56(4):2541-6.

184. Gallo A, Esposito F, Sacco R, Docimo R, Bisecco A, Della Corte M, et al. Visual resting-state network in relapsing-remitting MS with and without previous optic neuritis. Neurology. 2012 Oct 2;79(14):1458-65.

185. Gabilondo I, Rilo O, Ojeda N, Pena J, Gomez-Gastiasoro A, Mendibe Bilbao M, et al. The influence of posterior visual pathway damage on visual information processing speed in multiple sclerosis. Mult Scler. 2016 Nov 01:1352458516676642.

186. Shao Y, Cai F, Zhong Y, Huang X, Zhang Y, Hu P, et al. Altered intrinsic regional spontaneous brain activity in patients with optic neuritis: a resting-state functional magnetic resonance imaging study. Neuropsychiatr Dis Treat. 2015 -12-11;11:3065-73.

187. Beckmann CF, Smith SM. Probabilistic independent component analysis for functional magnetic resonance imaging. IEEE Trans Med Imaging. 2004 Feb;23(2):137-52.

188. Hyvarinen A, Oja E. A Fast Fixed-point Algorithm for Independent Component Analysis. Neural Comput. 1997 October;9(7):1483-1492.

189. Salimi-Khorshidi G, Douaud G, Beckmann CF, Glasser MF, Griffanti L, Smith SM. Automatic denoising of functional MRI data: combining independent component analysis and hierarchical fusion of classifiers. Neuroimage. 2014 Apr 15,;90:449-68.

190. Griffanti L, Salimi-Khorshidi G, Beckmann CF, Auerbach EJ, Douaud G, Sexton CE, et al. ICA-based artefact removal and accelerated fMRI acquisition for improved resting state network imaging. Neuroimage. 2014 Jul 15,;95:232-47.

191. Jenkinson M, Smith S. A global optimisation method for robust affine registration of brain images. Med Image Anal. 2001 Jun;5(2):143-56.

192. Jenkinson M, Bannister P, Brady M, Smith S. Improved Optimization for the Robust and Accurate Linear Registration and Motion Correction of Brain Images. Neuroimage. 2002 October;17(2):825-41.

193. Beckmann CF, Mackay CE, Filippini N, Smith SM. Group comparison of resting-state FMRI data using multi-subject ICA and dual regression. Neuroimage. 2009 07/01;47:S148.

194. Filippini N, MacIntosh BJ, Hough MG, Goodwin GM, Frisoni GB, Smith SM, et al. Distinct patterns of brain activity in young carriers of the APOE-epsilon4 allele. Proc Natl Acad Sci U S A. 2009 Apr 28,;106(17):7209-14.

195. Power JD, Barnes KA, Snyder AZ, Schlaggar BL, Petersen SE. Spurious but systematic correlations in functional connectivity MRI networks arise from subject motion. Neuroimage. 2012 -2-1;59(3):2142-54.

196. Power JD, Mitra A, Laumann TO, Snyder AZ, Schlaggar BL, Petersen SE. Methods to detect, characterize, and remove motion artifact in resting state fMRI. Neuroimage. 2014 -1;84.

197. Langkilde AR, Frederiksen JL, Rostrup E, Larsson HBW. Functional MRI of the visual cortex and visual testing in patients with previous optic neuritis. Eur J Neurol. 2002 May;9(3):277-86.

198. Satterthwaite TD, Elliott MA, Gerraty RT, Ruparel K, Loughead J, Calkins ME, et al. An improved framework for confound regression and filtering for control of motion artifact in the preprocessing of resting-state functional connectivity data. Neuroimage. 2013 Jan 01,;64:240-56.

199. Roosendaal SD, Schoonheim MM, Hulst HE, Sanz-Arigita E, Smith SM, Geurts JJG, et al. Resting state networks change in clinically isolated syndrome. Brain. 2010 Jun;133:1612-21.

200. ClinicalTrials.gov [Internet]. Bethesda (MD): National Library of Medicine (US). 2000 Feb 29 Identifier NCT01879527 Amiloride Hydrochlorothiazide as Treatment of Acute Inflammation of the Optic Nerve, June 18 2013, [cited Oct 2017]. About 3 screens, available from https://clinicaltrials.gov/ct2/show/record/NCT01879527.

201. Diem R, Molnar F, Beisse F, Gross N, Druschler K, Heinrich SP, et al. Treatment of optic neuritis with erythropoietin (TONE): a randomised, double-blind, placebo-controlled trial study protocol. BMJ Open. 2016 /03;6(3):e010956.

202. Chataway J, Chandran S, Miller D, Connick P, Giovannoni G, Pavitt S, et al. THE MS-SMART TRIAL IN SECONDARY PROGRESSIVE MS– CURRENT UPDATE J Neurol Neurosurg Psychiatry 2016;87:e1.

.